

Huifei Jin

Dielectric Strength and Thermal Conductivity of Mineral Oil based Nanofluids

Dielectric Strength and Thermal Conductivity of Mineral Oil based Nanofluids

Huifei Jin

April 2015

Dielectric Strength and Thermal Conductivity of Mineral Oil based Nanofluids

Proefschrift

ter verkrijging van de graad van doctor

aan de Technische Universiteit Delft,

op gezag van de Rector Magnificus prof. ir. K.C.A.M. Luyben,

voorzitter van het College voor Promoties,

in het openbaar te verdedigen op vrijdag 10 april 2015 om 10.00 uur

door

Huifei Jin

Master of Electrical Engineering,
Delft University of Technology, the Netherlands

geboren te Jinzhou, China

This dissertation has been approved by the

promotor: Prof. dr. J. J. Smit and
copromotor: Dr. Ir. P. H. F. Morshuis

Compositions of the doctoral committee:

Rector Magnificus,
Prof. dr. J.J. Smit, promotor
Dr. ir. P.H.F. Morshuis, copromotor
Prof. dr. P. Palensky, other, not independent member

Independent members:

Prof. dr. S.J. Picken, Department of Chiminal Engineering, TU Delft
Prof. dr. Z. Wang, University of Manchester
Prof. dr. S. Li, Xi'an JiaoTong University
Dr. R. Kochetov, ABB Corporate Research

This research was funded by the following companies:

Philips Healthcare GTC, Hamburg, Germany
Comet AG, Flamatt, Switzerland
Jensen Capacitors, Broendby, Denmark
Thales Electron Devices, Ulm, Germany
SebaKMT, Radeburg, Germany

ISBN: 978-94-6182-552-0

Printed by: Off Page, Amsterdam, The Netherlands

Copyright © 2015 by H. Jin

All rights reserved. No part of this work may be reproduced in any form
without the permission in writing from the Publisher.

Summary

In many applications of high voltage engineering, electrical and thermal stresses increase due to an ongoing decrease of product dimensions. In particular, the electrical industry is interested in applying nanofluids in transformers to be able to decrease transformer size and weight. The requirement for nanofluids is to enhance the electrical insulation as well as the thermal conductivity of transformer oil. The focus of this thesis is to investigate how to improve the dielectric strength and thermal conductivity of mineral oil by introducing a low concentration of nanoparticles as well as to understand the possible mechanism behind the property changes.

Stable dispersed nanoparticles are vital for the investigation of the properties of nanofluids. However, it can be a challenge to maintain the nano-meter size of nanoparticles due to the attractive force between nanoparticles, which can lead to the formation of agglomerations which eventually settle out of suspension. In this thesis, good and stable dispersed nanoparticles in mineral oil have been achieved by magnetic stirring and ultrasonic vibration at a relatively low concentration. The two types of nanofillers which were used to achieve stable dispersed nanofluids are silica and fullerene nanoparticles.

The results of AC breakdown test results on nanofluids with up to 0.02 wt.% silica and nanofluids with up to 0.1 wt.% fullerene showed that both types of nanofluids exhibited enhanced breakdown strength compared with mineral oil. The enhancement increases with an increase of mass fraction. The effect is more significant at higher moisture content. The enhancement of the AC breakdown voltage due to silica nanoparticles is larger than for fullerene nanoparticles. Since silica is an insulating material and fullerene is a semi conductive material, the phenomena can't be explained by the theory of conductive nanoparticles acting as electron traps. Besides, moisture content plays an important role in the breakdown behaviour of mineral oil. So one possible explanation behind the enhanced AC breakdown voltage of silica nanofluids is that moisture is adsorbed on the surface of silica nanoparticles. However, fullerene is hydrophobic, therefore moisture adsorption can't be the reason for the enhanced breakdown strength of fullerene nanofluids.

Partial discharge (PD) measurements gave more detailed information on the pre-breakdown phenomenon of dielectric nanofluids by recording the discharge pulse shape, inception voltage, total discharge magnitude and single discharge pulse amplitude. The PD results of mineral oil, 0.01 wt.% silica and fullerene nanofluids showed that silica nanoparticles increase the inception voltage, and decrease both the total discharge magnitude and the pulse amplitude of mineral oil significantly. The effect due to fullerene nanoparticles is similar but less than the effect of silica nanoparticles. The possible explanation of this phenomenon is that organic acid is adsorbed on the surface of the nanoparticles. The increased inception voltage and decreased PD discharge magnitudes of silica and fullerene nanofluids can be due to the decreased acidity in the nanofluids. The larger effect of silica nanoparticles on the dielectric strength of mineral oil compared with fullerene nanoparticles can be a result of the combination of acid and moisture adsorption on the surface of the nanoparticles.

The effect of silica and fullerene nanoparticles up to 0.1% mass fraction on the thermal conductivity and viscosity of mineral oil is negligible. This is mainly due to the low concentration and limitation of stability of nanofluids.

The stability and possible harmful effects of nanoparticles on health and environment are also discussed in this thesis.

Finally, it was concluded that the dielectric strength of mineral oil is improved by adding a low concentration of nanoparticles. The possible explanation for this achievement and recommendations for further research are also described.

Samenvatting

In veel toepassingen van de hoogspanningstechniek is er een toename van elektrische en thermische belasting door een voortdurende afname van de productafmetingen. De elektrische industrie in het bijzonder is geïnteresseerd in de toepassing van nanovloeistoffen in transformatoren om de grootte en het gewicht van transformatoren te kunnen verminderen. Een eis aan deze nanovloeistoffen is dat de elektrische isolerende eigenschappen en de thermische geleidbaarheid van transformatorolie worden verbeterd. De focus van dit proefschrift is te onderzoeken hoe de diëlektrische sterkte en thermische geleidbaarheid van minerale olie zijn te veranderen door de toevoeging van een lage concentratie van nanodeeltjes en tevens om het mogelijke mechanisme achter deze verandering van eigenschappen te achterhalen.

Een stabiele verspreiding van nanodeeltjes is vitaal voor verder onderzoek naar de eigenschappen van nanovloeistoffen. Maar het is een uitdaging om de nanometergrootte van nanodeeltjes te handhaven vanwege de aantrekkingskracht tussen nanodeeltjes. Deze aantrekkingskracht kan leiden tot agglomeratie en uiteindelijk tot het bezinken uit de suspensie. In dit proefschrift werd stabiele nanovloeistof met een relatief lage concentratie op basis van minerale olie verkregen met magnetisch roeren en ultrasonische trillingen. De twee soorten vulstof waarmee stabiel gedispergeerde nanovloeistoffen bereid werden zijn silica en fullereen nanodeeltjes.

De testresultaten van de AC doorslagspanning van silica nanovloeistoffen tot 0,02 gew.% en fullereen nanovloeistoffen tot 0,1 gew.% lieten zien dat beide typen nanovloeistoffen verhoogde doorslagsterkte vertoonden ten opzichte van minerale olie. De verhoging van de doorslagsterkte neemt toe met een toename van de massafractie. Het effect is groter bij een hoger vochtgehalte. Silica nanodeeltjes veroorzaken een hogere AC doorslagspanning dan fullereen nanodeeltjes. Omdat silica een isolerend materiaal is en fullereen een halfgeleidend materiaal, kunnen de verschijnselen niet verklaard worden met de theorie waarin geleidende nanodeeltjes fungeren als elektronenvanger. Bovendien speelt het vochtgehalte een belangrijke rol in het doorslagspanningsgedrag van minerale olie. Een mogelijke verklaring achter de versterkte AC

doorslagspanning van silica nanovloeistoffen is dat vocht wordt geadsorbeerd aan het oppervlak van silica nanodeeltjes. Maar fullereen is hydrofoob, dus vochtadsorptie kan niet de reden voor de verhoogde doorslagsterkte van fullereen nanovloeistoffen zijn.

Het meten van de partiële ontladingen (PD) gaf meer gedetailleerde informatie over de pre-doorslagfenomenen van diëlektrische nanovloeistof. Gemeten werden de ontladingspulsvorm, de ontsteekspanning, de totale ontlading en de puls amplitude. De PD resultaten van minerale olie, silica en fullereen nanovloeistoffen lieten zien dat silica nanodeeltjes de ontsteekspanning verhogen en de grootte van de totale ontlading en de pulsamplitude van minerale olie aanzienlijk verminderen. Het effect van fullereen nanodeeltjes is vergelijkbaar maar minder groot dan het effect van silica nanodeeltjes. De mogelijke verklaring voor dit verschijnsel is dat organisch zuur wordt geadsorbeerd op het oppervlak van de nanodeeltjes. De verhoogde ontsteekspanning en verminderde ontlading van silica en fullereen nanovloeistoffen kunnen worden toegeschreven aan de afname van de zuurgraad in de nanovloeistoffen. Het grotere effect van silica nanodeeltjes op de diëlektrische sterkte van minerale olie ten opzichte van fullereen nanodeeltjes kan worden toegeschreven aan de combinatie van zuur- en vochtadsorptie aan het oppervlak van de nanodeeltjes.

Het effect van silica en fullereen nanodeeltjes tot 0,1 gew.% op de thermische geleidbaarheid en de viscositeit van minerale olie is verwaarloosbaar. Dit is voornamelijk te wijten aan de lage concentratie en de beperkte van de stabiliteit van nanovloeistoffen.

De stabiliteit en de mogelijke schadelijke effecten van nanodeeltjes voor de gezondheid en het milieu worden ook besproken in dit proefschrift.

Ten slotte werd geconcludeerd dat de doorslagsterkte van minerale olie wordt verbeterd door de toevoeging van een lage concentratie nanodeeltjes. De mogelijke verklaring voor dit resultaat en aanbevelingen voor verdere onderzoek worden ook beschreven.

Contents

1	INTRODUCTION	- 1 -
1.1	DEVELOPMENT OF THE CONCEPT OF NANOFUIDS	- 1 -
1.2	APPLICATIONS OF NANOFUIDS	- 2 -
1.3	STATE OF ART	- 3 -
1.4	GOAL OF THIS THESIS	- 4 -
1.5	STRUCTURE OF THE THESIS	- 6 -
1.6	REFERENCES	- 7 -
2	SYNTHESIS OF NANOFUIDS.....	- 11 -
2.1	GENERAL ISSUES OF CONCERN	- 11 -
2.1.1	NATURE OF COLLOIDAL STATE	- 11 -
2.1.2	DISPERSION METHOD.....	- 15 -
2.1.3	SURFACE MODIFICATION	- 15 -
2.1.4	REQUIREMENTS AND PRECAUTIONS.....	- 18 -
2.2	MATERIALS USED	- 18 -
2.2.1	HOST MATERIAL.....	- 18 -
2.2.2	FILLER MATERIAL.....	- 19 -
2.2.3	SURFACTANT AND COUPLING AGENT	- 20 -
2.3	SYNTHESIS PROCEDURE	- 21 -
2.3.1	NANOPARTICLE CHARACTERIZATION	- 21 -
2.3.2	NANOPARTICLE SURFACE MODIFICATION.....	- 25 -
2.3.3	DISPERSION PROCEDURE	- 27 -
2.3.4	PARTICLE DISTRIBUTION EXAMINATION	- 28 -
2.4	SUMMARY	- 31 -
2.5	REFERENCES	- 32 -
3	AC BREAKDOWN STRENGTH OF NANOFUIDS	- 35 -
3.1	INTRODUCTION	- 35 -
3.2	BREAKDOWN MECHANISM IN INSULATING LIQUID	- 36 -
3.3	AC BREAKDOWN IN MINERAL OIL.....	- 37 -
3.3.1	INFLUENCE OF WATER CONTENT	- 38 -

3.3.2	INFLUENCE OF PARTICLES.....	- 38 -
3.3.3	INFLUENCE OF VISCOSITY	- 39 -
3.4	EXPERIMENTAL TEST SET-UP FOR BREAKDOWN MEASUREMENTS	- 39 -
3.5	STATISTICAL ANALYSIS OF BREAKDOWN DATA	- 41 -
3.6	AC BREAKDOWN STRENGTH OF SILICA NANOFLUIDS.....	- 42 -
3.6.1	SAMPLE PREPARATION	- 42 -
3.6.2	MEASUREMENT RESULTS.....	- 42 -
3.6.3	DATA ANALYSIS.....	- 43 -
3.6.4	VISCOSITY.....	- 48 -
3.6.5	DISCUSSION	- 49 -
3.6.6	SUMMARY	- 50 -
3.7	AC BREAKDOWN VOLTAGE OF SURFACE MODIFIED SILICA NANOFLUIDS	- 51 -
3.7.1	SAMPLE PREPARATION	- 51 -
3.7.2	MEASUREMENT RESULTS.....	- 52 -
3.7.3	DATA ANALYSIS.....	- 53 -
3.7.4	DISCUSSION	- 58 -
3.7.5	SUMMARY	- 59 -
3.8	AC BREAKDOWN STRENGTH OF FULLERENE NANOFLUIDS.....	- 60 -
3.8.1	SAMPLE PREPARATION	- 60 -
3.8.2	MEASUREMENT RESULTS.....	- 61 -
3.8.3	DATA ANALYSIS.....	- 62 -
3.8.4	VISCOSITY.....	- 65 -
3.8.5	DISCUSSION	- 66 -
3.8.6	SUMMARY	- 67 -
3.9	REFERENCES	- 67 -
4	<u>PARTIAL DISCHARGE DYNAMICS IN NANOFLUIDS.....</u>	<u>- 71 -</u>
4.1	INTRODUCTION	- 71 -
4.2	PRE-BREAKDOWN PHENOMENA IN LIQUID DIELECTRICS.....	- 71 -
4.2.1	POSITIVE STREAMER	- 72 -
4.2.2	NEGATIVE STREAMER.....	- 73 -
4.3	FUNDAMENTALS OF PARTIAL DISCHARGE	- 74 -
4.3.1	CHARACTERISTIC PARAMETERS OF PD IN LIQUID DIELECTRICS.....	- 74 -
4.3.2	PD MEASUREMENT CIRCUIT AND EXPERIMENTAL SETUP.....	- 75 -
4.4	EXPERIMENTAL RESULTS OF PD IN MINERAL OIL AND NANOFLUIDS	- 79 -
4.4.1	TEST SAMPLES	- 79 -

4.4.2	RESULTS UNDER POSITIVE DC VOLTAGE	- 80 -
4.4.3	RESULTS UNDER NEGATIVE DC VOLTAGE	- 86 -
4.5	DISCUSSION	- 92 -
4.6	SUMMARY	- 93 -
4.7	REFERENCES	- 94 -
<u>5</u>	<u>THERMAL CONDUCTIVITY</u>	<u>- 97 -</u>
5.1	INTRODUCTION	- 97 -
5.2	CONDUCTION HEAT TRANSFER IN LIQUIDS	- 98 -
5.3	THERMAL CONDUCTIVITY OF NANOFUIDS	- 99 -
5.4	THERMAL CONDUCTIVITY MEASUREMENT TECHNIQUES FOR NANOFUIDS. -	101 -
5.5	EXPERIMENTAL RESULTS OF THE THERMAL CONDUCTIVITY OF SILICA AND FULLERENE NANOFUIDS	- 102 -
5.5.1	TEST SETUP.....	- 103 -
5.5.2	THERMAL CONDUCTIVITY IN FUNCTION OF TEMPERATURE	- 104 -
5.5.3	THERMAL CONDUCTIVITY AS A FUNCTION OF TIME	- 106 -
5.5.4	SUMMARY	- 107 -
5.6	MODELLING RESULTS OF THE THERMAL CONDUCTIVITY OF SILICA AND FULLERENE NANOFUIDS	- 108 -
5.7	EXPERIMENTAL RESULTS OF THERMAL CONDUCTIVITY OF OTHER TYPES OF NANOFUIDS	- 112 -
5.8	DISCUSSION AND SUMMARY	- 113 -
5.9	REFERENCES	- 114 -
<u>6</u>	<u>STABILITY, HEALTH AND ENVIRONMENTAL ASPECTS</u>	<u>- 117 -</u>
6.1	STABILITY TESTS OF NANOFUIDS	- 117 -
6.1.1	NANOFUIDS STABILITY TEST SET-UP	- 118 -
6.1.2	NANOFUIDS STABILITY TEST RESULTS	- 120 -
6.1.3	SUMMARY AND DISCUSSION	- 122 -
6.2	HEALTH AND ENVIRONMENTAL ASPECTS	- 123 -
6.3	FUTURE RESEARCH	- 124 -
6.4	REFERENCES	- 125 -
<u>7</u>	<u>CONCLUSIONS AND RECOMMENDATIONS.....</u>	<u>- 127 -</u>

7.1 CONCLUSIONS.....	- 127 -
7.2 RECOMMENDATIONS.....	- 130 -
7.3 REFERENCES	- 131 -
<u>APPENDIX A. DYNAMIC LIGHT SCATTERING</u>	<u>- 133 -</u>
A.1 INTRODUCTION	- 133 -
A.2 COLLECTING DATA.....	- 133 -
A.3 DATA ANALYSIS	- 134 -
REFERENCES.....	- 135 -
<u>APPENDIX B. MOISTURE CONTENT MEASUREMENT</u>	<u>- 137 -</u>
REFERENCES.....	- 138 -
<u>APPENDIX C. BANDWIDTH OF PARTIAL DISCHARGE DETECTION SYSTEM . -</u>	<u>139 -</u>
REFERENCES.....	- 140 -
<u>APPENDIX D. THERMAL CONDUCTIVITY CALCULATION OF NANOFUIDS IN</u>	<u>COMSOL MULTIPHYSICS HEAT TRANSFER MODULE..... - 141 -</u>
<u>APPENDIX E. FOURIER TRANSFORM INFRARED TERAHERTZ</u>	<u>SPECTROMETER</u>
<u>- 143 -</u>	
REFERENCES.....	- 145 -
<u>LIST OF SYMBOLS AND ABBREVIATIONS</u>	<u>- 146 -</u>
<u>ACKNOWLEDGMENTS</u>	<u>- 149 -</u>
<u>PUBLICATIONS</u>	<u>- 151 -</u>
<u>CURRICULUM VITAE</u>	<u>- 153 -</u>

1 Introduction

Today high-performance cooling is a top challenge facing high-tech industries [1-3]. However in the electrical power industry, conventional insulating fluids are inherently poor heat transfer fluids. Therefore, new and strong innovative concepts are needed to achieve high-performance cooling in thermal management systems. Nanofluids exhibit enhanced properties, for instance as thermal transfer fluids as well as insulation. Therefore nanofluids are considered to be used in many engineering applications ranging from power cooling systems to automotive industry [1]. The electrical power industry is interested in transformer cooling application of nanofluids for reducing transformer size and weight. The request for nanofluids is to enhance the thermal conductivity of transformer oil without compromising the required electrical insulation of the oil [2]. A study related to the thermal conductivity, dielectric strength and viscosity of transformer oil based nanofluids has indicated that the breakdown voltage increased along with an improvement of heat transfer characteristics [3].

1.1 Development of the concept of nanofluids

The base concept of dispersing solid particles in fluid to enhance the thermal conductivity is not new. It can be traced back to 1873, when Maxwell presented a theoretical basis for predicting the effective thermal conductivity of liquid/solid suspension [4]. Solid particles are added because they conduct heat much better than liquids. For more than 100 years, scientists and engineers have made great efforts to enhance the inherently poor thermal conductivity of traditional heat transfer liquids, such as water, oil and ethylene glycol [1]. Numerous theoretical and experimental studies of the effective thermal conductivity of suspensions that contain solid particles have been conducted [5-7]. However, all of the studies have been confined to millimetre- or micrometre-size particles. The major problem with the use of millimetre- or micrometre-size particles is the rapid settling of the particles in fluids [1]. The large size particles and the difficulty in production of small particles are the limiting factors for liquid/solid suspension to be investigated for practical applications.

Nanotechnology helps to overcome these problems by stably suspending in fluids nanometre-sized particles instead of millimetre- or micrometre-

sized particles [2]. An important step in the development of nanoscience was the assessment of the nano-meter size of molecules in the beginning of the 20th century [8]. The concept of nanotechnology was introduced in the famous lecture of Richard Feynman “There is enough space at the bottom” in 1959 [9]. The invention of the scanning tunnelling microscope triggered the growth of nanotechnology in the 1980’s [10]. In 1995, Stephen Choi from Argonne National Laboratory presented at the annual winter meeting of the American Society of Mechanical Engineers “the remarkable possibility of increasing the convection heat transfer coefficients by using high-conductivity nanofluids instead of increasing pump power” [2]. After that, Choi and Eastman have tried to suspend various metal and metal oxides nanoparticles in several different fluids. The results showed that nanoparticles stay suspended longer than larger particles and nanofluids exhibit excellent thermal properties and cooling capacity [11-14]. Since then numerous research groups have investigated thermal conductivity, convective heat transfer and breakdown strength of nanofluids [15-31]. The nanofluid technology is still in its early phase and scientists are working now to help using nanofluids as a tool to solve technological problems of industry [10].

1.2 Applications of nanofluids

Nanofluids can be used in a great deal of engineering applications ranging from the automotive industry to the medical arena and to power plant cooling systems as well as computers [32]. The applications of nanofluids related with heat transfer and energy saving are introduced below.

- Industrial cooling applications

The application of nanofluids in industrial cooling systems can result in energy savings and emission reduction [33]. In 2008, a project that employed nanofluids for industrial cooling was started by Routbort et al. [34]. It showed that the replacement of cooling and heating water with nanofluids has the potential to conserve 1 trillion Btu of energy for U.S. industry. For power industry, 10 to 30 trillion Btu can be saved per year by using nanofluids in closed-loop cooling cycles. The associated emissions reductions would be approximately 5.6 million metric tons of carbon dioxide, 8600 metric tons of nitrogen oxides and 21000 metric tons of sulphur dioxides [1]. The performance of a flow-loop cooling apparatus filled with polyalphaolefin based exfoliated graphite nanoparticles fibres

were tested by Nelson et al. in 2009 [35]. It was observed that several properties of palyalphaolefin was enhanced after adding the nanoparticles: the specific heat is increased by 50%, the thermal diffusivity was increased by 4 times due to nanoparticles and the convective heat transfer was enhanced by around 10%.

- Nuclear reactors

The possible applications of nanofluids in nuclear reactors are pressurized water reactor primary coolant, standby safety systems, accelerators targets and plasma diverters [36]. A study showed that the use of nanofluids as a coolant can be used in emergency cooling systems, there they can cool down overheat surfaces more quickly leading to an improvement in power plant safety [37, 38]. Despite the concerns regarding the loss of nanoparticles through the boiling vapour and the safety measures for the disposal of nanofluids, nanofluids can be regard as a promising further application in nuclear reactors [1].

- Automotive applications

Engine oils, automatic transmission fluids, coolants, lubricants and other synthetic high-temperature heat transfer fluids found in conventional automotive systems have inherently poor heat transfer properties. Those fluids could benefit from the high thermal conductivity resulted from the addition of nanoparticles [39, 40].

- Electronic applications

The high thermal conductivity enables the nanofluids to cool the microchips very quickly [10]. Nanofluid was discovered to be effective in engineering the wettability of a surface and its surface tension, which can be used to control the microfluidic systems [41]. An experiment showed that droplets of nanofluid have changeable contact angles, which have the potential of allowing new methods for focusing lenses in miniature cameras and for cooling microcomputer chips [42].

1.3 State of art

Nanofluids have some potential features which make them special for various engineering applications [32]. A large number of research groups focused on the drastically enhanced thermal properties of nanofluids, especially the thermal conductivity and convective heat transfer [15-22]. The advantages of nanofluids for heat transfer properties are [23]:

- Better stability than the liquid/solid suspensions with millimetre or micrometre sized particles
- Rise in thermal conductivity beyond expectation and much higher than theoretical predictions
- Adjustable thermal conductivity by varying the particle concentration
- Reduced necessary pumping power of forced convection for circulating cooling liquid

Compared to the huge attention for thermal properties of nanofluids, only a small fraction of the research groups focused on the electrical properties of nanofluids. In 1998, Segal et al. measured increased AC impulse breakdown strength of a magnetite nanofluid based on transformer oil [24]. Based on this result, O’Sullivan et al. simulated the streamer propagation in mineral oil and in mineral oil based nanofluids. The simulation results indicated that conductive nanoparticles inhibit the streamer propagation, since conductive nanoparticles can act as electron traps in mineral oil [25, 26]. Thus, they suggested that nanofluids based on either conventional transformer oil or vegetable oil can be used to quickly replace mineral oil in power transformers. This hypothesis is not universally accepted due to the fact that it can’t explain the enhanced breakdown strength of nanofluids with insulating nanoparticles, such as titania and silica [27, 28] Until now, several publications have shown that magnetite, silica, alumina and titania nanoparticles can improve the breakdown strength of mineral oil [27-31]. For vegetable oil based nanofluids, Li et al. observed that surface modified magnetite nanofluids had a 20% higher AC breakdown voltage than the pure oil and also a higher positive and negative lightning impulse breakdown voltage [30].

1.4 Goal of this thesis

The main goals of this thesis are:

- To investigate how the dielectric strength and thermal conductivity of mineral oil can be optimized by adding a low concentration of nanoparticles.
- To understand the mechanisms by which the mentioned properties of mineral oil are changed.

The dielectric strength of nanofluids is investigated using AC breakdown strength and partial discharge measurements. The influence of filler material, filler concentration, and moisture content on the dielectric strength of the base fluids has been investigated. Recent studies showed that one possible mechanism behind the dielectric behaviour of nanofluids is that conductive nanoparticles can act as electron traps in the liquid and this can help to increase the dielectric strength of the base fluids [25, 26]. This mechanism is verified in our study by testing the breakdown strength of nanofluids containing nanoparticles with different conductivities. In our study, another possible mechanism behind the enhanced dielectric strength of nanofluids is proposed, which is the adsorption of moisture and acid on the surface of nanoparticles.

Regarding the thermal conductivity of nanofluids, we used the transient hot wire method. The effect of different fillers, agglomerations of nanoparticles and particle concentrations on the thermal conductivity of nanofluids is investigated. A model is built to analyse the effect of thermal barriers on the surface of nanoparticles due to phonon scattering.

We addressed more specifically the following research questions:

- How to achieve stable nanofluids on basis of mineral oil?
- What is the effect of different nanoparticles, particle concentration and moisture content on the AC breakdown strength of mineral oil?
- What is the effect of water adsorption on the surface of silica nanoparticles on the AC breakdown strength of mineral oil?
- What is the difference between the partial discharge behaviour of nanofluids containing insulating nanoparticles and nanofluids containing semiconducting nanoparticles?
- What is the influence of nanoparticles on the thermal conductivity of mineral oil? How to measure it?

To answer these questions, we used the following methods:

- Ultrasonic preparation method of mineral oil based nanofluids; examining the particle size distribution in the nanofluids with dynamic light scattering

- Assessment of the AC breakdown strength of nanofluids; analysis the breakdown voltage data with Weibull software
- Partial discharge measurements of nanofluids under DC voltage
- Thermal conductivity measurement of nanofluids using transient hot-wire method; analysis of the thermal conductivity of nanofluids with COMSOL software

1.5 Structure of the thesis

Chapter 2 describes the synthesis of nanofluids. This chapter starts with the interfacial mechanism in nanofluid – the nature of colloidal system. Then, the dispersion method, function of surfactants and requirement and precaution during the synthesis are introduced. In the second section, the host fluids, nanofillers and surfactant used in this study are described. In the third section, the synthesis procedure of nanofluids is described step by step. After this, the characterization examination and surface modification of nanoparticles and the particle size distribution in nanofluids are presented.

In chapter 3, the measurement results and data analysis of the AC breakdown strength of mineral oil and nanofluids are presented. The effect of different nanoparticles, particle concentration and moisture content on the AC breakdown strength of mineral oil is investigated. The AC breakdown results show that the effect of nanoparticles on the breakdown strength of mineral oil strongly depends on the moisture content. So a possible mechanism is proposed that the hydrophilic surface of silica can adsorb moisture which leads to less effect of moisture content on the breakdown strength of mineral oil. This hypothesis is verified with the comparison of the AC breakdown strength of untreated silica nanofluid and surface modified silica nanofluid.

Investigation on the partial discharge behaviour of nanofluids under DC voltage is described in chapter 4. Partial discharge measurements give a more detailed view on the pre-breakdown phenomenon of dielectric liquid by recording the discharge pulse shape, inception voltage, total discharge magnitude and single discharge pulse amplitude. The partial discharge measurement results of two types of nanofluids containing nanoparticles with different conductivities and mineral oil are compared and analysed. The investigation of the mechanism behind the partial discharge behaviour

of nanofluids is focusing on the adsorption of moisture and acid on the surface the nanoparticles.

Chapter 5 deals with the thermal conductivity of nanofluids. The experimental results of thermal conductivity of mineral oil and different types of nanofluids are investigated. The effect of different fillers, agglomerations of nanoparticles and concentrations on the thermal conductivity of nanofluids is investigated. A model is built to analyse the thermal resistance on the surface of nanoparticles.

Chapter 6 raises the issue about some practical aspects of nanofluids. The stability of nanofluids under the condition of forced convection is studied. The health and environmental aspects of nanofluids is discussed.

Chapter 7 provides the concluding remarks on this thesis. It also proposes the future research directions.

1.6 References

- [1] K.V. Wong and O. de Leon, "Applications of Nanofluids: Current and Future", *Advances in Mechanical Engineering*, Vol. 2010, pp. 1-11, 2010.
- [2] S.K. Das, S.U.S. Choi, W. Yu and T. Pradeep, *Nanofluids: Science and Technology*, Wiley-Interscience, 2008.
- [3] M. Chiesa and S.K. Das, "Experimental Investigation of the Dielectric and Cooling Performance of Colloidal Suspensions in Insulating Media", *Colloids and Surfaces A: Physicochemical and Engineering Aspects*, Vol. 335, pp. 88-97, 2009.
- [4] J.C. Maxwell, *A Treatise on Electricity and Magnetism*, 1st Edition, Clarendon Press, Oxford, U.K, 1873.
- [5] A.S. Ahuja, "Augmentation of Heat Transport if Laminar Flow of Polystyrene Suspensions. I. Experiments and Results", *Journal of Applied Physics*, Vol. 46, pp. 3408-3416, 1975.
- [6] R.L. Hamilton and O. K. Crosser, "Thermal Conductivity of Heterogeneous Two Component Systems", *I&EC Fundamentals*, Vol. 1, pp. 3125-3131, 1962.
- [7] R.R. Bonnecaze and J.F. Brady, "The Effect Conductivity of Random Suspensions of Spherical Particles", *Proceedings of Royal Society London*, Vol. A432, pp. 445-465, 1991.
- [8] C.K. Mangrulkar and V.M. Kriplani, "Nanofluid Heat Transfer-A Review", *International Journal of Engineering and Technology*, Vol. 3, pp. 136-142, 2013.
- [9] R.P. Feynman, "There's Plenty of Room at the Bottom", *American Physical Society Meeting*, Pasadena, CA, USA, 1959.
- [10] K.R. Sreelakshmy, S. Nair Aswathy, K.M. Vidhya, T.R. Saranya and C. Nair Sreeja, "An Overview of Recent Nanofluid Research", *International Research Journal of Pharmacy*, Vol. 4, pp. 239-243, 2014
- [11] S. Lee, S.U.S. Choi, S. Li and J.A. Eastman, "Measuring Thermal Conductivity of Fluids Containing Oxide Nanoparticles", *Transactions of ASME*, Vol. 121, pp. 280-288, 1999.
- [12] J.A. Eastman, S.U.S. Choi, S. Li, W. Yu and L.J. Thompson, "Anomalously Increased Effective Thermal Conductivities of Ethylene Glycol-based Nanofluids Containing Copper Nanoparticles," *Applied Physics Letters*, Vol. 78, pp. 718-720, 2001.
- [13] X. Wang, X. Xu, and S.U.S. Choi, "Thermal Conductivity of Nanoparticle-fluid Mixture", *Journal of Thermophysics and Heat Transfer*, Vol. 13, pp. 474-480, 1999.

- [14] J.A. Eastman, S.U.S. Choi, L.J. Thompson and S. Lee, "Enhanced Thermal Conductivity through the Development of Nanofluids", Materials Research Society Symposium Proceedings, pp. 3-11, 1996.
- [15] M. Liu, M. Lin, I. Huang and C. Wang, "Enhancement of Thermal Conductivity with CuO for Nanofluids", Chemical Engineering & Technology, Vol. 29, pp. 72-77, 2006.
- [16] Y. Hwang, H.S.K. Par, J.K. Lee and W.H. Jung, "Thermal Conductivity and Lubrication Characteristics of Nanofluids", Current Applied Physics, Vol. 6, pp.67-71, 2006.
- [17] W. Yu, H. Xie, L. Chen and Y. Li, "Investigation of Thermal Conductivity and Viscosity of Ethylene Glycol based ZnO Nanofluid", Thermochemica Acta, Vol. 491, pp. 92-96, 2009.
- [18] H.A. Mintsa, G. Roy, C.T. Nguyen and D. Doucet, "New Temperature Dependent Thermal Conductivity Data for Water-based Nanofluids", International Journal of Thermal Sciences, Vol. 48, pp. 363-371, 2009.
- [19] S. Zeinali Heris, M. Nasr Esfahany and S.G. Etamad, "Experimental Investigation of Convective Heat Transfer of Al₂O₃/water Nanofluid in Circular Tube", International Journal of Heat and Fluid Flow, Vol. 28, pp. 203-210, 2007.
- [20] D. Kim, Y. Kwon, Y. Cho, C. Li, S. Cheong and Y. Hwang, "Convective Heat Transfer Characteristics of Nanofluids under Laminar and Turbulent Flow Conditions", Current Applied Physics, Vol. 9, pp. 119-123, 2009.
- [21] J.Y. Jung, H.S. Oh and H.Y. Kwak, "Forced Convective Heat Transfer of Nanofluids in Microchannels", Internal Journal of Heat and Mass Transfer, Vol. 52, pp. 466-472, 2009.
- [22] K.V. Sharma, L.S. Sundar and P.K. Sarma, "Estimation of Heat Transfer Coefficient and Friction Factor in the Transition Flow with Low Volume Concentration of Al₂O₃ Nanofluid Flowing in a Circular Tube and with Twisted Tape Insert", International Communications in Heat and Mass Transfer, Vol. 36, pp. 503-507, 2009.
- [23] R. Saidur, K.Y. Leong and H.A. Mohammad, "A Review on Applications and Challenges of Nanofluids", Renewable and Sustainable Energy Reviews, Vol. 15, pp. 1646-1668, 2011.
- [24] V. Segal, A. Hjorsberg, A. Rabinovich, D. Natrass and K. Raj, "AC (60Hz) and Impulse Breakdown Strength of a Colloidal Fluid based on Transformer Oil and Magnetite Nanoparticles", Conference Record of the 1998 IEEE International Symposium on Electrical Insulation, USA, 1998.
- [25] F.M. O'Sullivan, "A Model for the Initiation and Propagation of Electrical Streamers in Transformer oil and Transformer Oil based nanofluids", PhD thesis, Massachusetts Institute of Technology, 2007.
- [26] J.G. Hwang, F.M. O'Sullivan, M. Zahn, O. Hjordstam, L.A.A. Petterson and R. Liu. "Modelling of Streamer Propagation in Transformer Oil based Nanofluids", Annual Report Conference on Electrical Insulation and Dielectric Phenomena, pp. 361-366, 2008.
- [27] Y. Du, Y. Lv, J. Zhou, X. Li and C. Li, "Breakdown Properties of Transformer Oil based TiO₂ Nanofluid," Annual Report Conference on Electrical Insulation and Dielectric Phenomena, pp.1-4, 2010.
- [28] Y. Lv, L. Wang, X. Li, Y. Du, J. Zhou and C. Li, "Experimental Investigation of Breakdown Strength of Mineral Oil based Nanofluids", IEEE international Conference on Dielectric Liquids, pp. 1-3, 2011.
- [29] D.E.A. Mansour, E.G. Atiya, R.M. Khattab and A.M. Azmy, "Effect of Titania Nanoparticles on the Dielectric Properties of Transformer Oil-Based Nanofluids," Annual Report Conference on Electrical Insulation and Dielectric Phenomena, pp. 295-298, 2012.
- [30] J. Li, Z. Zhang, P. Zou and S. Grzybowski, "Preparation of a Vegetable Oil-based Nanofluid and Investigation of its Breakdown Dielectric Properties," Electrical Insulation Magazine, Vol. 28, pp. 43-50, 2012.
- [31] B. Du, J. Li, B. Wang and Z. Zhang, "Preparation and Breakdown Strength of Fe₃O₄ Nanofluid based on Transformer Oil," International Conference on High Voltage Engineering and Application, pp. 311-313, 2012.
- [32] S. Mukherjee and S. Paria, "Preparation and Stability of Nanofluids-A Review", IOSR Journal of Mechanical and Civil Engineering, Vol. 9, pp. 63-69, 2013.
- [33] N. R. Ramakoteswaa, G. Leena and S.V. Ranganayakulu, "Synthesis, Applications and Challenges of Nanofluids – Review", IOSR International Conference on Advances in Engineering & Technology, pp. 21-28, 2014.

- [34] J. Routbort, et al., Argonne National Lab, Michellin North America, St. Gobain Corp., 2009, http://www1.eere.energy.gov/industry/nanomanufacturing/pdfs/nanofluids_industrial_cooling.pdf.
- [35] I.C. Nelson, D. Banerjee and R. Ponnappan, "Flow Loop Experiments Using Polyalphaolefin Nanofluids," *Journal of Thermophysics and Heat Transfer*, Vol. 23, pp. 752-761, 2009.
- [36] J. Buongiorno, L.-W. Hu, S.J. Kim, R. Hannink, B. Truong, and E. Forrest, "Nanofluids for Enhanced Economics and Safety of Nuclear Reactors: an Evaluation of the Potential Features Issues, and Research gaps", *Nuclear Technology*, Vol. 162, pp. 80-91, 2008.
- [37] S.J. Kim, I.C. Bang, J. Buongiorno and L.W. Hu, "Study of Pool Boiling and Critical Heat Flux Enhancement in Nanofluids," *Bulletin of the Polish Academy of Sciences—Technical Sciences*, Vol. 55, pp. 211-216, 2007.
- [38] S.J. Kim, I.C. Bang, J. Buongiorno, and L. W. Hu, "Surface Wettability Change during Pool Boiling of Nanofluids and its Effect on Critical Heat Flux," *International Journal of Heat and Mass Transfer*, Vol. 50, pp. 4105-4116, 2007.
- [39] W. Yu, D.M. France, J.L. Routbort, and S.U.S. Choi, "Review and Comparison of Nanofluid Thermal Conductivity and Heat Transfer Enhancements," *Heat Transfer Engineering*, Vol. 29, pp. 432-460, 2008.
- [40] M. Chopkar, P.K. Das, and I. Manna, "Synthesis and Characterization of Nanofluid for Advanced Heat Transfer Applications," *Scripta Materialia*, Vol. 55, pp. 549-552, 2006.
- [41] S. Vafaei, T. Borca-Tasciuc, M.Z. Podowski, A. Purkayastha, G. Ramanath and P.M. Ajayan, "Effect of Nanoparticles on Sessile Droplet Contact Angle," *Nanotechnology*, Vol. 17, pp. 2523-2527, 2006.
- [42] R.K. Dash, T. Borca-Tasciuc, A. Purkayastha and G. Ramanath, "Electrowetting on Dielectric-actuation of Microdroplets of Aqueous Bismuth Telluride Nanoparticle Suspensions", *Nanotechnology*, Vol. 18, pp. 1-6, 2007.

2 Synthesis of nanofluids

2.1 General issues of concern

Nanofluids are two-phase colloidal systems, which can be classified in terms of a dispersion phase and a dispersion medium [1]. In a nanofluid, the dispersion phase is solid and the dispersion medium is liquid. In a two-phase system, it is important to prevent sedimentation and obtain a stable nanofluid. The factors of high importance when considering a nanofluid synthetic approach are:

- Colloidal system status
- Dispersion of particles in the fluid
- Nanoparticle surface modification

2.1.1 Nature of colloidal state

The word “colloid” comes from the Greek word for glue, refers to protein or gelatin solutions. Colloidal dispersions can be formed either spontaneously or by mixing. The result of a spontaneous dispersion is called a lyophilic colloid, such as a protein solution. The dispersion which requires energy input is called lyophobic. In this study, the dispersion medium is mineral oil. The lyophilic dispersions require hydrophobic nanoparticles, while lyophobic dispersions contain hydrophilic nanoparticles [2].

For the stability of a colloidal system, there are two terms of importance: kinetic stability and thermodynamic stability. Lyophilic colloids are thermodynamically stable, which means the system achieves its chemical equilibrium or exists in its lowest energy state. The thermodynamic potential depends on the temperature and pressure. The majority of colloidal systems are lyophobic and they are kinetically stabilized. Typical examples of lyophobic colloids are the hydrosols and organosols of metals, oxides, and sulfides. In a colloid system, due to Brownian motion or external forces the particles collide. Brownian motion is a random movement of particles suspended in a fluid resulting from their collision with quick atoms or molecules in the liquid. Whether the particles will stick together or will separate depends on the interaction between the particles [3]. The two basic interactions between particles are due to the attractive Van der Waals potential and the repulsive electrostatic potential [1]. The

total interaction which is the sum of the attractive potential and the repulsive potential is shown in Fig.2.1.

The Van der Waals force is due to interaction between two dipoles, including the dipole-dipole force, dipole-induced dipole force and dispersion forces. The Van der Waals force is always attractive between particle surfaces of the same materials, and can be repulsive between dissimilar materials. The Van der Waals force is a weak force which becomes significant only at a very short distance. Brownian motion ensures the nanoparticles colliding with each other, and these results in the formation of agglomeration of particles due to the Van der Waals force [4]. The illustration of Van der Waals force between two atoms is shown in Fig.2.2.

The electrostatic force is due to the fact that particles often carry an electrical charge and therefore repel or attract each other. A repulsive electrostatic potential is the result of the interaction between the electrical double layers surrounding the particles. An electrical double layer consists of three parts: surface charge, stern layer and diffuse layer. Surface charge is due to adsorbed charged ions on the particle surface. The Stern layer consists of counterions which are attracted to the particle surface and closely attached to it by the electrostatic force. The diffuse layer is a film of the dispersion medium adjacent to the particles, which contains free ions with a higher concentration of counterions [1]. The schematic illustrating of the electrical double layer structure and electrical potential near the solid surface is shown in Fig.2.3.

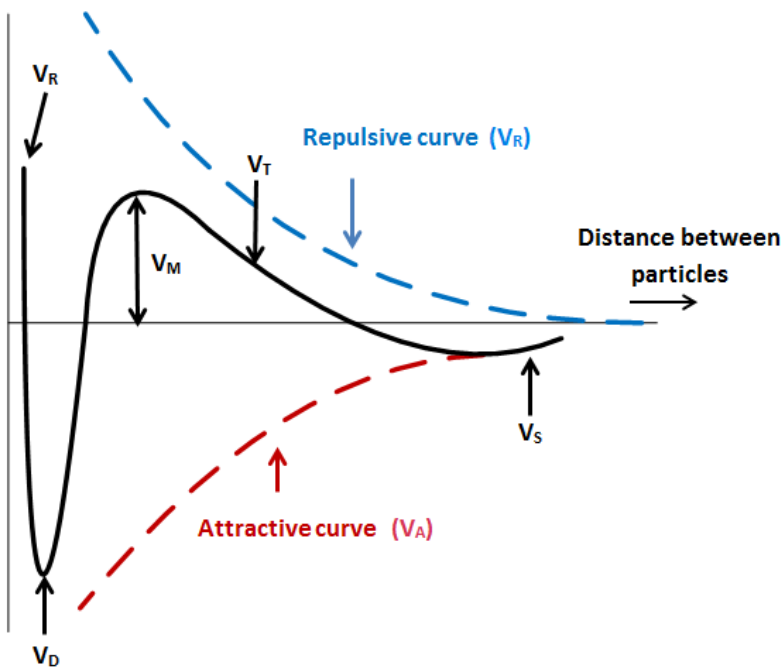


Figure 2.1 Plots of potential energy versus the distance between two particles. When the particles are far apart, both attractive Van der Waals (V_A) and repulsive electrostatic (V_R) potential reduce to zero. As two particles approach, they overcome the energy barrier V_M , leading to attractive aggregation V_D [5].

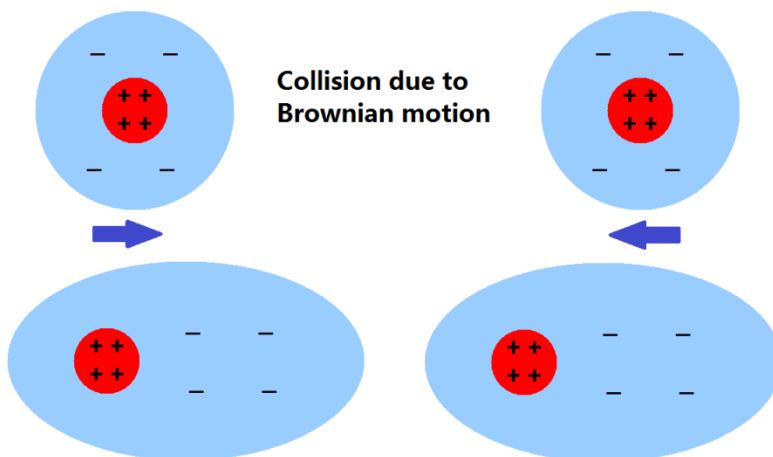


Figure 2.2 Diagram of Van der Waals force between two atoms.

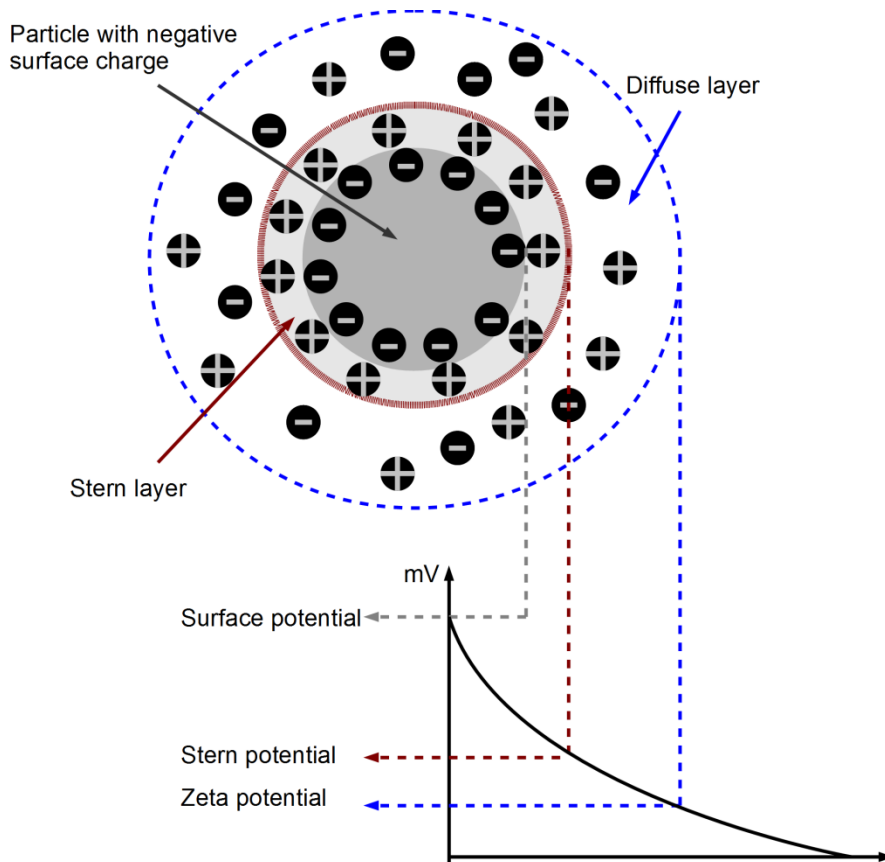


Figure 2.3 Schematic illustrating the electrical double layer structure and the electrical potential near the particle surface with Stern and diffuse layer indicated. Surface charge is assumed to be negative.

The sum of attractive and repulsive forces between particles determines whether there will be aggregation in a colloid system. If the attractive potential prevails over the repulsive potential, then there are clusters due to particles that aggregate. Hence, if the repulsive potential is larger than the attractive potential, aggregation can be prevented. The stability of a colloid system can be improved in two ways [6]:

- Increase the repulsive energy between particles by forming electric layers on the surface of nanoparticles to achieve electrostatic stabilization.
- Decrease the attractive energy between particles by increasing the distance between particles. This can be done by attaching macromolecules to the surface of particles such as polymers or

surfactants, which provide a steric barrier to prevent particles coming close to each other.

2.1.2 Dispersion method

Nanofluids are not simply binary solid-liquid mixtures; there are several essential requirements for creating a useful nanofluid. One of the most important requirements is the stability of nanofluids. The dispersion method is crucial for the final properties of nanofluids. Nanofluids tend to form agglomerations and clusters due to the sum of attractive and repulsive force [3]. In order to achieve a well dispersed nanofluid, two methods can be applied: the so-called two-step method and one-step method. The two-step method is the most widely used method for preparing nanofluids. Two-step means nanofillers and nanofluids are prepared in two different steps. The nanofillers are firstly produced as dry powders by chemical or physical methods. Then the nanopowders are dispersed into the dispersion medium with the help of a magnetic stirrer, ultrasonication, high-shear mixing or homogenizing. Due to the fact that nanopowder synthesis techniques are already scaled up to industry production levels, the two-step method is an economic method to synthesizing nanofluids. Due to the metastable status of nanofluids, nanoparticles tend to form aggregations and clusters. To enhance the stability of nanofluids, surfactants are often used [7].

The one-step physical vapour condensation method was developed by Eastman et al. [14]. The one-step method is designed to reduce agglomerations of nanoparticles. This method produces and disperses nanoparticles in the fluid simultaneously. This method avoids the procedures of drying, storage and transportation of nanopowder. Thus, the agglomerations of nanopowders are minimized. Due to the high cost of the one-step method, it cannot be used to synthesize nanofluids at a large scale. Another important disadvantage of the one-step method is that impurities can exist in the nanofluids due to the fact that residual reactants are left in the nanofluids due to incomplete reaction or stabilization.

2.1.3 Surface modification

Surface modification by adding surfactants or coupling agents is an easy and economical way to enhance the stability of nanofluids. Surface modification can improve the contact of the two materials [7]. In nanofluids, surfactants or coupling agents tend to locate at the interface of

the two phases, where it introduces a degree of contiguity between the nanoparticles and base fluids. In order to disperse inorganic particles into an organic fluid, hydrophobic groups and hydrocarbon chains should be formed on the surface of particles by various surface modification methods. Surfactants and silane coupling agents have been used to modify the surface of metal or metal oxide directly [9].

A. Surfactants

Surfactants are amphiphilic materials, which have the tendency to reside at the interface between polar and non-polar materials. This is due to their special structure: a surfactant consists of a hydrophilic polar head group and a hydrophobic tail group, usually a long hydrocarbon chain. Surfactants can be divided into four types according to the composition of the hydrophilic head group: non-ionic surfactants, anionic surfactants, cationic surfactants and zwitterionic surfactants. The schematic illustration of the four types of surfactant is shown in Fig.2.4.

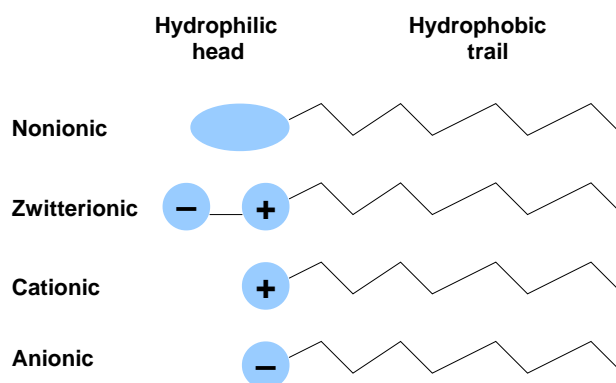


Figure 2.4 Schematic illustration of the four types of surfactants [10].

All non-ionic surfactants have HLB values, HLB stands for hydrophilic-lipophilic balance. The HLB value is a measure of the degree to which it is hydrophilic or lipophilic, determined by calculating values for different regions of a molecule. The hydrophilic group is usually a polyhydric alcohol or ethylene oxide. The lipophilic group is usually a fatty acid or a fatty alcohol. The HLB value can be calculated as [11]:

$$HLB = 20 * \frac{M_h}{M} \quad (2.1)$$

Where M_h is the molecular weight of the hydrophilic group and M is the molecular weight of the surfactant.

The HLB value can be used to predict the surfactant properties, Table 2.1 shows the HLB value and the surfactants applications.

Table 2.1 HLB values and applications of surfactants [12].

HLB value	Applications
1-3	Mixing unlike oils together
4-6	Water-in-oil emulsions
7-9	Wetting powers into oils
8-12	Oil-in-water emulsion
13-15	Formulating detergent solutions

Anionic surfactants have negative charged groups in its hydrophilic head group. Cationic surfactants are with positively charged head groups. Amphoteric surfactants contain pH depended zwitterionic head groups.

The selection of surfactants is a key issue to enhance the stability of a nanofluid. The basic principle is to choose the surfactant according to the dispersion medium. If the base fluid is oil, the surfactants should be oil soluble. In case of water based nanofluid, the surfactant should be water soluble. For non-ionic surfactant, the selection can be based on its HLB value. For ionic surfactants, the choice can be based on the zeta potential of the nanoparticles. A suitable surfactant can be effective to improve the stability of nanofluids. However, surfactants can also have negative effects on the nanofluid, such as an increase of the thermal resistance between nanoparticles and base fluid [7].

B. Silane coupling agent

A silane coupling agent has the ability to form a durable bond between organic and inorganic materials [13]. The general formula of a silane coupling agent is shown in Fig.2.5. In the formula, X is a hydrolysable group, typically an alkoxy, acyloxy, halogen or amine. Following hydrolysis, a reactive silanol group is formed, which can condense with other silanol groups. The R group is a non-hydrolysable organic radical that may possess a functionality that imparts desired characteristics.

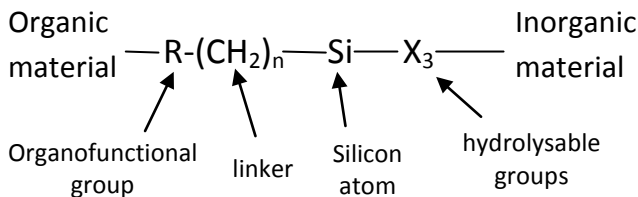


Figure 2.5 General formula of silane coupling agent.

When a silane coupling agent is used to modify the surface of inorganic nanoparticles, first hydrolysis of the hydrolysable groups occurs. Then condensation of oligomers follows. The oligomers bond with the OH group of the inorganic materials. Finally, during drying or curing, a covalent linkage is formed with the inorganic materials [15].

2.1.4 Requirements and precautions

During synthesis procedures, a nanopowder can be harmful for the human body if they accumulate in the organs, especially the lungs [16]. As soon as the nanopowders are dispersed into base fluid, they are not that dangerous due to the bonding between nanofillers and base fluids. Precautions should be taken to prevent direct contact between human body and nanopowders [17]. The use of a fume hood, protective working clothing, impervious gloves and safety glasses are necessary during synthesizing nanofluids, in order to prevent breathing, hand, body and eye contact with nanopowers. It is recommended to work and store at a small under-pressure area to prevent nanopowders moving to other work areas. Filters in the ventilation systems should be nanocertified to prevent outflow of nanoparticles to the environment [18, 19]. The health and environmental aspects of nanofluids will be discussed in chapter 6.

2.2 Materials used

2.2.1 Host material

The host fluid used in this study is Shell Diala S3ZXIG mineral oil. This type of oil is widely used in HV transformers and power supplies of X-ray systems. The principle chemical components of mineral oil are complex mixtures of hydrocarbons. For a further reduction of product size and product weight, it is essential to improve both the electrical and the thermal properties of mineral oil. Recently, great progress has been made in improving the electrical breakdown strength and heat transfer of mineral oils by introducing nanoparticles. It is important to investigate the

effect of nanoparticles on the electrical and thermal properties of Diala S3ZXIG mineral oil. The properties of Diala mineral oil are shown in Table 2.2, in which the thermal conductivity was measured in the lab and other properties were provided by the data sheet [20].

Table 2.2 Properties of Shell Diala S3ZXIG according to the data sheet.

Properties	Temperature [°C]	Method	Diala S3 ZXIG
Density [kg/m ³]	15	ISO 3675	890
	20		886
Kinetic viscosity [mm ² /s]	40	ISO 3104	8
	-30		1100
Breakdown voltage-untreated [kV]	ambient	IEC 60156	>30
Breakdown voltage-treated [kV]	ambient	IEC 60156	>70
Thermal conductivity [W/(m·K)]	20	Hot-wire	1.14
	40		1.09
	60		1.06
	80		1.04

2.2.2 Filler material

The list of nanoparticles used as dispersion phases is shown in Table 2.3. In this study, three types of nanoparticles were chosen: silica, fullerene and titania nanoparticles. The choice was made according to the dispersion stability, breakdown strength and thermal conductivity behaviour in mineral oil [21-24]. Fullerene nanoparticles are oil soluble, so they don't need surface modification to be dispersed in mineral oil. For other two types of nanoparticles, the nanofluids without surface modification have lower stability compared with fullerene nanofluid.

Table 2.3 List of filler materials, properties according to the respective data sheet [25-27].

Filler Material	silica	fullerene	titania
Chemical property	inorganic	organic	inorganic
Average size in nm	15	1	<25
Shape	spherical	buckyball	spherical
Thermal conductivity [W/(m·K)]	1.38	0.4	11.7
Relative permittivity	3.8 – 5.4	4.0 – 4.5	86 – 173
Electrical Conductivity [S/m]	10 ⁻¹⁶ to 10 ⁻¹²	9.86×10 ⁻⁴	10 ⁻¹⁴

2.2.3 Surfactant and coupling agent

In this study, surfactant sorbitan monooleate (span 80) and silane coupling agent Z6011 are used to modify the surface of nanoparticles. Span80 was used to prevent sedimentations in titania nanofluids; the surface modification was experimentally done in this study. Silane coupling agent Dow Corning Z6011 (Z6011) was used to modify the surface property of silica nanoparticles. The Z6011 modified silica nanoparticles were purchased from Nanoamour, USA.

Span80 has been proven to successfully prevent agglomeration in oil based nanofluids in several papers [28-30]. The reason for choosing span 80 is its HLB value of 4.3. From Table 2.1, it can be seen that surfactants with an HLB value from 4-9 can be used for wetting power into oils. The molecule structure of span80 is shown in Fig. 2.6. The hydroxyl group of span 80 molecules can build a connection with the hydroxyl groups on the surface of titania particles via a hydrogen bond. The chain group of span 80 molecules will turn to the mineral oil side. By this, span 80 can cover the surface of titania nanoparticles and agglomerations among nanoparticles are reduced.

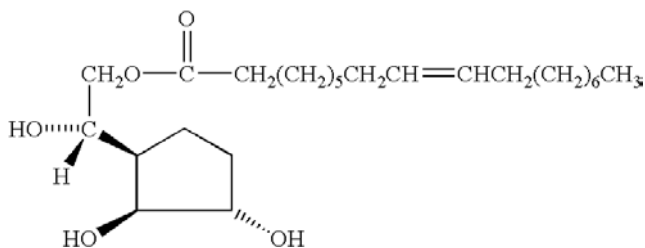


Figure 2.6 Molecule structure of Span80.

Silane coupling agent Z6011 was used to modify the surface property of silica nanoparticles from hydrophilic to hydrophobic. The purpose is to make silica nanoparticles soluble in mineral oil. Z6011 is a reactive chemical containing an aminopropyl organic group and a triethoxysilyl inorganic group. Z6011 silane can react with the surface of inorganic materials such as fiberglass and silica. The molecule structure of Z6011 is shown in Fig.2.7.

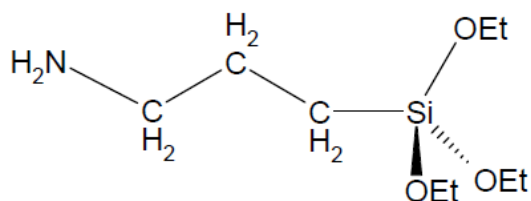


Figure 2.7 Molecule structure of Dow Corning Z6011, the abbreviated Et represents an ethyl group with the formula $-C_2H_5$.

2.3 Synthesis procedure

2.3.1 Nanoparticle characterization

The dry nanopowders were examined with transmission electron microscopy (TEM). TEM is a microscopy technique whereby a beam of electrons is transmitted through an electron transparent (around 100 to 150 nm thick) specimen, interacting with the specimen as it passes through. An image is formed from the interaction of the electrons transmitted through the specimen, and the imaging is magnified and focused onto an imaging device. Fig.2.8 shows the TEM result of titania nanoparticles. To examine the nanoparticles with TEM, the nanoparticles need to be dispersed in ethanol or water. It can be seen that the size of titania agglomerations is around 100 nm.

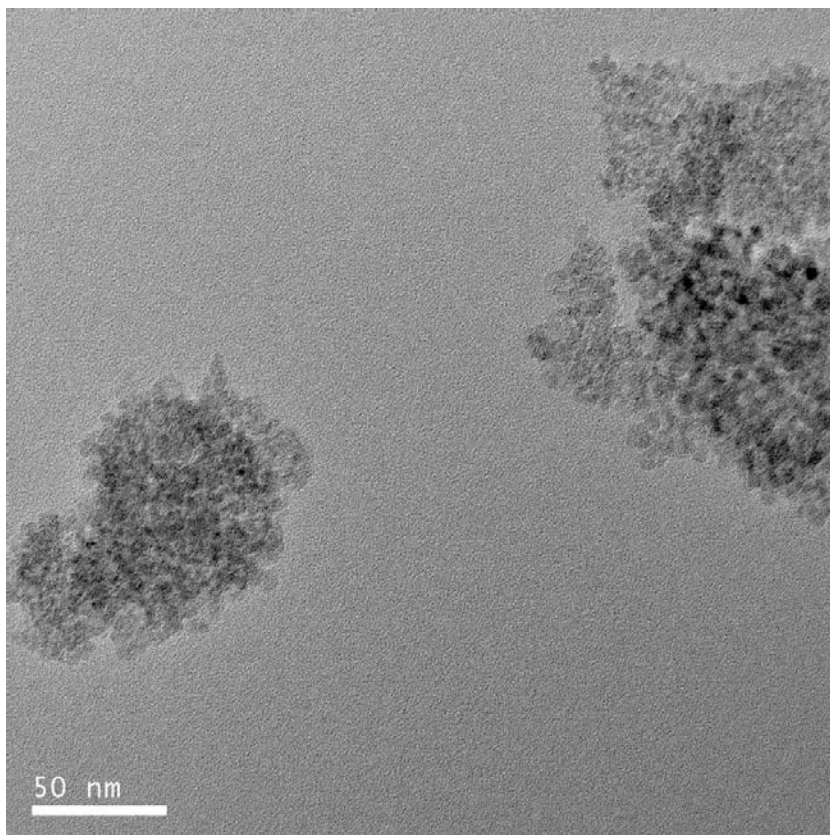


Figure 2.8 TEM results of titania nanoparticles in 50 nm scale.

Fig. 2.9 and 2.10 show the TEM results of untreated silica and Z6011 treated silica nanoparticles in 50 nm and 0.2 μm scales. It can be seen clearly that the surface modified silica nanoparticles are easier to be distinguished. The shape of the modified silica nanoparticles is round, and the size is roughly 20-30 nm. Pure silica nanoparticles have abrupt edges and are difficult to be distinguished. Hence, the surfactant helps to break the silica nanoparticle agglomerations and clusters.

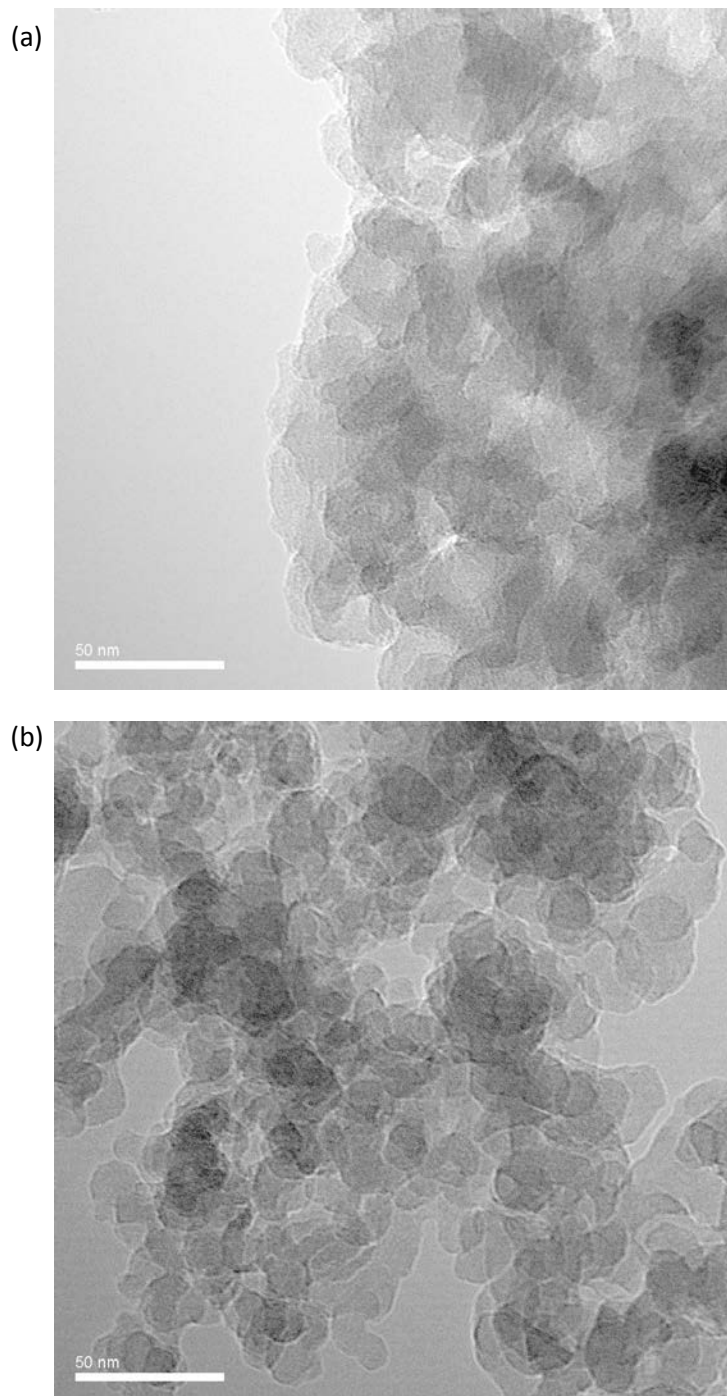


Figure 2.9 TEM results of (a) untreated silica and (b) Z6011 treated silica nanoparticles in 50 nm scale.

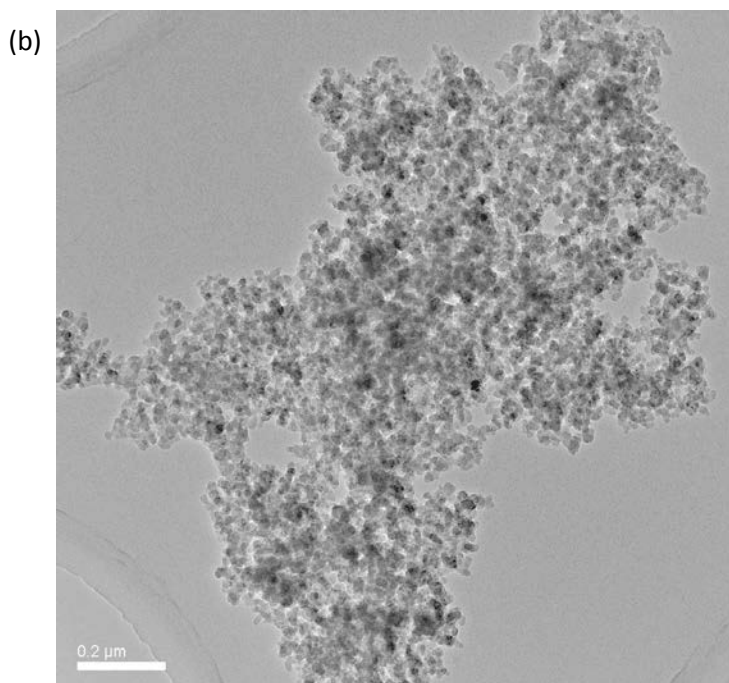
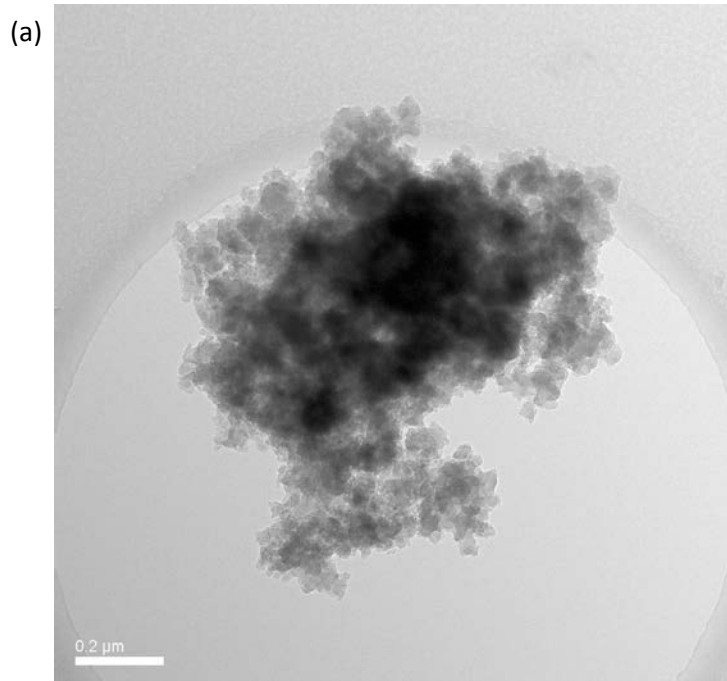


Figure 2.10 TEM results of (a) untreated silica and (b) Z6011 treated silica nanoparticles in 0.2 μm scale.

2.3.2 Nanoparticle surface modification

The titania nanoparticles were modified with surfactant span 80. Span80 connects to the surface of nanoparticles via hydrogen bond. So, to determine the amount of surfactant used in surface modification, it is necessary to check the mass of the hydroxyl groups on the surface of the nanoparticles. The surfactants have a hydrophilic head and hydrophobic tail, so if there are excess amounts of surfactants, they may start to build bonds between themselves. Fig. 2.11 shows the schematic illustration of the effect of excess surfactants. An appropriate amount of surfactant can modify the particle surface into hydrophilic property. But, if the surfactant amount is two times more than necessary, the hydrophobic tail of the surfactants may connect together via covalent bonds of hydrocarbons and the hydrophilic head of the surfactants will extend to the base fluids. The surface of the particle may appear hydrophilic again. Excess amount of surfactants may also lead to weak bonds between particles and base fluid.

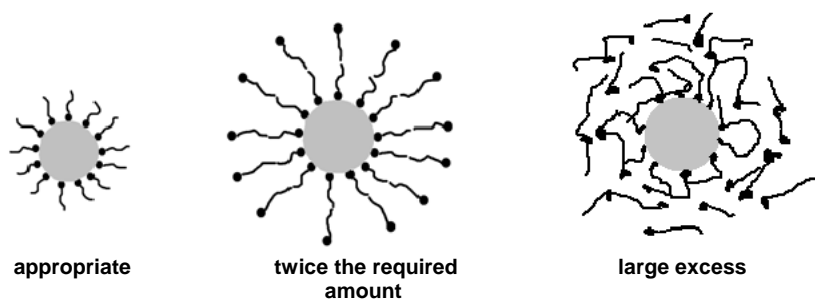


Figure 2.11 Schematic illustration of the effect of excess surfactants.

The surface properties of nanoparticles were examined with thermal gravimetric analysis (TGA). TGA is a method of thermal analysis in which changes in physical and chemical properties of materials are measured as a function of increasing temperature (with constant mass loss). TGA can provide information about physical phenomena, such as second-order phase transitions, including vaporization, sublimation, absorption and desorption. Likewise, TGA can provide information about chemical phenomena including chemisorptions, desolvation (especially dehydration), decomposition and solid-gas reaction (e.g. oxidation or reduction).

Fig.2.12 shows the TGA test result of titania nanoparticles. The covalent bond of hydroxyl group on the surface of titania nanoparticles are breaking

up at temperature ranges between 450 to 600 °C. Between 25 to 200 °C, the weight loss is due to the evaporation of physical or chemical bonded water. For titania nanoparticles, the OH group takes 0.282% of the total mass.

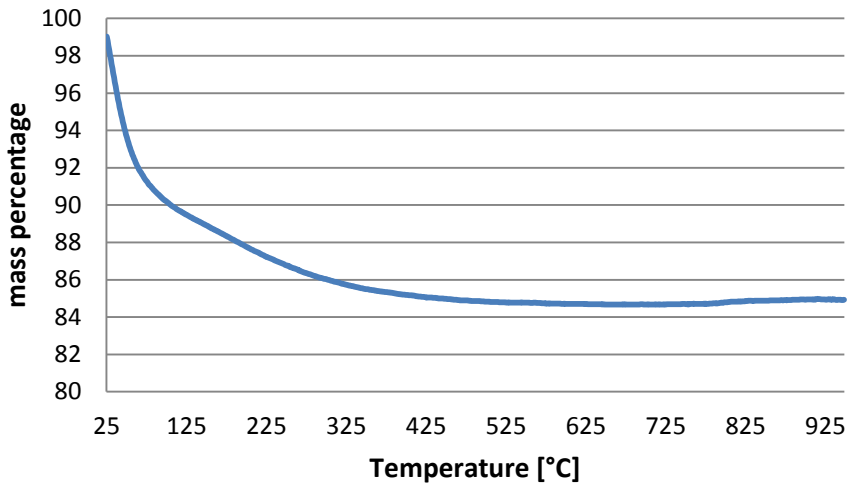


Figure 2.12 TGA results of titania nanoparticles.

According to the TGA result, for 1 g titania nanoparticles, there are 2.82 mg hydroxyl groups on the surface. For 1 mole OH group, the mass is 17 g. So the amount of OH groups on 1g titania nanoparticles are 1.659×10^{-4} moles. When the Span80 molecules cover the surface of the titania nanoparticles, at least one hydroxyl group on the head of span80 will build a hydrogen bond with the hydroxyl group on the surface of titania nanoparticles. For 1 g titania nanoparticles, the mass of span 80 that should be added can be calculated as:

$$\begin{aligned}
 m_{span80} &= v_{span80} * M_{span80} = v_{OH} * M_{span80} \\
 &= 1.659 \times 10^{-4} mol * \frac{428.62g}{mol} = 0.0711g
 \end{aligned}$$

Where m_{span80} is the mass of span80, M_{span80} is the molecular weight of span80, v_{OH} is the amount in moles of OH groups on the surface of 1 g titania nanoparticles, v_{span80} is the amount in moles of span80.

The calculated amount and practical amount of surfactant may be different because in a nanofluid, not all the molecules of the surfactant will

build bond with the nanoparticles. To determine the appropriate amount of surfactant, various amounts of surfactants were added to the nanofluids. The results of nanoparticle distribution of titania nanofluids show that for 1 g titania nanoparticles, span80 with around 0.7 g leads to the best stability, which will be shown in section 2.3.4.

2.3.3 Dispersion procedure

For the nanofluid preparation in this study, the two-step method is used. The nanofluid dispersion process is shown in Fig.2.13. All the preparations were done under a fume-hood. The preparation of nanofluids starts with the weighing of nanoparticles in a glove box. Then the nanoparticles are mixed with mineral oil and surfactant if necessary. After this, the mixture is stirred with a magnetic stir at ambient temperature for 30 minutes. Finally the mixture is put under ultrasonication for 2 hours to get a well dispersed nanofluid. The magnetic stirring helps to disperse the nanopowders evenly in the base fluid, but the energy is not enough to break any agglomeration of nanoparticles. So an ultrasonic bath is used to break the agglomerations of nanoparticles.

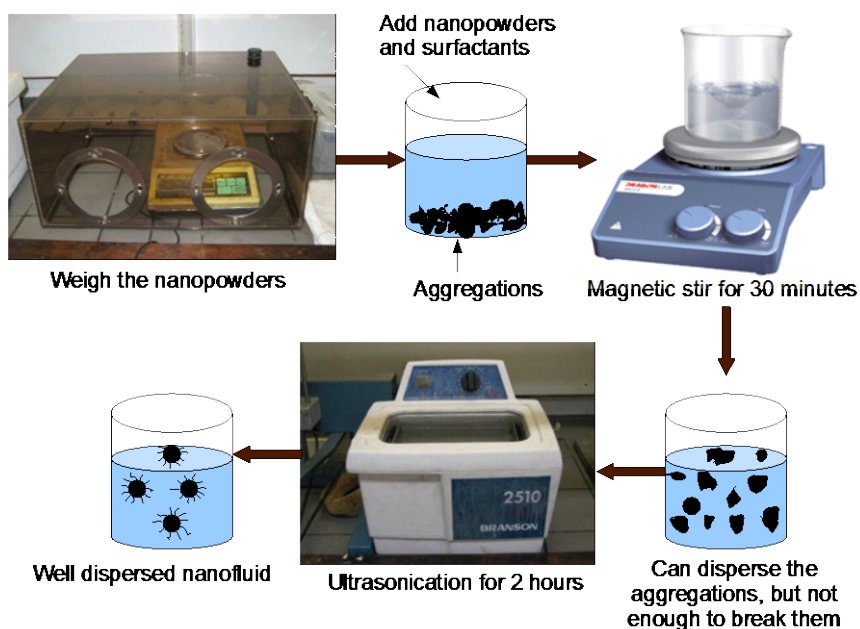


Figure 2.13 Schematic diagram of nanofluids preparation.

2.3.4 Particle distribution examination

The particle size distribution in nanofluids was measured with dynamic light scattering (DLS). DLS is a technique that can be used to determine the size distribution profile of small particles in a suspension. The laser light of the analyser is scattered by the particles of the suspension measured, the scattered light signal is then collected with an array of sensors. The particle size distribution is calculated from the received light signal. The measuring range of the instrument is 0.4 nm to 10 μm , The DLS technique is introduced in detail in appendix A.

Before examining the particle distribution in nanofluids, it is important to check the particle distribution in the pure mineral oil. Fig.2.14 shows the DLS result of mineral oil. The result indicated that there are particles with diameters of 58 to 147 nm existing in the oil. The peak value of the particle size is around 91 nm. So if a nanofluid shows a similar result as that of mineral oil, it means that the DLS result of the nanofluid may only show the existing particles in the oil.

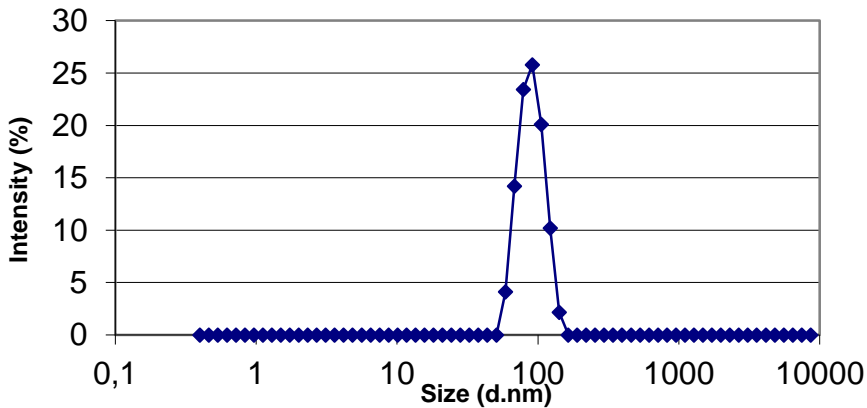


Figure 2.14 DLS result of mineral oil.

Fig.2.15 show the span80 modified titania nanofluids with 0.01% mass fraction. To determine the appropriate amount of the surfactant span80, various amounts of span80 were added to the nanofluids. When the mass ratio between the titania nanoparticles and span80 is 1 : 0.7, the particle size distribution of the nanofluid achieves the smallest. With a titania/span80 mass ratio of 0.07, which is the calculated amount introduced in section 2.32, the size distribution is the highest among the

three nanofluids. The reason can be that not all the molecules of the surfactant will build bond with the nanoparticles. The titania nanofluid with a large excess of span80 shows a larger particle size distribution than the nanofluid with appropriate amount of span80. This result proves the theory in section 2.3.2. The dry titania nanoparticles have a size smaller than 50 nm. So the appropriate mass ratio between titania nanoparticles and span80 prevent aggregation of titania nanoparticles is 1: 0.7.

The diameters of the particles in the nanofluid with titian/span80 mass ratio of 1/0.7 are 32 to 50 nm, with the peak value of 37 nm. The size of the particles in titania nanofluid has no overlap with that of mineral oil, which means the intensity of titania nanoparticles is much higher than that of the particles in mineral oil.

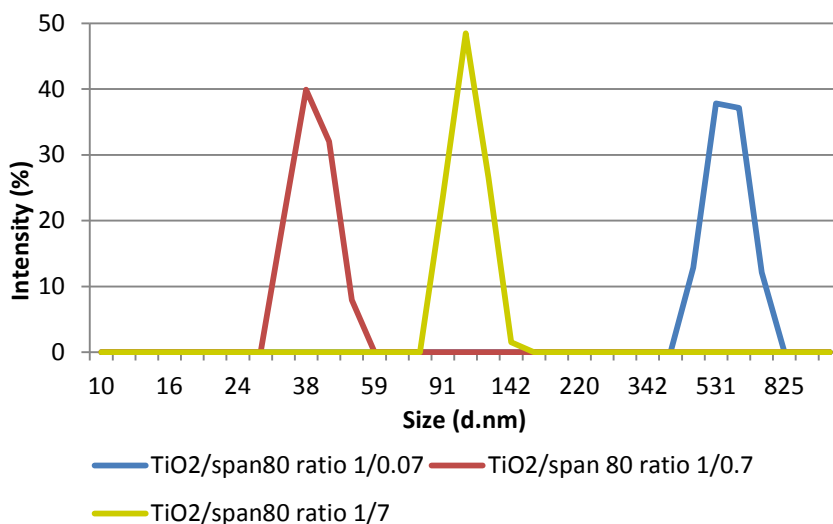


Figure 2.15 DLS result of 0.01% titania nanofluids with various amount of span80.

The DLS result of 0.01 wt.% untreated silica nanofluid is shown in Fig. 2.16. The particle sizes are 37 to 712 nm, with a peak value of 122 nm. The range of the size of particles has overlap with that of mineral oil. But since the peak values are different and the range of particle size is much larger than that of mineral oil. The DLS result shows the distribution of silica nano-clusters in the fluid. The dry silica nanoparticles have a size of 10 to 20 nm. So without surface modification, there are only silica-clusters in the nanofluid. However, various of surfactants were used to treat the

nanoparticles, but none of them can increase the stability of silica nanofluid. The DLS results of the silane coupling agent Z6011 modified silica nanofluids showed similar results as untreated silica nanofluids.

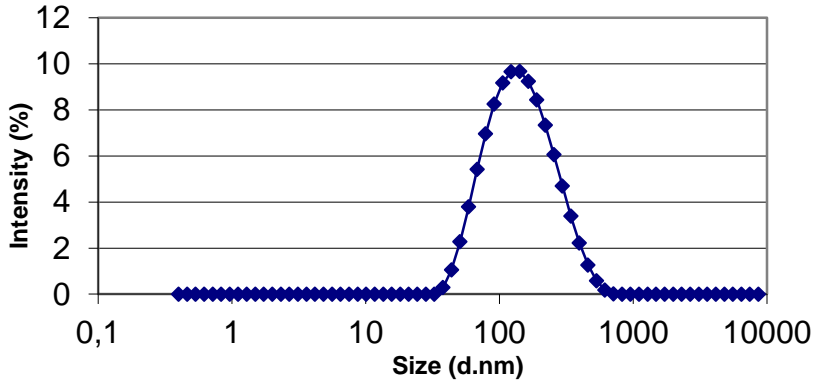


Figure 2.16 DLS result of 0.01 wt.% untreated silica nanofluids.

Fig. 2.17 shows the DLS result of 0.05 wt.% fullerene nanofluid. The diameters of the fullerene nanoparticles are 22 to 68 nm, with the peak value of 37 nm. The particle distribution is also different from that of mineral oil, so the DLS results indicate the fullerene particle distributions in the nanofluid.

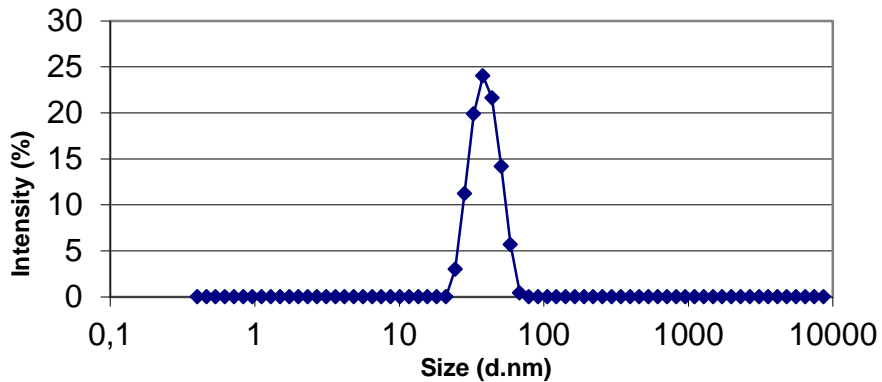


Figure 2.17 DLS result of 0.05 wt.% fullerene nanofluid.

It was observed that fullerene nanofluids show the best long-term stability. Three years after synthesis, there is no observed sedimentations and the particle size distribution doesn't increase. In silica nanofluids with 0.01% mass fraction, sedimentations were observed within one month. For 0.02%

silica nanofluids, visible sedimentations appeared within one week. In titania nanofluids, there are observed sedimentations after 24 hours after synthesis.

2.4 Summary

A nanofluid is a two-phase colloidal system, which contains a solid dispersion phase and a liquid dispersion medium. The three most important issues for nanofluids synthesis are: colloid system status, efficient dispersion method and nanoparticle surface modification. The majority of colloids are kinetic stable systems. In this system, the two basic interactions between particles are: attractive force due to Van de Waals interaction and repulsive force due to electrostatic interaction. There are two ways to prevent aggregation between particles: forming electric layers on the surface of particles to increase the repulsive energy and increasing the distance between particles to decrease the attractive energy.

In this study, the two-step method was used to prepare nanofluids. Due to the fact that nanopowder synthesis techniques are already scaled up to industry production levels, two-step method is an economic method and the most widely used way to synthesizing nanofluids. The nanoparticles were all purchased. Three types of nanoparticles were used in this study, silica, fullerene and titania. To achieve a stable dispersion, titania nanoparticles were modified with surfactant span80. To modify the surface of silica nanoparticles into hydrophobic, silane coupling agent Z6011 was used.

Before dispersion into the base fluid, the characterisation of nanoparticles can be examined with a TEM test. The test results show the shape and the size of the nanoparticles. The TGA test can further be used to investigate the surface properties of nanoparticles. Surface modification can be performed according to the TGA test results. The preparation of nanofluids starts with the weighing of nanoparticles in a glove box. Then the nanoparticles are mixed with mineral oil and surfactant if necessary. After this, the mixture is stirred with a magnetic stir at ambient temperature for 30 minutes. Finally the mixture is put under ultrasonication for 2 hours to get a well dispersed nanofluid. After dispersion, the particle distribution in the nanofluids can be examined with a DLS test.

2.5 References

- [1] S.K. Das, S.U.S. Choi, W. Yu and T. Pradeep, *Nanofluids: Science and Technology*, Wiley-Interscience, 2008.
- [2] P. Ghosh, *Colloid and Interface Science*, PHI Learning Pvt. Ltd, 2009.
- [3] G.J.M. Koper, *An Introduction to Interfacial Engineering*, VSSD, 2007.
- [4] G. Cao and Y. Wang, *Nanostructures and Nanomaterials*, Imperial College Press, 2004.
- [5] G.D. Parfitt, *Dispersion of Powders in Liquids with Special Reference to Pigments*, Applied Science, 1981.
- [6] S. Mukherjee and S. Paria, "Preparation and Stability of Nanofluids - A Review", *Journal of Mechanical and Civil Engineering*, Vol. 9, pp. 63-69, 2013.
- [7] W. Yu and H. Xie, "A Review on Nanofluids: Preparation, Stability Mechanisms and Applications", *Journal of Nanomaterials*, Vol. 2012, pp. 1-17, 2012.
- [8] J.A. Eastman, S.U.S. Choi, S. Li, W. Yu and L.J. Thompson, "Anomalous Increased Effective Thermal Conductivities of Ethylene Glycol-based Nanofluids Containing Copper Nanoparticles," *Applied Physics Letters*, Vol. 78, pp. 718–720, 2001.
- [9] L. Chen, H. Xie, Y. Li and W. Yu, "Nanofluids Containing Carbon Nanotubes Treated by Mechanochemical Reaction," *Thermochimica Acta*, Vol. 477, pp. 21–24, 2008.
- [10] I. Som, K. Bhatia and M. Yasir, "Status of Surfactants as Penetration Enhancers in Transdermal Drug Delivery", *Journal of Pharmacy & BioAllied Sciences*, Vol. 4, pp. 2-9, 2012.
- [11] W.C. Griffin, "Calculation of HLB Values of Non-Ionic Surfactants", *Journal of the Society of Cosmetic Chemists*, Vol. 5, pp. 249-256, 1954.
- [12] W.C. Griffin, "Classification of Surface-Active Agents by 'HLB'", *Journal of the Society of Cosmetic Chemists*, Vol. 1, pp. 311-326, 1949.
- [13] B. Arkeles, "Silane Coupling agents Connecting Across Boundaries V2.0", Gelest, Inc, 2006.
- [14] M. Hosokawa, K. Nogi, M. Naito and T. Yokoyama, *Nanoparticles Technology Handbook*, Elsevier B.V, 2008.
- [15] B. Arkles and G. Larson, *Silicon Compounds: Silanes and Silicones*, Gelest, 2008.
- [16] R. Kochetov, P.H.F. Morshuis, J.J. Smit, T. Andritsch and A. Krivda, "Precautionary Remarks Regarding Synthesis of Nanocomposites", *Electrical Insulation Conference*, pp. 51-54, 2014.
- [17] J. Nijenhuis and V.C.L. Butselaar-Orthlieb, *TNW nanosafety guidelines*, Delft University of Technology, 2008.
- [18] P. A. Schulte and F. Salamance-Buentello, "Ethical and Scientific Issues of Nanotechnology in Workplace", *Environmental Health Perspectives*, Vol. 115, pp. 5-12, 2007.
- [19] S. Agarwal, E. Tatli, N.N. Clark and R. Gupta, "Potential Health Effects of Manufactured Nanomaterials: Nanoparticle Emission Arising from Incineration of Polymer Nanocomposites", *International Symposium on Polymer Nanocomposites Science and Technology*, Boucherville, Canada, 2005.
- [20] Material Safety Data Sheet, Shell Diala S3 ZX-IG version 1.0, Effective Data 15. 09. 2010, Regulation 1907/2006/EC.
- [21] A. Roustaei, S. Saffarzadeh and M. Mohammadi, "An Evaluation of Modified Silica Nanoparticles' Efficiency in Enhancing Oil Recovery of Light and Intermediate Oil Reservoirs", *Egyptian Journal of Petroleum*, Vol. 22, pp. 427-433, 2013.
- [22] D. Shin and D. Banerjee, "Enhanced Specific Heat of Silica Nanofluid", *Journal of Heat Transfer*, Vol. 133, pp. 1-4, 2011.
- [23] Y. Du, Y. Lv, J. Zhou, X. Li and C. Li, "Breakdown Properties of Transformer Oil-based TiO₂ Nanofluid", *Conference on Electrical Insulation and Dielectric Phenomena*, pp. 1-4, 2010.
- [24] P. Aksamit, D. Zmarzly, T. Boczar and M. Szmechta, "Aging Properties of Fullerene Doped Transformer Oils", *Conference Record of the 2010 IEEE International Symposium on Electrical Insulation*, pp. 1-4, 2010.
- [25] Safety Data Sheet, Silicon Dioxide, according to Regulation (EC) No. 1907/2006, Version 4.2, Revision Data 08.04.2011.
- [26] <https://sesres.com/PhysicalProperties.asp>

- [27] Safety Data Sheet, Titanium (IV) oxide (anatase), according to Regulation (EC) No. 1907/2006, Version 4.0, Revision Data 27.03.2010.
- [28] A. Amraei, Z. Fakhroueian and A. Bahramian, "Influence of New SiO₂ Nanofluids on the Surface Wettability and Interfacial Tension Behaviour between Oil-water Interface in EOR Processes", Journal of Nano Research, Vol. 26, pp. 1-8, 2013.
- [29] Z. Han, "Nanofluids with Enhanced Thermal Transport Properties", PhD thesis, University of Maryland at College Park, 2008.
- [30] S.M. Sohel Murshed, S. Tan and N. Nguyen, "Temperature Dependence of Interfacial Properties and Viscosity of Nanofluids for Droplet-based Microfluidics", Journal of Physics D: Applied Physics, Vol. 41, pp. 1-5, 2008.

3 AC Breakdown Strength of Nanofluids

3.1 Introduction

In a transformer, the liquid dielectric is used both for providing insulation and cooling effects. The widespread use of dielectric liquids is due to their inherent properties. It appears as though they would be more useful as insulating materials than either solids or gasses. The reason for this is that liquid insulators have greater electrical breakdown strength and thermal conductivity than gaseous insulators. In addition, the flexibility to complex geometries and the self-healing ability of liquid dielectrics means that they are often more practical to use than solid insulators. Unfortunately, the failure of liquid insulation can cause catastrophic damage to the power equipment, pollution in the surrounding environment and financial loss. So for many years, scientists and engineers have been trying to understand the mechanism behind electrical breakdown and reduce the likelihood of breakdown in dielectric liquid, particularly in transformer oils [1, 2].

The AC breakdown test is generally used as one of the quality checks and acceptance tests for transformer liquids before filling new transformers or during routine maintenance [3]. So it is important to evaluate the ability of nanofluids to withstand the electrical stress. In this chapter, the AC breakdown voltage of three types of nanofluids were investigated and compared with that of mineral oil. The three types of nanofluids are unmodified silica, surface modified silica and fullerene nanofluids. The reasons for choosing these nanofluids are not only that a stable dispersion can be achieved in mineral oil, but also that they exhibit better breakdown strength compared to mineral oil. The influences of water content, filler type, filler concentration and viscosity on the breakdown behaviour of nanofluids are also investigated.

In this chapter, section 3.2 gives an overview of breakdown mechanism in insulating liquid. The factors which influence the AC breakdown strength of mineral oil are introduced in section 3.3. In section 3.4, the measurement setups for AC breakdown test and humidity test are described. Section 3.5 gives a short introduction of Weibull statistical technique, which is used in this study to analyse the data of breakdown voltages. From section 3.6 to section 3.8, the AC breakdown voltages of mineral oil, silica nanofluids and

fullerene nanofluids are compared and analysed. The mechanism behind the change of breakdown strength due to nanoparticles is discussed.

3.2 Breakdown mechanism in insulating liquid

For the breakdown mechanism in insulating liquid, there is not yet a single theory that can explain all the experimental results or that is generally accepted. The developments of the breakdown theories in liquid dielectrics can be divided into three steps: ionization theory, weakest-link theory and streamer theory [3].

The ionization theory was used to explain the breakdown mechanism in insulating liquids before the 1940s. The theory assumes that at high voltage field emission of electrons at the cathode is the dominant factor, and the accumulative collision ionization and avalanche formation leads to final breakdown in the liquid. However, Felici pointed out that collision ionization cannot exist for field strengths up to several MV/cm [4]. One reason is that electrons will be more inelastically scattered and will not gather enough kinetic energy for collision ionization. Another reason is that most electrons are attached to liquid molecules in the form of negative ions. So the number of free electrons is by far less than enough to trigger a breakdown.

Between the 1940s and 1980s, the weakest-link theory was put forward. Researchers realized that a single hypothesis or factor is not possible to explain the observed breakdown phenomena in insulating liquids. The weakest-link theory postulates that the breakdown in liquid dielectrics starts with a local instability caused by either defects in the bulk liquid or on the surface of the electrode. These defects in the liquid can be impurities, chemical additives, dissolved water or dissolved gasses. The geometry, material, surface condition of the electrodes and gap distance between them can also influence the breakdown of the insulating liquid. Other influential factors are: hydrostatic pressure, the wave shape of the applied voltage and so on [5].

With the development of high speed imaging techniques, the streamer theory was developed in the early 1970s. The theory is also called “bubble theory”, from the observation of gas bubbles in the liquid before breakdown occurs [1]. Microscopic techniques started to be applied for breakdown investigations after the 1980s. This enabled researchers to

investigate in detail the breakdown processes in liquid dielectrics. The study results showed that in a divergent field generated by a needle-plane electrode configuration, the first visible phenomenon was the generation of a gas bubble in front of the needle electrode [6, 7]. The gas bubble is generated due to the generation of joule heat by the motion of carriers in a high electrical field. The local heat causes a temperature rise and a low density region or gas bubble generation in the liquid. The breakdown mechanism in the gas bubble is considered similar to that in air. Depending on the electrical field the low density conductive structure will propagate in the liquid and a streamer forms. The term "streamer" in liquids has been borrowed from gas discharge mechanisms. Raether defined a streamer as follows: "A narrow, luminous channel formed within a gas in an electric field at pressures that are close to and above atmospheric in the stage preceding the electrical breakdown of the gas" [8]. When the streamer propagates through the liquid, electrical breakdown occurs. In recent years, the streamer theory has been widely accepted. The streamer theory states that the breakdown process in liquids is composed of streamer initiation, streamer propagation and final breakdown. Streamer initiation depends on various testing conditions such as voltage polarity, electrode geometry, hydrostatic pressure, liquid types and additives [9-12]. The streamer propagation is also controlled by various experimental conditions. However, gap distance between the two electrodes has a larger impact on the streamer propagation than electrode tip radius [13, 14]

3.3 AC Breakdown in mineral oil

The dielectric strength of mineral oil in industrial applications is in the range of 0.1 MV/cm to 1 MV/cm [15]. In this range the electrical field is high enough to allow streamer propagation until the final breakdown. Under AC voltage, the streamer propagation mode in mineral oil depends on the gap distance [3]. At small gap distance, a single streamer occurs in an AC cycle, which will propagate into the liquid gap until breakdown occurs [16]. At large gaps, an AC cycle does not give enough time for the streamer to cross through the gap, so "burst" breakdown happens [16]. The "burst" means the breakdown is preceded by a streamer "burst" produced at previous cycles, and only the last streamer leads to breakdown [3].

The factors which influence the breakdown in mineral oil under AC voltage are water content, particles and viscosity.

3.3.1 Influence of water content

It is generally accepted that water in microscopic amounts is the cause of more electrical breakdowns than any other impurities. Therefore oils are cleaned and dried prior to transformer filling [17]. Water may be introduced to the oil by leaking gaskets, ingress from the atmosphere and aging products [18]. There are three forms in which water may be present in oil. They are: dissolved water, chemically bound water and free water.

Water content in mineral oil represents the amount of dissolved water. The breakdown strength of mineral oil depends strongly on the water content. One possible explanation is that the boiling point of water is much lower than that of mineral oil [19]. So water vapour bubbles are more easily formed. This leads to streamer formation at lower voltage in the mineral oil with higher water content. Thus, breakdown occurs in the oil at lower voltage due to the presence of dissolved water [3]. The effect of water content on the breakdown strength of mineral oil is also related to the gap distance. A study showed that the effect of water is more significant at small gaps than at larger gaps [19].

Chemically bound water is characterized by a small number of dissolved water molecules tightly linked to the polar/charge groups of the particles/liquid molecules by hydrogen bonds [20]. Chemically bound water will be released into the oil when oxidized. Free water is water which has settled out of the oil in a separate layer when water content in the oil approaches the saturation level.

3.3.2 Influence of particles

Solid particles also have a considerable effect on the electrical breakdown process in mineral oil. The solid impurities in the oil can be the by-product of oil oxidation and aging, partial discharge and cellulose pieces released under influence of insulation aging. Also metallic particles can be left in the transformer tank during manufacturing process. Experts have identified that carbon, iron; copper and cellulose fibre are the main existence of particles in transformer oil [3].

Usually, those solid particles, especially metallic particles, have higher permittivity value than mineral oil. Therefore when the particles are polarized or charged, they are attracted to the area of high electrical fields. The particles may partly bridge the liquid gap in the form of chains, which would lead to a decreased breakdown voltage [21]. However, recent studies showed that carbon particles have a high affinity to dissolved water in the oil. Therefore, after carbon particles are added into the liquid, the water content reduced and breakdown strength increased [22, 23]. For cellulose particles, they have much smaller dielectric constant, so the motion of cellulose particles is much slower than that of metallic particles. But when cellulose particles are moisturized, their dielectric constant will increase from 3.2 to 70, and their mobility in the oil is enhanced remarkably [24].

3.3.3 Influence of viscosity

It has been proved that the breakdown strength of transformer oils is related to their viscosities [25]. Viscosity is a measure that describes the resistance of a fluid to flow. The viscosity depends strongly on the temperature and liquid type. It is concluded that a reduction of viscosity can decrease the breakdown voltages of mineral oils [26]. For mineral oil, the reduction of viscosity results in the increased mobility of charge carriers. This can lead to a higher possibility of partial discharges. Therefore a lower breakdown voltage of the oil occurs [27, 28]. For the additional particles in the oil, the mobility is higher at lower viscosity. Thus, at lower viscosity, the breakdown voltage of mineral oil would reduce even more in the presence of particles [28].

3.4 Experimental Test Set-up for Breakdown Measurements

The AC breakdown voltage was measured with an OPG-100A insulating oil tester according to the IEC60156 standard. The electrode configuration consisted of two spherical brass electrodes with 2.5 mm gap distance. The rate of voltage rise was 2 kV/s. Fig. 3.1 shows the OPG-100A insulating oil tester.



Figure 3.1 OPG-100A insulating oil tester.

The AC breakdown voltage of the liquids was measured at two moisture content levels, 25 ppm and 15 ppm. Due to the high ambient humidity, the moisture content in the oil and nanofluids at room temperature is around 25 ppm. After 24 hours drying in the vacuum oven at 60 °C, the moisture content in the oil and nanofluids is around 15 ppm. The moisture contents of mineral oil and nanofluid were measured with a Vaisala MM70 moisture and temperature meter, shown in Figure 3.2. This device obtains the moisture content value by measuring the water activity in the oil. Water activity is a measure of the energy status of the water in a system, which is defined as the vapour pressure of water in a substance divided by that of pure water at the same temperature. A detailed description of the Vaisala MM70 is provided in appendix B.

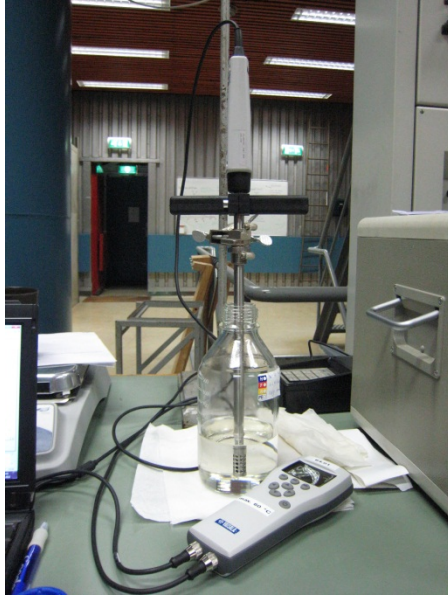


Figure 3.2 Vaisala MM70 moisture and temperature meter.

3.5 Statistical Analysis of Breakdown Data

The AC breakdown strength is measured to evaluate the quality of mineral oil. Usually the mean breakdown values are determined to estimate the quality of an insulating liquid. However, transformers are designed according to the minimum withstand voltage level of the insulation, rather than the mean withstand voltage. Weibull statistical techniques can be used to estimate the breakdown voltage obtained from AC breakdown data for lower failure probabilities [29].

For the data analysis of AC breakdown results of mineral oil and nanofluids, 2-parameter and 3-parameter Weibull plots are used. This is due to the fact that the Weibull distributions show better fits than other distributions, such as normal distribution and exponential distribution. For the 2-parameter Weibull analysis, the breakdown probabilities are calculated according to:

$$F(x) = 1 - \exp\{-(x/\eta)^\beta\}, \quad (3.1)$$

where $F(x)$ is the cumulative probability of breakdown; x is the AC breakdown voltage. β is the shape parameter, also known as the Weibull slope, which gives the Weibull distribution its flexibility. Depending on the value of shape parameter, a distribution is allowed to take on a variety of

shapes. η is the scale parameter, which determines the range of the distribution. The scale parameter is also known as the characteristic life or 63.2 percentile in 2-parameter Weibull plot. Besides the parameters shown in equation (3.1), there is a correlation coefficient ρ , which is a measure of how well the linear regression model fits the data.

For a 3-parameter Weibull plot, the breakdown probabilities are calculated by:

$$F(x) = 1 - \exp\left\{-\left[\frac{(x - \gamma)}{\eta}\right]^\beta\right\}, \quad (x \geq \gamma) \quad (3.2)$$

Where γ is the location parameter, which is used to define a failure-free zone. By definition, the probability of failure below the value γ is zero. The other parameters are the same as in equation (3.1) [29].

3.6 AC breakdown strength of silica nanofluids

3.6.1 Sample preparation

Silica nanofluids were prepared without surface modification according to the procedure described in chapter 2. Silica nanofluids with 0.01% and 0.02% were prepared. Ten samples were prepared for each type of fluid and for each sample, 12 tests were performed. After synthesis, the moisture contents of the fluids were around 25 ppm. To achieve 15 ppm moisture content, the samples were dried under vacuum in an oven for 24 hours at 70 °C

3.6.2 Measurement results

Fig.3.3 shows the 63.2% AC breakdown voltage (scale parameter) as well as the minimum and maximum values for mineral oil, 0.01% and 0.02% silica nanofluids. Table 3.1 shows the 62.3% AC breakdown voltage enhancement of mineral oil due to the presence of silica nanoparticles. It can be seen in Fig.3.3, that the AC breakdown voltage is increased with increasing nanoparticle concentration. As expected, the moisture content has a great effect on the AC breakdown voltage of all three fluids. The AC breakdown voltage decreases with an increase of the moisture content. At lower humidity level, the breakdown voltage enhancement is smaller than that at higher humidity level.

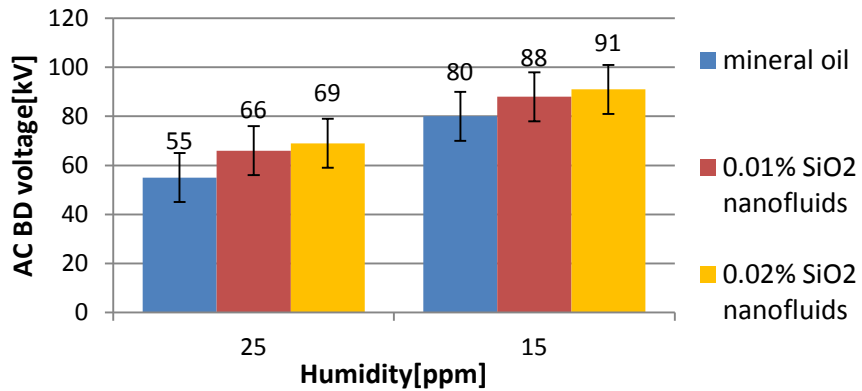


Figure 3.3 Comparison of 63.2% AC breakdown voltage of mineral oil and silica nanofluid, including the standard deviations.

Table 3.1 63.2% AC breakdown voltage enhancement in nanofluids.

Humidity mass fraction	0.01% silica NF	0.02% silica NF
25 ppm	20%	25%
15 ppm	10%	14%

3.6.3 Data analysis

3.6.3.1 AC breakdown results at 25 ppm humidity

Fig. 3.4 shows the 2-parameter Weibull analysis of the AC breakdown voltage of mineral oil, 0.01% and 0.02% silica nanofluids at 25 ppm humidity with 95% confidence bounds.

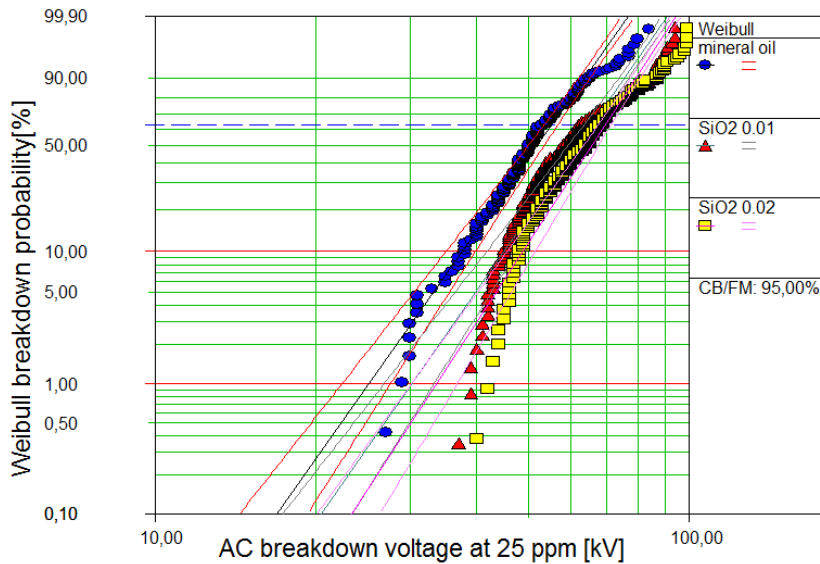


Figure 3.4 2-parameter Weibull plot of the AC breakdown voltage of mineral oil, 0.01% and 0.02% silica nanofluids at 25 ppm.

The parameters and correlation coefficient of the Weibull plot are shown in Table 3.2. Table 3.3 shows the AC breakdown voltage of mineral oil and 0.01% and 0.02% silica nanofluids at different breakdown probabilities. From Table 3.3, it can be seen that the 0.1% quantile of mineral oil is increased by 21% due to the presence of 0.01% silica nanoparticles and 38% due to the presence of 0.02% silica nanoparticles.

Table 3.2 Parameters and correlation coefficient of the 2-parameter Weibull plot in Fig.3.4.

parameters	Mineral oil	0.01% silica NF	0.02% silica NF
β	5.84	5.93	6.32
η	55.26	66.64	69.66
ρ	0.98	0.94	0.96

Table 3.3 AC breakdown at different breakdown probabilities of mineral oil and silica nanofluids at 25 ppm with 2-parameter Weibull calculation.

BD probabilities [%]	Mineral oil	0.01% silica NF		0.02% silica NF	
	BD[kV]	BD [kV]	change	BD [kV]	increase
0.1	17 (± 2)	21 (± 2)	+21%	23 (± 3)	+38%
1	25 (± 2)	30 (± 3)	+20%	34 (± 3)	+34%
5	33 (± 2)	40 (± 3)	+20%	44 (± 3)	+31%
63.2	55 (± 2)	66 (± 2)	+19%	69 (± 2)	+25%

In Table 3.2, the correlation coefficients ρ of the three fluids are 0.98, 0.94 and 0.96. To achieve a good fit, the value of ρ needs to be at 0.98 to 0.99. Hence the data doesn't fit well with the 2-parameter Weibull plot, which can be also seen in Fig. 3.4. Because of this, a 3-parameter Weibull plot is used to analyse the AC breakdown voltage of the three fluids. Fig. 3.5 shows the 3-parameter Weibull plot of the breakdown voltage of mineral oil, 0.01% and 0.02% silica nanofluids.

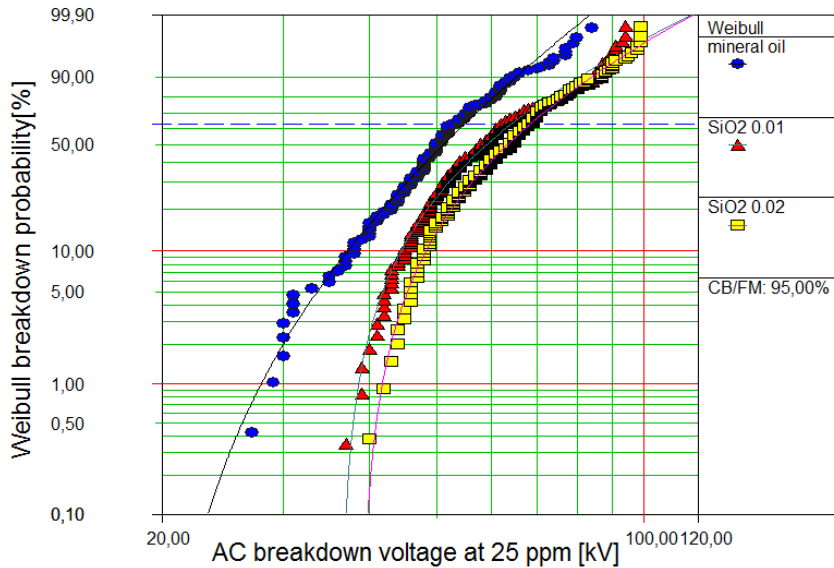


Figure 3.5 3-parameter Weibull plot of the AC breakdown voltage of mineral oil, 0.01% and 0.02% silica nanofluids at 25 ppm.

It can be seen from Fig.3.5 and from the values for ρ in Table 3.4, that the data fits the Weibull distribution well after adding the location parameter. Table 3.4 shows the parameters of the Weibull plot taken from Fig. 3.5. In Table 3.4, the correlation coefficient ρ of the three Weibull fits are 0.99, 0.99 and 1, which means the data fits the plot much better than the 2-parameter Weibull plot.

Table 3.5 compiles the values for the AC breakdown voltage at different breakdown probabilities of mineral oil, 0.01% silica nanofluid and 0.02% silica nanofluid at 25 ppm. In Table 3.6, the 0.1% quantile of mineral oil is increased by 61% in case of 0.01% silica nanoparticles and 74% in case of 0.02% silica nanoparticles. The AC breakdown voltage at 63.2% probability

of mineral oil is increased by 16% due to 0.01% silica nanoparticles and 25% because of 0.02% silica nanoparticles.

Table 3.4 Parameters and correlation coefficient of the 3-parameter Weibull plot in Fig. 3.5.

parameters	Mineral oil	0.01% Silica NF	0.02% Silica NF
β	3.32	1.81	1.96
η	36.21	27.97	29.57
ρ	0.99	0.99	1.00
γ	18.8	36.36	38.90

Table 3.5 AC breakdown at different breakdown probabilities of mineral oil and silica nanofluids at 25 ppm with 3-parameter Weibull calculation.

BD probabilities [%]	Mineral oil	0.01% Silica NF		0.02% Silica NF	
	BD[kV]	BD [kV]	change	BD [kV]	change
0.1	23 (± 1)	37 (± 1)	+61%	40 (± 1)	+74%
1	28 (± 2)	39 (± 1)	+39%	42 (± 1)	+50%
5	34 (± 2)	42 (± 1)	+24%	45 (± 1)	+32%
63.2	55 (± 1)	64 (± 2)	+16%	69 (± 2)	+25%

Silica nanoparticles can apparently increase the breakdown voltage of mineral oil significantly at lower probabilities (0.1% to 5%). The enhancement of the breakdown voltage at 0.1% probability is remarkable. The breakdown voltage of silica nanofluids increases with increasing particle concentration.

3.6.3.2 AC breakdown results at 15 ppm humidity

Fig. 3.6 shows the 2-parameter Weibull analysis of the breakdown voltage of mineral oil, 0.01% and 0.02% silica nanofluids at 15 ppm moisture content with 95% confidence bounds. The Weibull plots of the two nanofluids overlap, which indicates that no distinction can be made between the breakdown behaviour of these two nanofluids. Table 3.6 shows the parameters and correlation coefficient of the Weibull fit.

The correlation coefficient ρ of the Weibull fits of the three fluids are 0.99, 0.98 and 0.98 according to Table 3.6, so the data fits the plot well. Thus for the AC breakdown voltage of the three fluids at 15 ppm, the 2-parameter Weibull fit is sufficient for analysis.

The breakdown voltage of the three fluids at different breakdown probabilities is shown in Table 3.7. The breakdown voltage at 0.1%

probability is increased by 58% with 0.01% silica nanoparticles and by 57% with 0.02% silica nanoparticles. The breakdown voltage at 63.2% probability of mineral oil is increased by 10% for 0.01% silica nanofluids and 13% for 0.02% silica nanofluids, compared to mineral oil at the same moisture content level.

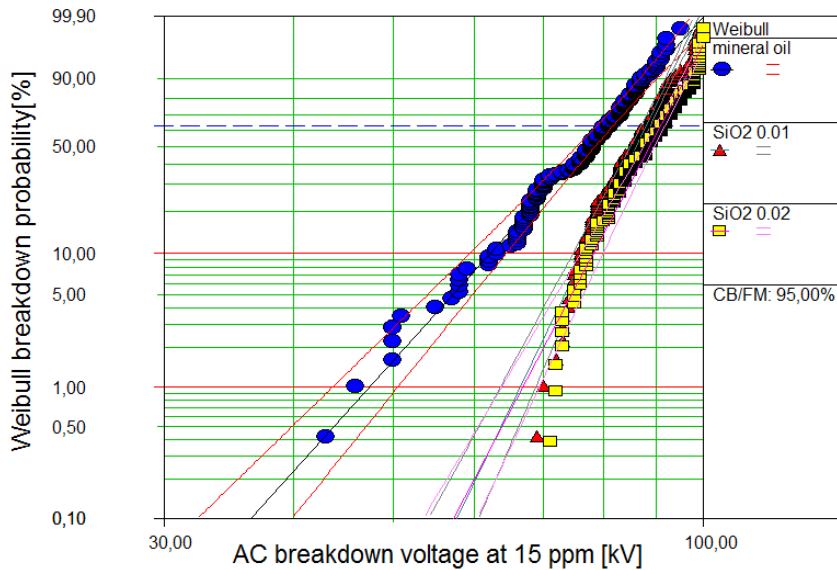


Figure 3.6 2-parameter Weibull analysis of the AC breakdown voltage of mineral oil, 0.01% and 0.02% silica nanofluids at 15 ppm.

Table 3.6 Parameters and correlation coefficient of the 2-parameter Weibull plot in Fig.3.6.

parameters	Mineral oil	0.01% Silica NF	0.02% Silica NF
β	8.72	16.31	14.93
η	80.34	88.01	90.87
ρ	0.99	0.98	0.98

Table 3.7 AC breakdown at different breakdown probabilities of mineral oil and silica nanofluids at 15 ppm with 2-parameter Weibull calculation.

BD Probabilities [%]	Mineral oil	0.01% Silica NF		0.02% Silica NF	
	BD[kV]	BD [kV]	change	BD [kV]	change
0.1	36 (± 4)	58 (± 1)	+58%	57 (± 3)	+57%
1	47 (± 3)	66 (± 2)	+40%	67 (± 2)	+41%
5	57 (± 3)	73 (± 2)	+29%	74 (± 2)	+30%
63.2	80 (± 1)	88 (± 2)	+10%	91 (± 1)	+13%

At 15 ppm moisture content level, silica nanoparticles show less of an effect on the breakdown voltage of mineral oil as they did at 25 ppm. Silica nanofluids still show up to 58% enhancement of the breakdown voltage at 0.1% probability. The particle concentration has less effect on the breakdown voltage of nanofluids than moisture content.

3.6.4 Viscosity

Viscosity is an important physical property of mineral oil. It has an influence on both the electrical properties and the heat transfer performance of mineral oil. To understand the effect of silica nanoparticles on mineral oil, viscosity is a key parameter to be studied. The viscosity was measured with a rheology meter between 10°C and 80°C. Fig. 3.7 shows the viscosity of mineral oil, 0.005% and 0.1% silica nanofluids. The reason for choosing the 0.005% and 0.1% mass fraction instead of 0.01% and 0.02% is that the effects of silica nanoparticles with 0.01% and 0.02% on the viscosity of mineral oil are nearly identical and almost the same as with 0.005%. By comparing the viscosity of 0.005% and 0.1% silica nanofluids, the effect of nanoparticle mass fraction on the viscosity can be estimated for a larger spectrum of fill grades.

The green line with the lowest viscosity represents Diala S3ZXIG mineral oil; the purple line represents the 0.005% silica nanofluid; the blue line exhibiting the highest viscosity represents the 0.1% silica nanofluid. The change of viscosity due to the silica nanoparticles is negligible, especially above 30°C. This indicates that the effect of silica nanoparticles on the breakdown voltage of mineral oil is probably not due to a change of viscosity.

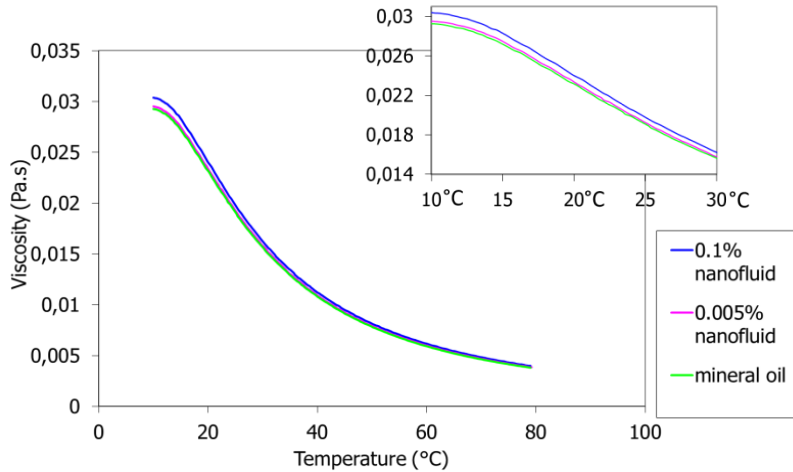


Figure 3.7 Viscosity of mineral oil, 0.005% and 0.1% silica nanofluids and detailed view for 10°C to 20°C.

3.6.5 Discussion

Several studies have proved that nanofluids can improve the breakdown strength of mineral oil, but the mechanism behind is still uncertain [30-33]. One possible explanation for the effect of conductive nanoparticles on the streamer propagation in mineral oil is that conductive nanoparticles act as electron traps [34]. Due to this, the streamer in the oil is decelerated. Since silica nanoparticles are not conductive, another mechanism must be involved in the observed breakdown strength enhancement.

The moisture content has a big influence on the AC breakdown strength of mineral oil. The breakdown voltage of both mineral oil and silica nanofluids increases with a decrease of the moisture content. However, silica nanofluids show a higher breakdown voltage than mineral oil, especially at the higher humidity level of 25 ppm. The surface of silica nanoparticles is hydrophilic, so it can bind water dispersed in the oil on the surfaces of the nanoparticles. This could be the reason why the moisture content could have less of an influence on the breakdown voltage of nanofluids than it has on mineral oil. At a humidity level of 15 ppm, it is possible that the water content is so small that with 0.01% silica nanoparticles, most of the water is adsorbed. Therefore, 0.01% and 0.02% silica nanofluids show similar AC breakdown results.

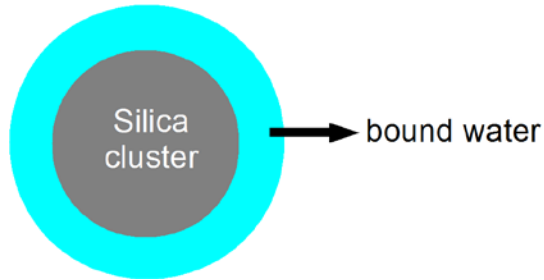


Figure 3.8 Illustration of an adsorbed water shell of silica nanoparticles.

This hypothesis can be verified by modifying the surface of silica nanoparticles with a surfactant that turns them hydrophobic. Then, the breakdown strength of the surface modified silica nanofluids can be measured and compared with that of non-modified silica nanofluids.

3.6.6 Summary

In this section, the AC breakdown voltage is investigated as a function of moisture content and viscosity of silica nanofluids. The mass fractions of the silica nanofluids are 0.01% and 0.02%. The results show that the addition of silica nanoparticles improves the AC breakdown voltage of mineral oil. The breakdown voltages of mineral oil and silica nanofluids strongly depend on the moisture content in the fluids.

At 25 ppm moisture content, silica nanoparticles increase the breakdown voltage of mineral oil, especially at lower probabilities. The enhancement of breakdown voltage at 0.1% failure probability is up to 74%. The breakdown voltage of silica nanofluids increases with particle concentration.

At 15 ppm moisture content, silica nanoparticles have less effect on the breakdown voltage of mineral oil, compared to 25 ppm humidity. However, there is still around 58% enhancement of the breakdown voltage at 0.1% failure probability. The particle concentration has less effect on the breakdown voltage of nanofluids than at 25 ppm moisture content.

Silica nanoparticles in mass concentrations between 0.005% and 0.1% have negligible effect on the viscosity of mineral oil. One possible reason for the enhanced breakdown strength of silica nanofluids is that the hydrophilic surface of silica nanoparticles adsorbs water in the oil. Due to this, the effect of moisture content on the breakdown strength of mineral

decreases. This assumption is verified by comparing the AC breakdown voltage of untreated silica nanofluid and surface modified silica nanofluid.

3.7 AC breakdown voltage of surface modified silica nanofluids

3.7.1 Sample preparation

The surface modified silica nanoparticles were purchased from Nanostructured & Materials Inc., USA. The average nanoparticle size is 20 to 30 nm according to the datasheet. The surfactant is silane coupling agent Z6011. The size of Z6011 modified silica nanoparticles is around 10 nm larger than the unmodified silica nanoparticles, which can be due to the coupling agent. The unmodified silica nanoparticles and the silica/Z6011 nanoparticles both have a spherical shape.

The thermogravimetric analysis (TGA) of pure silica and surface modified silica nanoparticles is shown in Fig. 3.9. Water is physical adsorbed at the surface of silica nanoparticles below 190°C. Hydroxyl groups bound through hydrogen bonds (vicinal silanols) are present on the silica surface up to 450°C, while germinal silanols are present up to 800°C, and free or isolated silanol groups up to a temperature of around 1000°C [35]. From the TGA curve, it can be seen that the mass loss of pure silica nanoparticles is much higher than that of silica/Z6011 at the temperature range 40 to 190°C. At this temperature range, the mass loss results mainly from the loss of water. This indicates that there is much more water adsorbed on the surface of the pure silica nanoparticles than on the hydrophobic Z6011 modified silica nanoparticles.

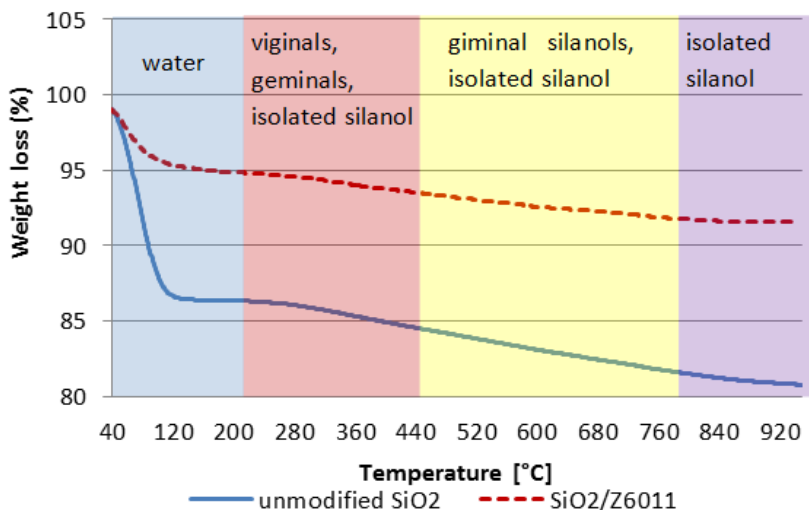


Figure 3.9 TGA results of unmodified silica and silica/Z6011 nanoparticles.

3.7.2 Measurement results

AC breakdown measurements were performed in the same way as for the unmodified silica nanofluids. Fig. 3.10 shows the 63.2% AC breakdown voltage as well as the minimum and maximum values of mineral oil, 0.01% unmodified silica and silica/Z6011 nanofluids (NF). Table 3.8 shows the enhancement of breakdown voltage of mineral oil due to silica nanoparticles. It can be seen that at 25 ppm humidity, the AC breakdown voltage of silica/Z6011 nanofluids is about half the value of pure silica nanofluids. 0.01% pure silica nanofluid increases the AC breakdown voltage of mineral oil by 20%. 0.01% silica/Z6011 nanofluid decreases the AC breakdown voltage of mineral oil by 37%. At 15 ppm humidity, the AC breakdown voltage of mineral oil and 0.01% silica/Z6011 is almost the same. Unmodified silica nanofluid with 0.01% concentration has a 12% higher AC breakdown voltage than the other two fluids.

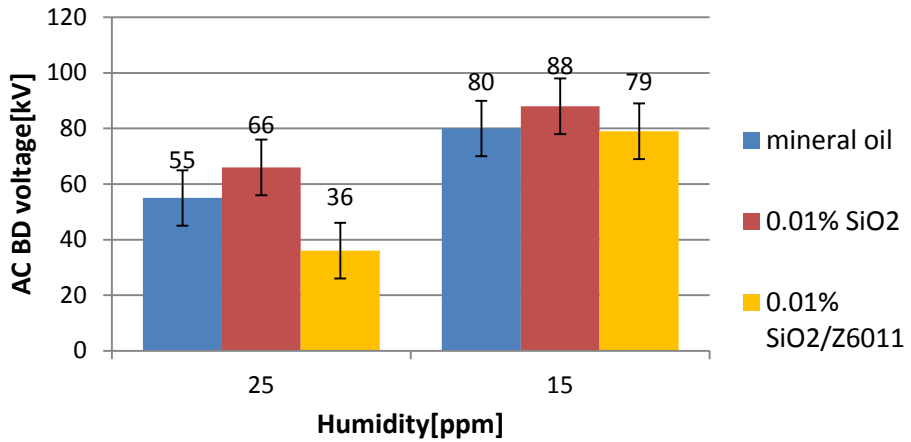


Figure 3.10 The 63.2% AC breakdown voltage of mineral oil, 0.01% silica nanofluid and 0.01% silica/Z6011 nanofluid.

Table 3.8 The 63.2% AC breakdown voltage change in nanofluids.

Humidity	Unmodified Silica	Silica/Z6011 NF
25 ppm	20%	-35%
15 ppm	10%	-1%

3.7.3 Data analysis

3.7.3.1 AC breakdown results at 25 ppm humidity

The measurement results of the AC breakdown voltage of silica/Z6011 nanofluid were also analysed with Weibull software and compared with that of untreated silica nanofluid and mineral oil. Fig. 3.11 shows the 2-parameter Weibull analysis of the AC breakdown voltage of mineral oil, 0.01% unmodified silica nanofluid and 0.01% silica/Z6011 nanofluid at 25 ppm humidity with 95% confidence bounds. The parameters and correlation coefficient of the Weibull plot are shown in Table 3.9. Table 3.10 shows the AC breakdown voltage at different breakdown probabilities.

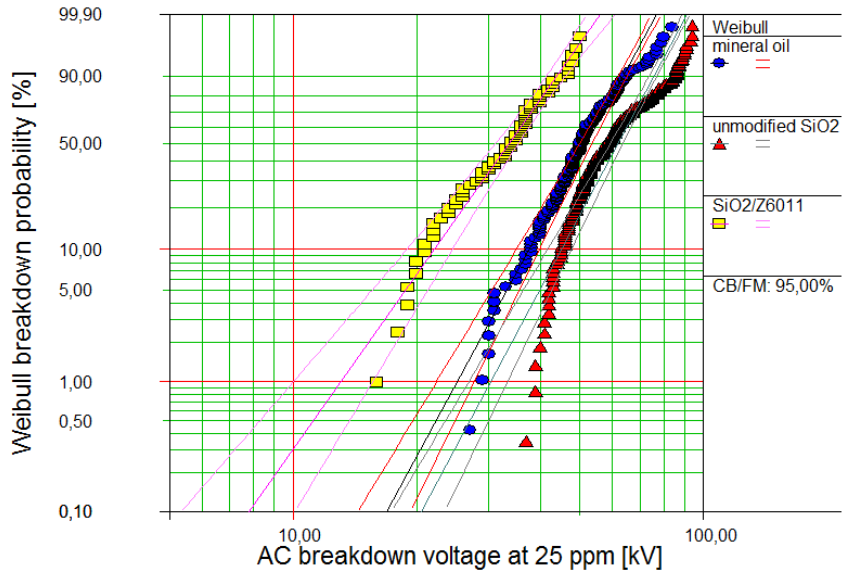


Figure 3.11 2-parameter Weibull plot of the AC breakdown voltage of mineral oil, 0.01% unmodified silica nanofluid and 0.01% silica/Z6011 nanofluid at 25ppm.

Table 3.9 Parameters and correlation coefficient of the 2-parameter Weibull plot in Fig. 3.11.

parameters	Mineral oil	unmodified Silica NF	Silica/Z6011 NF
β	5.84	5.93	4.49
η	55.26	66.64	36.32
ρ	0.98	0.94	0.98

Table 3.10 AC breakdown at different breakdown probabilities of mineral oil, 0.01% silica nanofluid and 0.01% silica/Z6011 nanofluid at 25 ppm.

BD probabilities [%]	Mineral oil	Unmodified silica		Silica/Z6011	
	BD[kV]	BD [kV]	change	BD [kV]	change
0.1	17 (± 2)	21 (± 2)	+21%	7 (± 3)	-59%
1	25 (± 2)	30 (± 3)	+20%	13 (± 3)	-48%
5	33 (± 2)	40 (± 3)	+20%	18 (± 2)	-45%
63.2	55 (± 2)	65 (± 2)	+19%	36 (± 2)	-34%

From Fig. 3.11 and Table 3.9, it can be seen after adding 0.01% unmodified silica nanoparticles into mineral oil, both scale and shape parameter increase. The shape parameter is the reciprocal of the slope of the fitted line. The scale parameter indicates the voltage at which 63.2% of the test specimens have failed. The confidence bounds of the silica/Z6011 AC breakdown voltage plot have no overlap with mineral oil. From Table 3.10,

it can be seen that unmodified silica nanoparticles can increase the AC breakdown voltage of mineral oil by 20% at all the failure properties. The Z6011 treated silica nanoparticles decrease the AC breakdown voltage of mineral oil. The correlation coefficient ρ values for the three fluids are 0.98, 0.94 and 0.98, which are a bit low for a good fitting. Hence, 3-parameter is used for a better fit.

Fig. 3.12 shows the 3-parameter Weibull analysis of the AC breakdown voltage of mineral oil, 0.01% unmodified silica nanofluid and 0.01% silica/Z6011 nanofluid at 25 ppm humidity. This figure only shows the location unadjusted plot for a better view. The parameters and correlation coefficient of the Weibull plot are shown in Table 3.11. The correlation coefficient values are all 0.99. Hence, the 3-parameter Weibull plot fits the data better than 2-parameter Weibull.

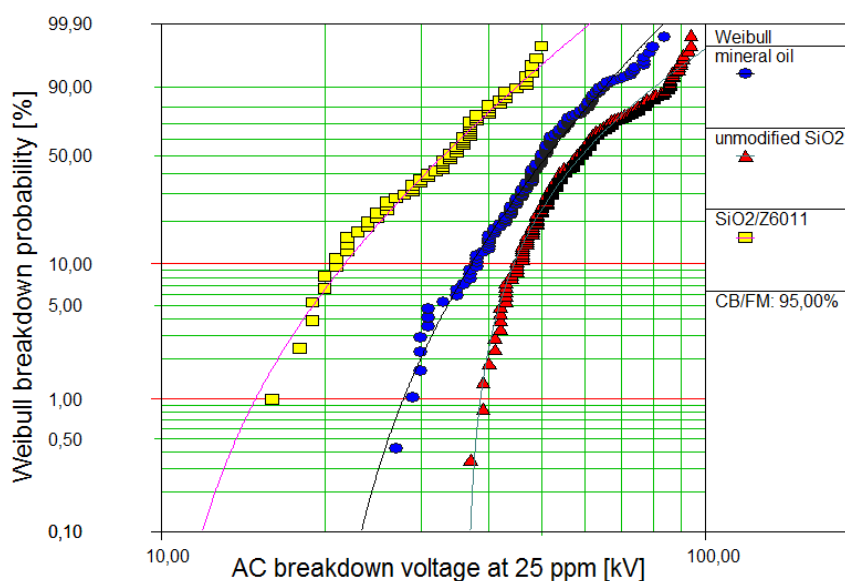


Figure 3.12 3-parameter Weibull plot of the AC breakdown voltage of mineral oil, 0.01% unmodified silica nanofluid and 0.01% silica/Z6011 nanofluid at 25ppm.

Table 3.11 Parameters and correlation coefficient of the 3-parameter Weibull plot in Fig. 3.12.

parameters	Mineral oil	Unmodified silica NF	Silica/Z6011 NF
β	3.32	1.81	2.9
η	36.21	27.97	26.73
ρ	0.99	0.99	0.99
γ	18.8	36.36	9.42

From Fig. 3.12, it can be seen that 0.01% nanofluid has a higher AC breakdown voltage than mineral oil. The Z6011 modified silica nanoparticles decrease the AC breakdown voltage of mineral oil. All the four Weibull plot parameters shown in Table 3.11 are the parameters after adjusting with location parameter. For the 3-parameter Weibull plot, the distribution assumes that no failure will take place under the value γ . The value γ is adjusted as a location parameter in the plot. For mineral oil, the distribution shows that the AC breakdown voltage won't be lower than 18.8 kV. By adding 0.01% unmodified silica nanoparticles, the threshold voltage is doubled. The threshold AC breakdown voltage is reduced by half due to 0.01% Z6011 treated silica nanoparticles.

Table 3.12 AC breakdown at different breakdown probabilities of mineral oil, 0.01% silica nanofluid and 0.01% silica/Z6011 nanofluid at 25ppm.

BD probabilities [%]	Mineral oil	Unmodified silica		Silica/Z6011	
	BD[kV]	BD [kV]	change	BD [kV]	change
0.1	23 (± 1)	37 (± 1)	+61%	12 (± 1)	-47%
1	28 (± 2)	39 (± 1)	+39%	15 (± 2)	-53%
5	34 (± 2)	42 (± 1)	+24%	19 (± 2)	-44%
63.2	55 (± 1)	64 (± 2)	+16%	36 (± 2)	-34%

Table 3.12 shows the AC breakdown voltage at different failure probabilities. The 0.01% silica nanoparticles increase the AC breakdown voltage of mineral oil remarkably, especially at low breakdown probabilities (0.1% to 1%). The surface treated silica nanoparticles have a negative effect on the AC breakdown behaviour of mineral oil.

3.7.3.2 AC Breakdown results at 15 ppm humidity

Fig. 3.13 shows the 2-parameter Weibull plot of mineral oil, 0.01% silica nanofluid and 0.01% silica/Z6011 nanofluid with 95% confidence bound. The parameters and correlation coefficient of the Weibull plot are shown in Table 3.13. Table 3.14 shows the AC breakdown voltage at different

breakdown probabilities. The correlation coefficient for the silica/Z6011 nanofluid is 0.97. However due to the fact that 3-parameter Weibull distribution adjusts a negative value to the plot of mineral oil, here, only 2-parameter Weibull plot is used to analyse the breakdown behaviour of the fluids.

At 15 ppm moisture content, silica nanoparticles show less of an effect on the breakdown voltage of mineral oil as they did at 25 ppm humidity. Unmodified silica nanofluids still show up to 58% enhancement of the breakdown voltage at 0.1% probability. The particle concentration has less effect on the breakdown voltage of nanofluids than humidity. The silica/Z6011 nanofluid has almost the same AC breakdown voltage as that of mineral oil.

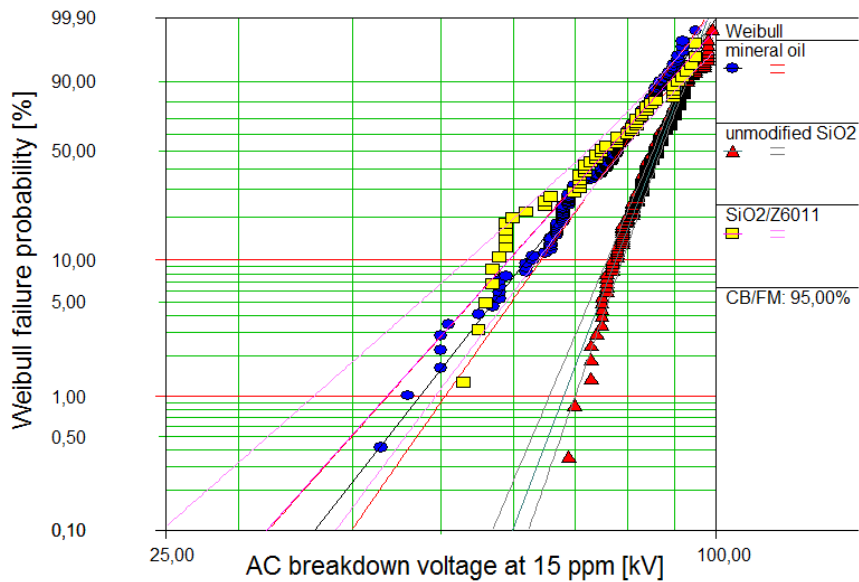


Figure 3.13 2-parameter Weibull analysis of the AC breakdown voltage of mineral oil, 0.01% silica nanofluid and silica/Z6011 nanofluid.

Table 3.13 Parameters and correlation coefficient of the 2-parameter Weibull plot in Fig. 3.13.

parameters	Mineral oil	Unmodified silica	Silica/Z6011
β	8.72	17.89	7.63
η	80.34	88.02	79.77
ρ	0.99	0.98	0.97

Table 3.14 AC breakdown at different breakdown probabilities of mineral oil and untreated silica and silica/Z6011 nanofluids at 15 ppm with 2-parameter Weibull calculation.

BD Probabilities [%]	Mineral oil	Unmodified silica		Silica/Z6011	
	BD[kV]	BD [kV]	change	BD [kV]	change
0.1	36 (± 4)	58 (± 1)	+58%	32 (± 6)	-11%
1	47 (± 3)	66 (± 2)	+40%	44 (± 6)	-6%
5	57 (± 3)	73 (± 2)	+29%	54 (± 5)	-5%
63.2	80 (± 1)	88 (± 2)	+10%	79 (± 3)	-1%

3.7.4 Discussion

The moisture content has a big influence on the AC breakdown voltage of mineral oil and silica nanofluids. The breakdown voltage of both mineral oil and silica nanofluids increases with a decrease of moisture content. Untreated silica nanoparticles have a hydrophilic surface, which can bind the water in the oil onto their surface. In practice, due to aging the humidity of the oil in transformer can increase from 5 ppm to 30 ppm. So silica nanoparticles can be useful in this situation.

According to the TGA tests, the water adsorbed on the surface of the unmodified silica nanoparticles takes around 11% of the total weight of the silica nanoparticles. The unit ppm represents parts per million in mass. The total mass of one silica nanofluid sample is 400 g. For 0.01% fill grade, the silica particle mass is around 0.04 g. Hence the weight of water adsorbed on the surface of unmodified silica nanoparticles is around 0.0044g. The silica nanofluid has more remarkable influence on the AC breakdown behaviour of mineral oil when the humidity is 25 ppm. At 25 ppm humidity, the water mass in the 400 g nanofluid is 0.01 g. Hence, up to 44% of the water in the silica nanofluid can be adsorbed on the surface of the silica nanoparticles. Bound water on the surface of nanoscale silica has less effect on the dielectric breakdown strength of the mineral oil than unbound water [36]. This is due to the fact that the mobility of water molecule of bound water is more limited than the unbound water. The silica nanoparticles thus may lead to a reduced effect of moisture content on the breakdown behaviour as long as the filler content is low enough to prevent percolation. For 0.02% silica nanofluid, the amount of bound water can be twice as much as that of 0.01% silica nanofluid. Hence, at 25

ppm moisture content, the breakdown strength of 0.02% silica nanofluid is higher than that of 0.01% silica nanofluid.

At 15 ppm water content, the water mass in the 400 g nanofluid is 0.006 g. Hence, due to 0.01% silica nanoparticles, up to 73% of water is adsorbed, which is most of the moisture content in the liquid. With 0.02% silica, the water adsorption can't be significantly increased further. Therefore particle concentration shows relatively less effect on the breakdown strength than that at higher moisture content.

Surface modified silica nanoparticles have a negative effect on the breakdown strength of mineral oil. One possible explanation is that without the affinity to water, silica nanoparticles show similar effect on the breakdown strength as additional particles. The particle effect was introduced in section 3.3.2. Due to the higher dielectric constant than mineral oil, charged particles are attracted to the high electrical field area. The particles may partly bridge the liquid gap in the form of chains, which would lead to a decreased breakdown voltage [21].

3.7.5 Summary

In this section, the AC breakdown voltage of mineral oil, 0.01% unmodified silica and silica/Z6011 nanofluid is compared. The goal is to verify the assumption that silica nanoparticles increase the AC breakdown strength of mineral oil due to the fact that their hydrophilic surface can bind the water in mineral oil.

The test results show that at 25 ppm moisture content, 0.01% unmodified silica nanofluid shows a 20% higher average AC breakdown voltage than mineral oil. While 0.01% silica/Z6011 nanofluid has a decreased AC breakdown voltage compared to mineral oil. At 0.1% failure probability, the change of AC breakdown strength of mineral oil due to 0.01% unmodified silica nanoparticles is 61% higher, while silica/Z6011 nanoparticles result in a 47% decrease.

At 15 ppm moisture content, the AC breakdown voltage of 0.01% silica/Z6011 nanofluid is almost the same as that of mineral oil, which is lower than that of unmodified silica nanofluid. The influence of silica nanoparticles on the breakdown strength of mineral oil at 15 ppm is less than that at 25 ppm. At 0.1% failure probability, the change of AC

breakdown strength of mineral oil is still 58% increased by introducing 0.01% unmodified silica nanoparticles, while we observe an 11% decrease when introducing nano-silica modified with Z6011.

The test results indicate that the hydrophilic silica nanoparticles have a positive effect on the AC breakdown strength of mineral oil. On the other hand, the hydrophobic silica/Z6011 reduces the AC breakdown voltage of the nanofluid. Since the surface modification is the key difference of the samples investigated, the hydrophilic surface is most likely the reason for the changes in AC breakdown strength of the silica nanofluids.

3.8 AC breakdown strength of fullerene nanofluids

3.8.1 Sample preparation

A C60 fullerene is a pure carbon molecule composed of 60 atoms of carbon. Fullerenes are spherical and also called buckyballs, since they resemble geodesic domes by Richard Buckminster Fuller [37]. The fullerenes were purchase from SES Research, USA.

There are two reasons for choosing fullerene nanoparticles:

- Fullerene has relative high electrical conductivity ($9.86 \times 10^{-4} \text{S/m}$), hence the polarization/ relaxation time constant is short relative to the streamer propagation in mineral oil. The theory will be discussed in section 3.8.5.
- Fullerene is oil soluble, which helps to achieve well-dispersed and stable mineral oil based nanofluids.

The host fluid is Diala S3ZXIG mineral oil. The particle concentrations are 0.05% and 0.1%. The synthesis procedure is the same as described in chapter 2. No surfactants were used for the synthesis. Fig. 3.14 shows the molecular structure of fullerene C60 and 0.05% fullerene nanofluid.



Fig.3.14 molecular structure of fullerene C60, 0.05% fullerene nanofluids.

As shown in chapter 2, the average particle size in the fullerene nanofluid is 37 nm, while the molecular size of fullerene C60 is 1 nm. So there are fullerene clusters in the nanofluids. The moisture content of the fullerene nanofluids after synthesis is around 35-40 ppm, which is higher than that of mineral oil (around 25ppm). To decrease the moisture content to the level of oil (around 25ppm), fullerene nanofluids were dried for 24 hours in a vacuum oven at 70°C. The reason for the high humidity of fullerene nanofluids could be that water was bounded in the aggregations of fullerene C60 molecules. After ultrasonication, the aggregations were broken and water was released into the oil. The lowest moisture content can be achieved for fullerene nanofluids is around 25 ppm.

For each type of fluid, 5 samples were prepared, and for each sample, 18 measurements were performed. Before breakdown test.

3.8.2 Measurement results

Fig. 3.15 shows the mean AC breakdown voltage as well as the minimum and maximum values of mineral oil, 0.05% and 0.1% fullerene nanofluids. The enhancement of the AC breakdown voltage of mineral oil is 19% due to 0.05% fullerene nanoparticles and 34% due to 0.1% fullerene nanoparticles.

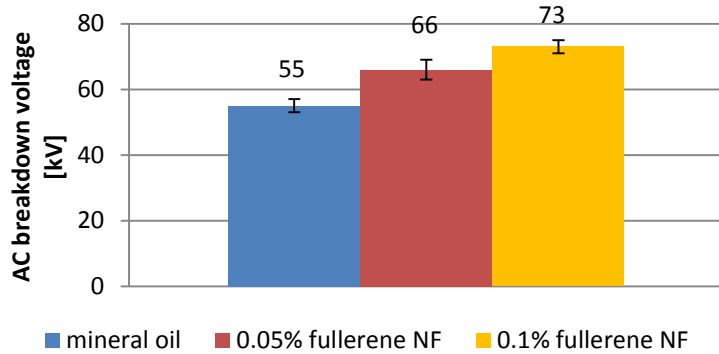


Figure 3.15 Comparison of mean AC breakdown voltage of mineral oil, 0.05% and 0.1% fullerene nanofluids.

3.8.3 Data analysis

All the AC breakdown results data were analysed with Weibull software. Fig. 3.16 shows the 2-parameter Weibull plot of the AC breakdown voltage of mineral oil, 0.05% and 0.1% fullerene nanofluids. The confidence bounds are 95%. The parameters and correlation coefficient of Weibull plot are shown in Table 3.15. Table 3.16 shows the AC breakdown voltage of mineral oil, 0.05% and 0.1% fullerene nanofluids at different breakdown probabilities.

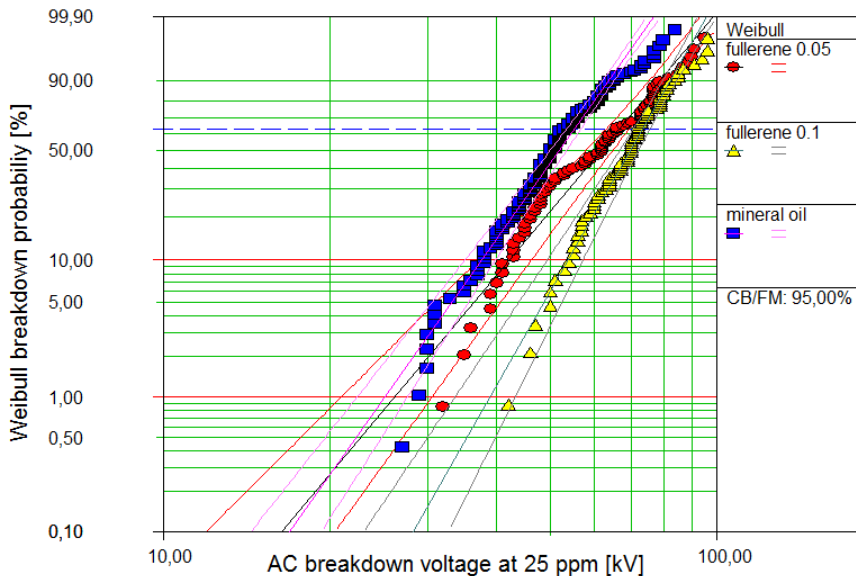


Figure 3.16 2-parameter Weibull plot of the AC breakdown voltage of mineral oil, 0.05% and 0.1% fullerene nanofluids.

From Fig. 3.16, it can be seen that the confidence bounds of the AC breakdown voltage of 0.05% fullerene nanofluid and mineral oil overlap at low failure probabilities. Hence there is no significant enhancement of breakdown voltage due to 0.05% fullerene nanoparticles. The 0.1% fullerene nanofluid on the other hand shows a significant increase of breakdown voltage compared to mineral oil.

Table 3.15 Parameters and correlation coefficient of the 2-parameter Weibull plot in Fig. 3.16.

parameters	Mineral oil	0.05% NF	0.1% NF
β	5.84	4.92	7.24
η	55.26	66.48	73.37
ρ	0.98	0.98	0.99

Table 3.16 AC breakdown at different breakdown probabilities of mineral oil and fullerene nanofluids at 25 ppm with 2-parameter Weibull calculation.

BD Probabilities [%]	Mineral oil	0.05% NF		0.1% NF	
	BD[kV]	BD [kV]	change	BD [kV]	change
0.1	17 (± 2)	16 (± 3)	-5%	28 (± 4)	+65%
1	25 (± 2)	26 (± 4)	+4%	39 (± 4)	+56%
5	33 (± 2)	36 (± 4)	+9%	48 (± 4)	+47%
63.2	55 (± 2)	66 (± 3)	+20%	73 (± 2)	+33%

From Table 3.16, it can be seen that the 0.1% quantile of mineral oil is decreased by 5% due to the presence of 0.5% fullerene. However, compared to the 63.2% quantile of mineral oil the nanofluid breakdown value is increased by 20%. By adding 0.1% fullerene nanoparticles, the breakdown strength of the 0.1% quantile is increased by 67% compared to pure mineral oil and that of the 63.2% quantile is increased by 33%. From Fig. 3.16, it can be seen that at lower breakdown probabilities (0.1% to 5%), the breakdown data of the three fluids is almost outside the confidence bounds. So the values given by the 2-parameter Weibull distributions at lower breakdown probabilities are not very reliable.

From Table 3.15, the correlation coefficients are 0.98, 0.98 and 0.99 for the three fluids. The 3-parameter Weibull plot of the breakdown voltage of mineral oil, 0.05% and 0.1% fullerene nanofluids shows higher correlation coefficients, shown in Table 3.17. Hence, the 3-parameter Weibull plot is also discussed. Fig.3.17 shows the 3-parameter Weibull plot of the

breakdown voltage of the three fluids. It can be clearly seen that the 0.1% fullerene nanofluid has a higher AC breakdown voltage than mineral oil. It can therefore be concluded that the breakdown voltage enhancement increases with an increase of nanoparticle concentration.

Table 3.18 compares the values of the AC breakdown voltage at different breakdown probabilities of mineral oil, 0.05% and 0.1% fullerene nanofluids. The breakdown voltage of 0.1% quantile of mineral oil is increased by 26% due to 0.05% fullerene nanoparticles and 57% due to 0.1% fullerene nanoparticles.

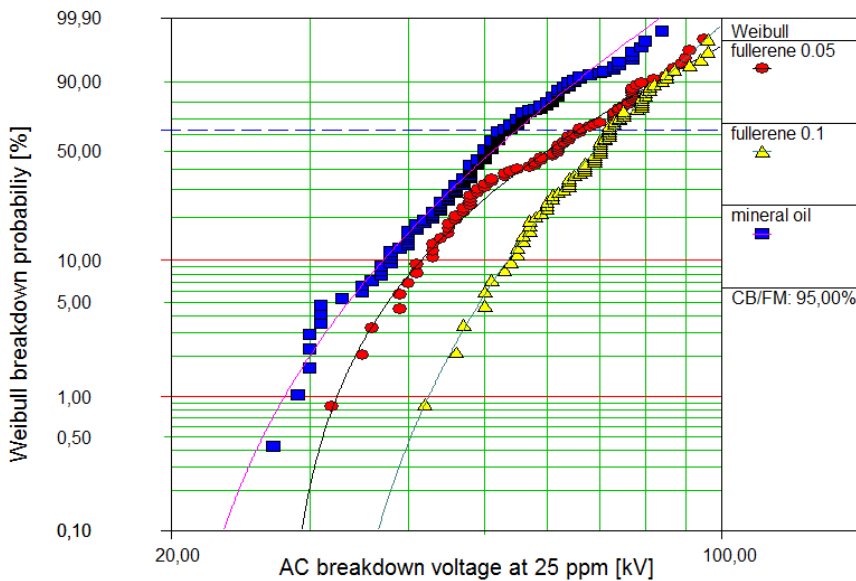


Figure 3.17 3-parameter Weibull plot of the AC breakdown voltage of mineral oil, 0.05% and 0.1% fullerene nanofluids.

Table 3.17 Parameters and correlation coefficient of the 3-parameter Weibull plot in Fig. 3.17.

parameters	Mineral oil	0.05% NF	0.1% NF
β	3.32	2.25	14.93
η	36.21	38.11	36.21
ρ	0.99	0.99	1
γ	18.80	27.54	29.82

Table 3.18 AC breakdown at different breakdown probabilities of mineral oil and fullerene nanofluids at 25 ppm with 3-parameter Weibull calculation.

BD Probabilities [%]	Mineral oil	0.05% NF		0.1% NF	
	BD[kV]	BD [kV]	change	BD [kV]	change
0.1	23 (± 1)	29 (± 1)	+26%	37 (± 3)	+61%
1	28 (± 2)	32 (± 2)	+14%	42 (± 3)	+50%
5	34 (± 2)	38 (± 2)	+12%	49 (± 3)	+44%
63.2	55 (± 1)	66 (± 4)	+20%	73 (± 2)	+33%

Fullerene nanoparticles can apparently increase the breakdown voltage of mineral oil, 0.1% fullerene nanofluid shows significant increased AC breakdown voltage. The breakdown voltage of fullerene nanofluids increases with increasing particle concentration.

3.8.4 Viscosity

To understand the effect of fullerene nanoparticles on mineral oil, viscosity is an important physical property to be studied. The viscosity was measured with a rheology meter between 10°C and 80°C. Fig. 3.18 shows the viscosity of mineral oil and 0.1% fullerene nanofluid. The blue line shows the viscosity of mineral oil and the red line shows that of 0.1% fullerene nanofluid. It can be seen that the viscosity of 0.1% fullerene nanofluid is almost the same as that of mineral oil especially at temperature above 30°C. There is around 2% increase of viscosity of mineral due to 0.1% fullerene nanoparticles at temperature below 30°C. So it can be concluded that fullerene nanofluids up to 0.1% mass fraction have negligible effect on the viscosity of mineral oil.

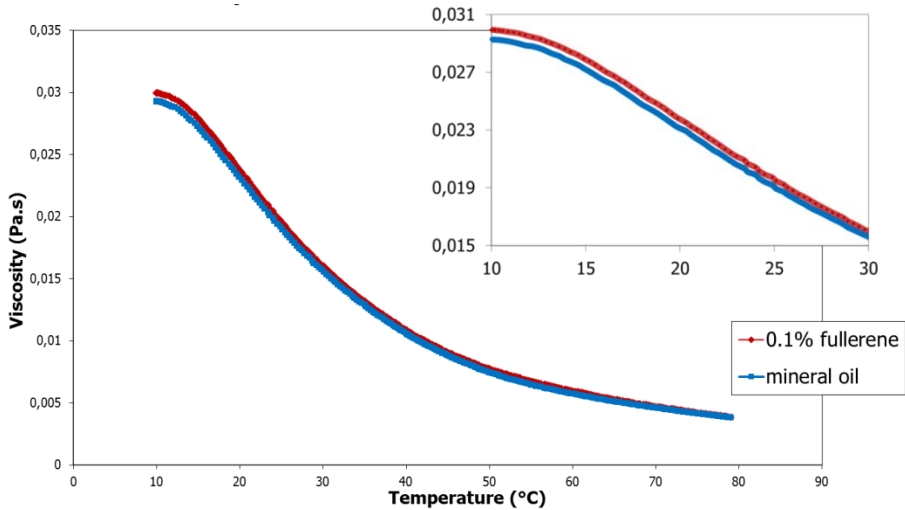


Figure 3.18 Viscosity of mineral oil and 0.1% fullerene nanofluid.

3.8.5 Discussion

Fullerene and silica nanoparticles can both improve the AC breakdown strength of mineral oil. The enhancement due to 0.05% fullerene nanoparticles is on average 19%. While the enhancement caused by 0.01% silica nanoparticles is on average 21%. So fullerene nanoparticles have less effect on the breakdown strength of mineral oil than silica nanoparticles. The differences between the fullerene and silica nanoparticles discussed in this study are surface property and electrical conductivity. The surface of fullerene nanoparticle is hydrophobic, and that of silica is hydrophilic. It was proved in section 3.7 that the moisture content adsorption on the hydrophilic surface of silica nanoparticles can be the reason for the enhanced breakdown strength of silica nanofluids. In contrast, the hydrophobic surface of fullerene nanoparticles won't adsorb any moisture content in mineral oil. However, except moisture content, the large surface area of nanoparticles may adsorb other additives in the oil, such as acid and particles caused by oxidation. The detailed comparison of the dielectric strength of fullerene and silica nanofluids and a further investigation of the surface adsorption of the two types of nanoparticles will be discussed in chapter 4.

The relative high electrical conductivity of fullerene particles can also be the reason for the enhanced breakdown strength of fullerene nanofluids. A recent study showed that conductive nanoparticles can act as electron

traps in mineral, which can improve the dielectric strength of the base oil [35]. The detailed explanation is that the charge relaxation time constant of the nano-material has a major bearing on the extent to which the electrodynamic processes in the liquid are modified. If the nanoparticles' relaxation time constant is short, relative to the timescales of interest for streamer growth, their presence in the oil will significantly modify the electrodynamics. On the other hand, if the nanoparticles' relaxation time constant is long relative to the timescales of interest for streamer growth, their presence will have little effect upon the electrodynamics. The charge relaxation time constant τ for the nanoparticles can be calculated as:

$$\tau = \frac{2\varepsilon_1 + \varepsilon_2}{2\sigma_1 + \sigma_2} \quad (3.3)$$

Where ε_1 and σ_1 are the permittivity and conductivity of mineral oil. The values for the materials tested are $\varepsilon_1 = 2.2\varepsilon_0$ and $\sigma_1 = 10^{-12}$ S/m; ε_2 and σ_2 are the permittivity and conductivity of fullerene nanoparticles, the values are $\varepsilon_2 = 4\varepsilon_0$ to $4.5\varepsilon_0$ and $\sigma_2 = 9.86 \times 10^{-4}$ S/m. After calculation, fullerene nanoparticles show relaxation time constants of 75 to 80 ns. Relative to the nanosecond to microsecond timescales involved in streamer propagation, the surface of fullerene nanoparticles can act as electron traps in mineral oil.

3.8.6 Summary

In this section, the AC breakdown voltage of 0.05%, 0.1% fullerene nanofluids were measured and the results were compared with that of mineral oil. The results show that 0.05% fullerene nanoparticles show no significant effect on the breakdown voltage of mineral oil at low failure probabilities. Fullerene nanoparticles with 0.1% mass fraction increase the AC breakdown voltage of mineral oil, especially at low failure probabilities, compared to pure mineral oil (0.1% to 5% probability of failure). The reason of AC breakdown enhancement of mineral oil due to fullerene nanoparticles can be that fullerene nanoparticles have a relaxation time constant of 75 to 80 ns. The streamer propagation in mineral oil is in nanosecond to microsecond range. That enables fullerene nanoparticles to act as charge traps in mineral oil.

3.9 References

- [1] Z. Krasucki, "Breakdown of Liquid Dielectrics", Proceedings of the Royal Society of London, Series A, Mathematical and Physical, Vol. 294, pp. 393-404, 1966.

- [2] H. Yamashita, H. Amano and T. Mori, "Optical Observation of Pre-breakdown and Breakdown Phenomena in Transformer Oil", *Journal of Physics D: Applied Physics*, Vol. 10, pp. 1753-1760, 1977.
- [3] X. Wang, "Partial Discharge Behaviours and Breakdown Mechanisms of Ester Transformer Liquid under AC Stress", PhD thesis, The University of Manchester, 2011.
- [4] N. Felici, "High-Field Conduction in Dielectric Liquids," *IEEE Transactions on Electrical Insulation*, Vol. EI-20, pp. 233-238, 1985.
- [5] M.G. Danikas, " Study of Some Factors Affecting the Breakdown Strength of Transformer oil", in 1988 International Conference on Dielectric Materials, Measurement and Applications, pp. 9-12, 1988.
- [6] O. Lesaint, "Streamer Generation and Propagation in transformer oil under ac Divergent Field Conditions", *Electrical Insulation*, Vol. 23, pp. 941-654, 1988
- [7] G. Massala, A. Saker and O. Lesaint, "Study of Streamer Propagation in Mineral Oil in Overvolted Gaps under Impulse Voltage", *Conference on Electrical Insulation and Dielectric Phenomena*, pp. 592-595, 1995.
- [8] H. Raether, *Elektronnye laviny i proboi v gazakh*, Moscow, 1968.
- [9] S. Ingebrigtsen, L.E. Lundgaard and P.O. Astrand, "Effect of Additives on Prebreakdown Phenomena in Liquid Cyclohexane: I. Streamer Initiation", *Journal of Physics D: Applied Physics*, Vol. 40, pp. 5161-5169, 2007.
- [10] O. Lesaint and T.V. Top, "Streamer Initiation in Mineral Oil part I", *IEEE Transactions on Dielectrics and Electrical Insulation*, Vol. 9, pp. 84-91, 2002.
- [11] T.V. Top and O. Lesaint, "Streamer Initiation in Mineral Oil part II", *IEEE Transactions on Dielectrics and Electrical Insulation*, Vol. 9, pp. 92-96, 2002.
- [12] P. Gournay and O. Lesaint, "On the Gaseous Nature of Positive Filamentary Streamers in Hydrocarbon Liquids. II: Propagation, Growth and Collapse of Gaseous Filaments in Pentane", *Journal of Physics D: Applied Physics*, Vol. 27, pp. 2117-2127, 1994.
- [13] G. Massala and O. Lesaint, "A Comparison of Negative and Positive Streamers in Mineral Oil at Large Gaps", *Journal of Physics D: Applied Physics*, Vol. 34, pp. 1525-1532, 2001.
- [14] O. Lesaint and G. Massala, "Positive Streamer Propagation in Large Oil Gaps", *IEEE Transactions on Dielectric and Electrical Insulation*, Vol. 5, pp. 360-370, 1998.
- [15] A.A. Zaky and R. Hawley, *Conduction and Breakdown in Mineral oil*, UK: Peter Peregrinus Ltd., 1973.
- [16] O. Lesaint, P. Gournay, A. Saker, R. Tobazeon, J. Aubin and M. Mailhot, "Streamer Propagation and Breakdown under AC in Mineral oil for Gaps up to 80 cm", *International Conference on Conduction and Breakdown in Dielectric Liquids*, pp. 251-254, 1996.
- [17] J.R. Lucas, *High Voltage Engineering*, University of Moratuwa, Sri Lanka, 2001
- [18] F.M. Clark, "Water Solution in High-Voltage Dielectric Liquids", *Transaction of the American Institute of Electrical Engineers*, Vol. 59, pp. 433-441, 1940.
- [19] M. Krins, M. Reuter, H. Borsi and E. Gockenbach, "Breakdown and Flashover Phenomena Related to the presence of High Absolute Water Contents in Clean and Carbonized Transformer oil", *Conference on Electrical Insulation and Dielectric Phenomena*, pp. 252-255, 2002.
- [20] D. Chandler, "Two Faces of Water", *Nature*, Vol. 417, pp. 491, 2002.
- [21] M. Krins, H. Borsi and E. Gockenbach, "Impact of Carbon Particles on the Electrical Strength of Different Solid/Liquid Interfaces in a Non-uniform Field", *IEEE International Symposium on Electrical Insulation*, pp. 623-626, 1998.
- [22] W.B. Wiegand, C.R. Boggess and D.W. Kitchin, "Effect of Carbon Black on Insulating Oils", *Journal of Industrial and Engineering Chemistry*, Vol. 23, pp. 273-276, 1931.
- [23] M. Krins, H. Borsi and E. Gockenbach, "Influence of Carbon Particles on the Breakdown and Partial Discharge Inception Voltage of Aged Mineral Based Transformer Oil", *International Conference on Dielectric Materials, Measurements and Applications*, pp. 251-254, 1996.

- [24] A. Ozawa, S. Mikkami, K. Nitta, M. Shinmura, S. Washizu and Y. Wadam, "Electrical Conduction and Polarization in Cellulose in Relation to its Water Content", International Conference on Conduction and Breakdown in Solid Dielectrics, pp. 433-436, 1989.
- [25] M. Pompili and C. Mazzetti, "Effect of Reduced Viscosity on the Electrical Characteristics of Transformer and Switchgear oils", IEEE International Symposium on Electrical Insulation, pp. 363-366, 2002.
- [26] F.M. Clark, "Dielectric Strength of Mineral Oils", Transactions of the American Institute of Electrical Engineers, Vol. 54, pp. 50-55, 1935.
- [27] C. Choi, K. Yatsuzuka and K. Asano, "Motion of a Conductive Particle in Viscous Fluid Simulating Liquified Plastic Waste", IEEE Conference on Industry Applications, vol. 3, pp. 1831-1836, 1999.
- [28] H. Kuirita, O. Usui, T. Hasegawa and H. Fujii, "Effect of Particles on Partial Discharge Inception in Oil Immersed Insulating System", IEEE International Conference on Dielectric Liquids, pp. 126-131, 1999.
- [29] R.B. Abernethy, *The New Weibull Handbook Fifth Edition, Reliability and Statistical Analysis for Predicting Life, Safety, Supportability, Risk, Cost and Warranty Claims*, North Palm Beach, Fla: R.B. Abernethy, 2006.
- [30] V. Segal, A. Hjorsberg, A. Rabinovich, D. Natrass and K. Raj, "AC (60Hz) and Impulse Breakdown Strength of a Colloidal Fluid based on Transformer Oil and Magnetite Nanoparticles," Electrical Insulation, pp.619-622, 1998.
- [31] B. Du, J. Li, B. Wang and Z. Zhang, "Preparation and Breakdown Strength of Fe₃O₄ Nanofluid based on Transformer Oil," International Conference on High Voltage Engineering and Application, pp.311-313, 2012.
- [32] Y. Du, Y. Lv, J. Zhou, X. Li and C. Li, "Breakdown Properties of Transformer Oil based TiO₂ Nanofluid," Annual Report Conference on Electrical Insulation and Dielectric Phenomena, pp.1-4, 2010.
- [33] D.E.A. Mansour, E.G. Atiya, R.M. Khattab and A.M. Azmy, "Effect of Tatiana Nanoparticles on the Dielectric properties of Transformer Oil-Based Nanofluids," Annual Report Conference on Electrical Insulation and Dielectric Phenomena, pp. 295-298, 2012.
- [34] F.M. O'Sullivan, "A Model for the Initiation and Propagation of Electrical Streamers in Transformer oil and Transformer oil based nanofluids", PhD thesis, Massachusetts Institute of Technology, 2007.
- [35] A. Rimola, D. Coasta, M. Sodupe, J.H. Lambert and P. Ugliengo, "Silica Surface Features and Their Role in the Adsorption of Biomolecules: Computational Modelling and Experiments", Chemical Reviews, pp. 4215-4313, 2013.
- [36] S.V. Kulkarni and S.A. Kharparde, *Transformer Engineering: Design and Practice*, Technology & Engineering, 2004.
- [37] V.K. Varadan, A.S. Pillai, D. Mukherji, M. Dwivedi and L. Chen, *Nanoscience and Nanotechnology in Engineering*, World Scientific, 2010.

4 Partial discharge dynamics in nanofluids

4.1 Introduction

As mentioned in chapter 3, a breakdown process in mineral oil is preceded by streamer initiation and propagation. Recent studies have shown that the details of the discharge event during streamer initiation and propagation in mineral oil can be studied with the help of an ultra-high frequency (in the range between 300 MHz to 3 GHz) oscilloscope. [1-4]. In general, voltage, current, total charge and light emission signals have been recorded during the initiation and propagation of streamers. The needle-plane electrode system is widely used to study the streamers. The reason is that needle electrodes can create a very high field to start streamer propagation. In this chapter, in order to evaluate the effect of nanoparticles on the dynamics of the discharge process, a time-resolved detection setup with needle-plane electrode was built.

The results of AC breakdown measurements of mineral oil, silica and fullerene nanofluids were analysed in chapter 3. It shows that silica nanofluid with 0.01% mass fraction and fullerene nanofluid with 0.1% both improve the AC breakdown strength of mineral oil. Breakdown occurs due to discharge initiation and propagation in the oil. The breakdown strength value provides little information on the discharge process. Therefore, it is also important to investigate the detailed discharge mechanisms of mineral oil and nanofluids. Hence, this chapter focuses on the partial discharge behaviour of mineral oil, silica and fullerene nanofluids. The total charge, voltage and pulse shape were recorded with the help of a high bandwidth oscilloscope. Since the discharge mechanism in mineral oil strongly depends on the polarity of applied voltage, in this chapter the applied voltages are positive and negative DC voltages.

4.2 Pre-breakdown phenomena in liquid dielectrics

For many years, scientists and engineers have been trying to understand the phenomenon leading to electrical breakdown in dielectric liquids, particularly in transformer oils. This pre-breakdown process is called “streamer”. A streamer is the phenomenon of electrical discharge observed during the initiation of electrical breakdown in a dielectric medium [5]. Depending on polarity of the electrode, a streamer is

classified as a positive or negative streamer. Positive streamers were found to be fast and filamentary [6-9, 13]. While negative streamers tend to be slow and bushy [10-13].

4.2.1 Positive streamer

For positive streamer initiation, the most widely accepted theory is the molecular ionization theory [14]. The hypothesis is when the field at the anode tip reaches a critical value, the liquid near the tip is ionized resulting into low mobility positive ions and high mobility electrons. The fast electrons migrate towards the anode resulting in joule heating and a net positive ions zone at the tip. The joule heat causes a temperature rise and generates a local low density region. In this low density region, once the electrical field is high enough to start an electron avalanche, a streamer is initiated. The net positive ions zone at the anode tip increases the local electrical field which allows the streamer to propagate [16]. The streamer is self-sustaining and propagates forward as a moving dissipative source. Field ionization and subsequent streamer propagation is an extremely fast process, which gives the characteristic filamentary appearance. A streamer will “die” if the electric field at its tip becomes too small to support propagation as a result of the potential drop along the streamer channels.

For the positive streamer propagation, four different modes were observed [6, 7]. The first mode was only observed under low applied voltage in short gaps with very sharp needle tip (1 μm). This mode expands a short distance in a bushy structure with a velocity of 100 m/s [6, 8, 9]. The second mode is a filamentary streamer which travels at a supersonic speed of some km/s. It was observed with an applied voltage close to breakdown voltage [7]. When the applied voltage is above the breakdown voltage, the third mode streamer occurs with the velocity of 10-20 km/s. The streamer composes of a number of thin filaments. The fourth mode occurs at voltage above the acceleration voltage, the velocity is around some 100 km/s. The shape is a very luminous channel surrounded by some side branches. The correlation between mode, shape, velocity and applied voltage of positive streamer propagations in mineral oil is shown in Fig. 4.1.

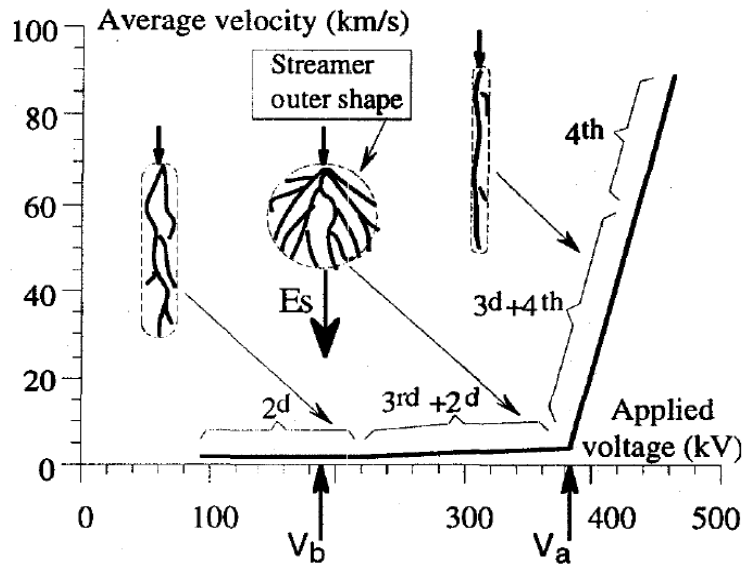


Figure 4.1 Correlation between mode (2nd to 4th), shape, velocity and applied voltage of positive streamers in mineral oil [7]. V_b is breakdown voltage and V_a is acceleration voltage.

4.2.2 Negative streamer

At negative polarity, the initiation of a streamer is due to the formation of micrometre-sized bubbles in front of the needle tip [10, 11]. This is due to a fast electronic avalanche which occurs in front of the needle tip. Following the avalanche by a few nanoseconds, a shock wave is radiated and a cavity develops [12]. Discharge occurs inside the gas phase which generates fast current pulses and a slow bushy-like streamer grows [12].

The negative streamer propagation was observed in four modes [6]. The first mode is a thin pencil-like structure with a diameter of a few micrometres, the speed is subsonic. The second mode is a bushy structure growing at a subsonic rate. The third mode is a thin structure at nearly sonic velocity. The shape of the fourth mode is similar to the third, but propagates an order of magnitude faster. Fig. 4.2 shows a typical streamer in a large paraffinic oil gap within a needle-plain electrode system.

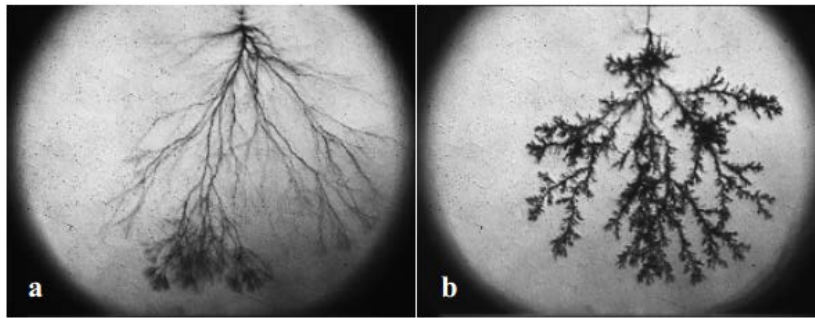


Figure 4.2 Typical streamers in paraffinic oil [13]. (a) positive streamer at 210 kV, (b) negative streamer at 390 kV.

4.3 Fundamentals of partial discharge

A partial discharge (PD) is defined as a localized electrical discharge which partially bridges the insulation between electrodes, such as a discharge in a bubble within a liquid dielectric [15]. The presence and magnitude of PD are important criteria for the early detection of degraded insulation systems and the assessment of manufactured product quality [17].

4.3.1 Characteristic parameters of PD in liquid dielectrics

Partial discharge in dielectric liquids is a complex process that involves a succession of inter-correlated phenomena, such as electronic, mechanical, thermal, etc. Moreover, experiments have shown that the characteristic features of a partial discharge greatly depend on the magnitude and shape of applied voltage, gap distance, electrode configuration, liquid nature and purity [18].

The availability of an electron in the low density region of a dielectric liquid is the first condition for a discharge to develop. In this case, the electron can initiate an electron avalanche which travel towards the anode. When an electrical avalanche contains about 10^8 electrons, the transition to a streamer is expected to take place [19]. The minimum voltage at which PDs can be detected is called the partial discharge inception voltage (PDIV). It is used as an important indicator for representing the integrity of liquid insulation [20].

The key parameter for PD monitoring is the discharge magnitude, which can be used to evaluate the intensity of PD in liquid. The value of the PD

charge can be determined by integrating the PD current value during the PD time interval:

$$q = \int_{t_1}^{t_2} i(t)dt \quad (4.1)$$

Where q is the charge, $i(t)$ is the current, and t is the time, t_1 and t_2 represent the start time and the end time of the discharge pulse.

The time-resolved PD measurement system can record the PD pulse shape, which is related to the charge carrier movement. The effect of additional nanoparticles, moisture content, acid value and additives due to oxidation on the charge carrier movement can be indicated by the PD pulse shape. The PD pulse shape in one PD sequence includes the PD repetition rate and a single pulse shape. A single pulse shape is determined by the rise time, pulse duration, fall time and pulse amplitude.

4.3.2 PD measurement circuit and experimental setup

In order to detect the electric pulse generated by the PD, different kinds of apparatus have been developed in the past. In the 1950s and 1960s, an ultra-wide band or time resolved system for study of the discharge process on a hundred nanosecond scale was used by Raether [19]. With the introduction of fast digitizers and digitizing oscilloscopes in the last decade, time-resolved measurements gained great importance for the study of discharge mechanisms. The bandwidth of a time-resolved detection system must be larger than the highest frequency component of the discharge signal. Besides, the discharge return path should be as short as possible to minimize travelling wave problems and it should be of low inductance to prevent oscillations [21]. The system is able to record the current pulse shape which has a direct correlation with the charge carrier movement in the discharge process.

The basic circuit of a time-resolved PD measurement is shown in Fig. 4.3. The method is based on the measurement of a charge displacement that causes a current in the leads to a sample. This is performed by placing an impedance Z in the circuit. In this way the external charge displacement which is related to the discharge is measured. This external charge displacement is directly related to the energy dissipation in a discharge. In the basic circuit, coupling capacitor K provides a closed circuit for the

discharge current. A high bandwidth oscilloscope is used to record the discharge pulse shape.

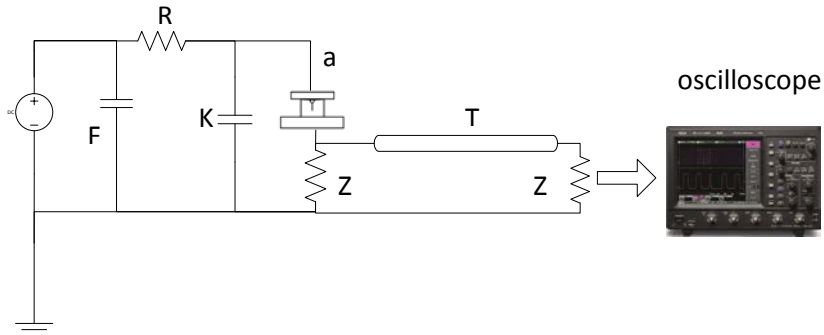


Figure 4.3 Experimental set-up for time-resolved PD measurement (a: test sample; K: coupling capacitor; Z: measuring impedance; T: 50 Ω coaxial cable; F: capacitor for shorting out high frequency noise from the DC source; R: resistor for limiting the current).

Fig. 4.4 shows the experimental PD measurement set-up. Capacitor F is connected with the HV DC source in parallel to filter out the high voltage noise from the source. The HV DC source can supply up to 40 kV voltage. The resistor R is connected with the HV DC source and test cell in series. The test cell is connected in series with impedance Z. The current shape of the PD is displayed on an oscilloscope.



(a) Capacitor F (10 nF)

(b) test cell



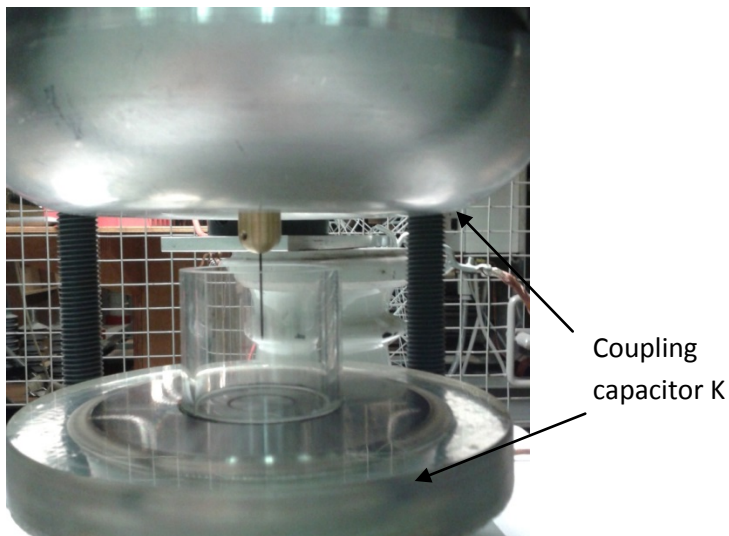
(c) HV DC source

(d) oscilloscope

Figure 4.4 PD measurement set-up.

Fig. 4.5 shows a detailed view of the needle-plane test cell. The radius of curvature of the needle tip is $1 \mu\text{m}$. The gap distance is 20 mm. The plane electrode consists of a 28 mm diameter measuring electrode and a concentric 180 mm diameter guard electrode. The electrode holder and the guard electrode act as coupling capacitor K. Impedance Z consists of six resistors of 300 Ohm in parallel to achieve 50 Ohm measuring impedance. This is visible at the back side of the plane electrode. The discharge signal is fed via a 50 Ohm coaxial cable to the oscilloscope. The sensitivity of the

detective system is around 0.2 pC. All the measurements were performed according to the standard IEC60270. The bandwidth of the oscilloscope is 400 MHz, the bandwidth of the detection system will be discussed in appendix C.



(a) Needle-plane test cell, oil sample container, electrode holder acts as coupling capacitor K.



(b) Backside of the electrode, impedance Z (6 impedances of 300 Ohm in parallel connected with plane electrode) and transmission line connected with the impedance Z.

Figure 4.5 Detailed view of needle-plane test set up.

4.4 Experimental results of PD in mineral oil and nanofluids

The quantities which are used for comparing the PD phenomena for mineral oil, 0.01% silica and fullerene nanofluids are: inception voltage, PD duration, PD rise time, total discharge magnitude and single PD voltage amplitude.

- The voltage rise of the PD tests was controlled by hand, with a rate of rise around 1 kV/s.
- The discharge magnitude is calculated by integrating the current amplitude of all the discharge pulses in one PD sequence.
- The single PD voltage amplitude represents the peak voltage value of the largest PD pulse in a PD sequence.

4.4.1 Test samples

In section 3.8.5, the theory of conductive nanoparticles acting as electron traps was introduced. The hypothesis of the theory is that the charge relaxation time constant of the nanoparticle may have a major bearing on the extent to which the electrodynamic processes in the liquid are modified [14]. The charge relaxation time constant τ for the transformer oil/nanoparticle system is:

$$\tau = \frac{2\varepsilon_1 + \varepsilon_2}{2\sigma_1 + \sigma_2} \quad (4.2)$$

Where ε_1 and σ_1 are the permittivity and conductivity of the mineral oil, the values are $\varepsilon_1 = 2.2 \varepsilon_0$ and $\sigma_1 = 1 \times 10^{-12} \text{ S/m}$; ε_2 and σ_2 are the permittivity and conductivity of the spherical nanoparticles. The permittivity, conductivity, and the calculated charge relaxation time of the nanoparticles and the mineral oil are shown in Table 4.1.

Table 4.1 Permittivity, conductivity and charge relaxation time of the tested liquids.

	mineral oil	silica	fullerene
Conductivity [S/m]	10^{-12}	10^{-16} to 10^{-12}	9.86×10^{-4}
Relative permittivity	2.2	3.8 to 5.4	4.0 to 4.5
Charge relaxation time constant	--	25 to 37 s	75 to 80 ns

The test samples in this study are mineral oil, silica and fullerene nanofluids. The particle concentration for both nanofluids is 0.01% mass fraction. The reason for choosing silica and fullerene nanofluids is that the conductivities of silica and fullerene are different. After calculation, the charge relaxation time constant of silica is 25 to 37 s. For fullerene, it is 75 to 80 ns. So, relative to the nanosecond to micro second time scales involved in streamer propagation, fullerene nanoparticles can act as charge traps in mineral oil, but silica nanoparticles cannot. To verify this assumption, the PD dynamics in 0.01% silica and fullerene nanofluids are measured and the results are compared with those of mineral oil.

For the PD tests, five samples were prepared for each fluid according to the procedure outlined in chapter 2. For each sample, 10 tests were performed.

4.4.2 Results under positive DC voltage

4.4.2.1 Inception voltage

The results of the PD inception voltage of mineral oil, 0.01% silica and fullerene nanofluids under positive DC voltage are shown in Fig. 4.6. The input voltage is increased by hand-control. The accuracy is around ± 1 kV. The inception voltage ranges of mineral oil, silica and fullerene nanofluids are 20 to 24 kV, 25 to 29 kV and 24 to 26 kV respectively. There is overlap between the inception voltage range of mineral oil and fullerene nanofluid. The inception voltage of silica nanofluid is some 20% higher than that of mineral oil, while the enhancement of the inception voltage due to fullerene nanofluid is not significant.

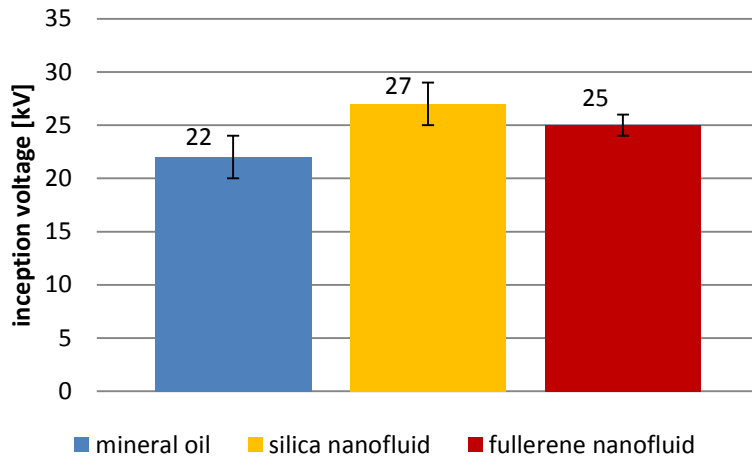


Figure 4.6 Inception voltage of mineral oil, 0.01% silica and fullerene nanofluids under positive DC voltage.

4.4.2.2 Observation of a PD sequence

In this section, the PD duration, PD rise time and the shape of a single PD pulse of the three liquids are compared. The duration of the pulses depends on the repetition rate of the pulses. Fig. 4.7 to 4.9 show the pulse shapes of the PD in the three fluids. It can be seen that the single impulse shapes of the discharge in three fluids are almost the same, only the voltage amplitude of mineral oil is higher than the two nanofluids. The rise time of the impulses for all three fluids is around 2 ns, which mainly depends on the circuit setup. The main difference shown in the three figures is the duration of the sequence of discharge pulses, which is for mineral oil much longer than the silica and fullerene nanofluids. Since the single discharge pulse durations of the three liquids are measured to be in the same range, the duration of the discharge pulses depends only on the number of discharge pulses in one PD sequence. So this indicates that the number of discharge pulses in one PD sequence for mineral oil is 3 times higher than that for silica nanofluid and 2 times higher than that for fullerene nanofluid. It was mentioned in chapter 2 that moisture content, acid and additive particles due to oxidation all have negative effect on the dielectric strength of mineral oil. A study has demonstrated that the pulse repetition rate is more sensitive to those additives than PD inception voltage and PD magnitude do [22]. It is possible that the additional nanoparticles can adsorb those additives on their surface, therefore the pulse repetition rate of nanofluids is smaller than mineral oil.

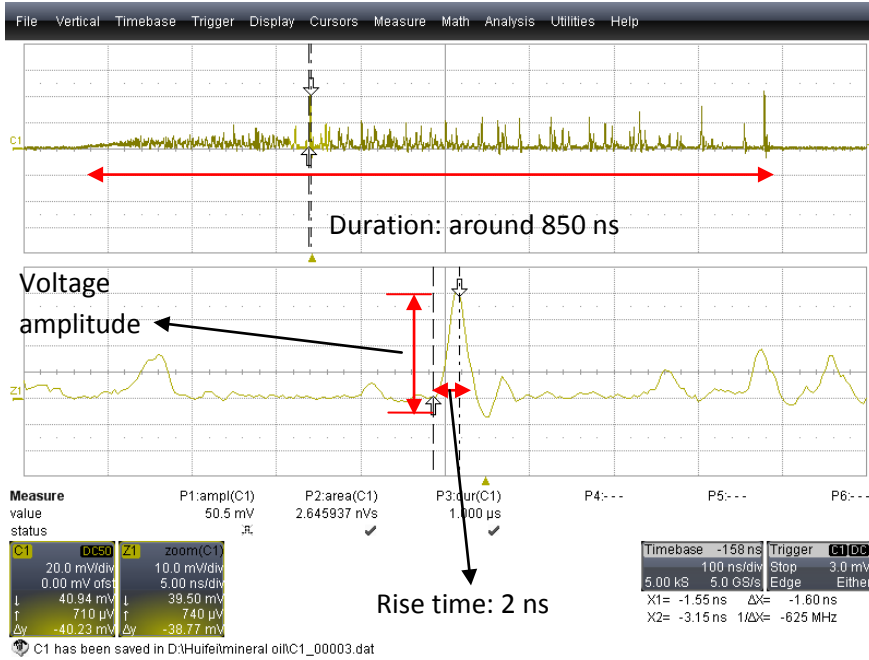


Figure 4.7 One PD sequence for mineral oil under positive DC voltage.

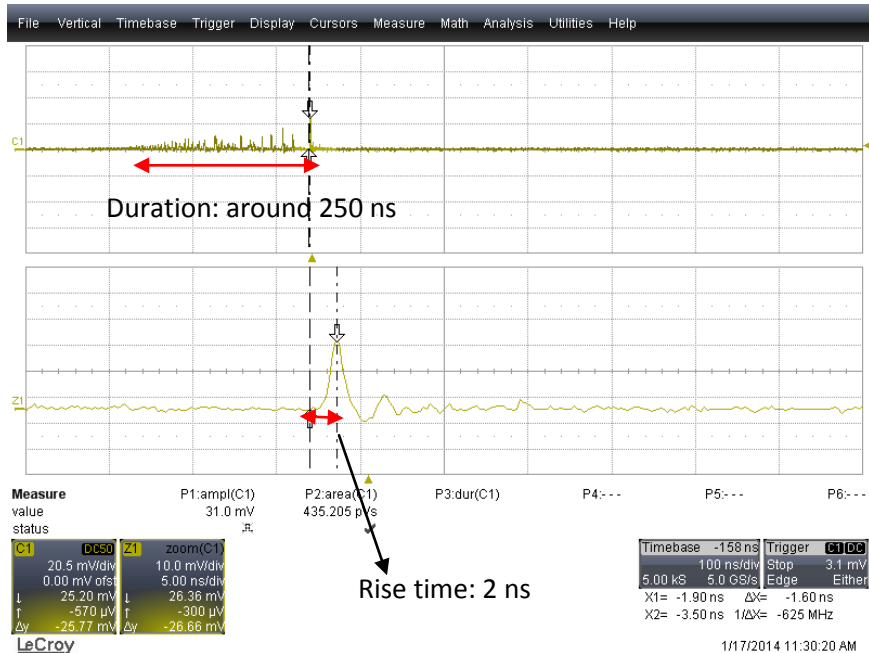


Figure 4.8 One PD sequence for silica nanofluid under positive DC voltage.

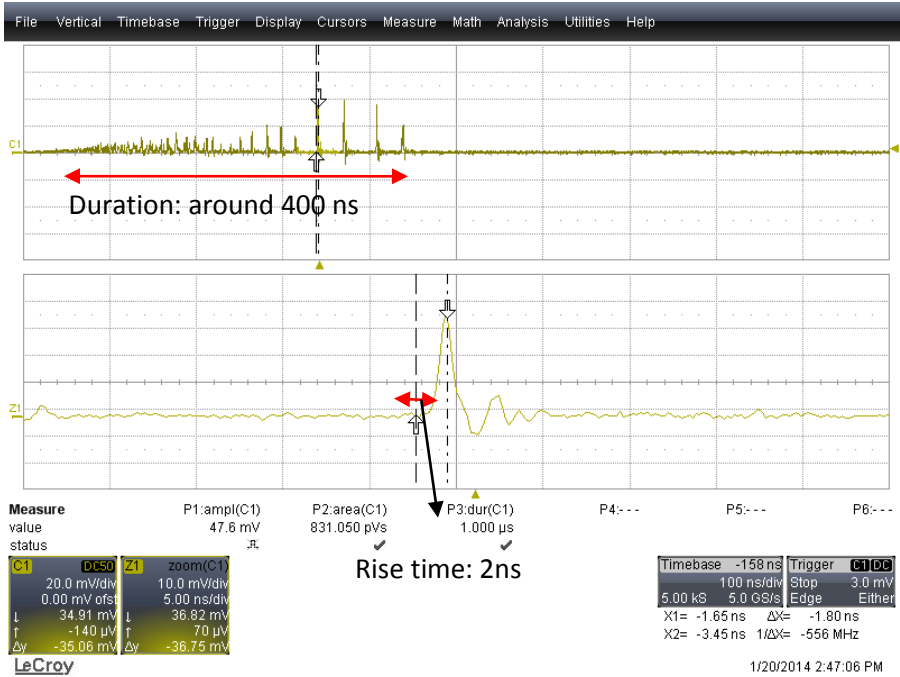
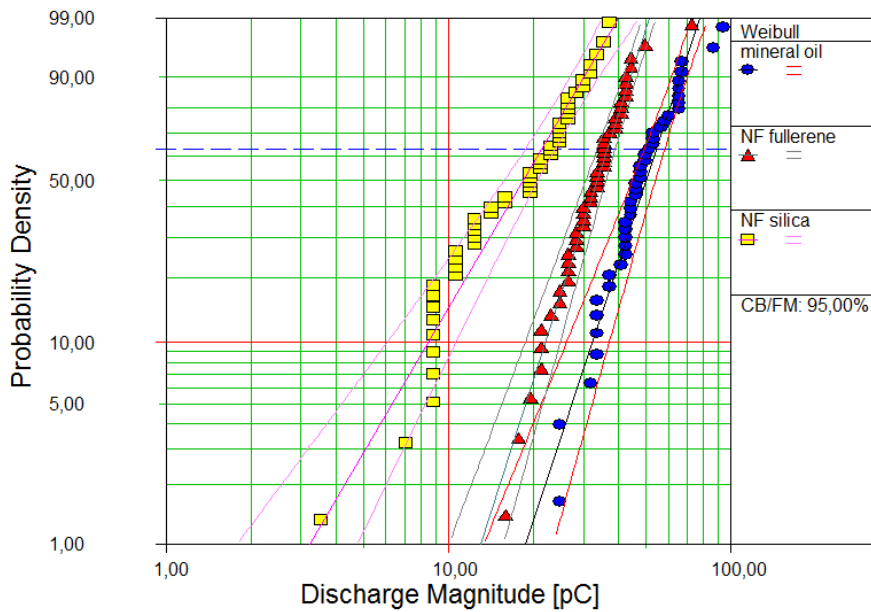


Figure 4.9 One PD sequence for fullerene nanofluid under positive DC voltage.

4.4.2.3 Total Discharge magnitudes

The results of the positive discharge magnitudes of mineral oil, silica and fullerene nanofluids were analysed with Weibull software to have a clear comparison among the PD behaviour of the three fluids. Fig. 4.10 shows the 2-parameter Weibull distributions of the discharge magnitude of the three fluids.



$\beta_1=4,32, \eta_1=54,24, \rho=0,97$
 $\beta_2=4,45, \eta_2=36,44, \rho=0,98$
 $\beta_3=2,44, \eta_3=21,35, \rho=0,97$

Figure 4.10 2-parameter Weibull distributions of the positive discharge magnitude in mineral oil, silica and fullerene nanofluids, including 95% confidence bounds.

From Table 4.2, it can be seen that the discharge magnitude in mineral oil is reduced by around 60% due to the addition of silica nanoparticles and around 33% due to fullerene nanoparticles. Table 4.2 shows the mean value and 63.2% Weibull plot discharge magnitude of the three fluids.

Table 4.2 Positive discharge magnitude of mineral oil, silica and fullerene nanofluids at 50% and 63.2% probabilities.

Probability density [%]	Mineral oil	0.01% SiO ₂ NF		0.01% fullerene NF	
	Discharge magnitude [pC]	Discharge magnitude [pC]	change	Discharge magnitude [pC]	change
50	49 (±4)	18 (±2)	-63%	33 (±3)	-33%
63.2	54 (±4)	21 (±3)	-61%	36 (±3)	-33%

4.4.2.4 PD Voltage amplitude

In this section, the PD voltage amplitudes of single discharge pulses in mineral oil, silica and fullerene nanofluids are compared. The difference of

discharge magnitudes of the three liquids can be due to the numbers of pulses occurred in one partial discharge sequence or the voltage amplitude of the pulses. So it is important to investigate the difference of all single discharge pulses of the three liquids. The results of wave shapes show that the single pulse voltage amplitudes of the three liquids are different. The 3-parameter Weibull distribution of the voltage amplitudes is shown in Fig. 4.11. The reason for using the 3-parameter Weibull distribution is that the correlation coefficient value for 2-parameter Weibull distribution is too low to get a good fit.

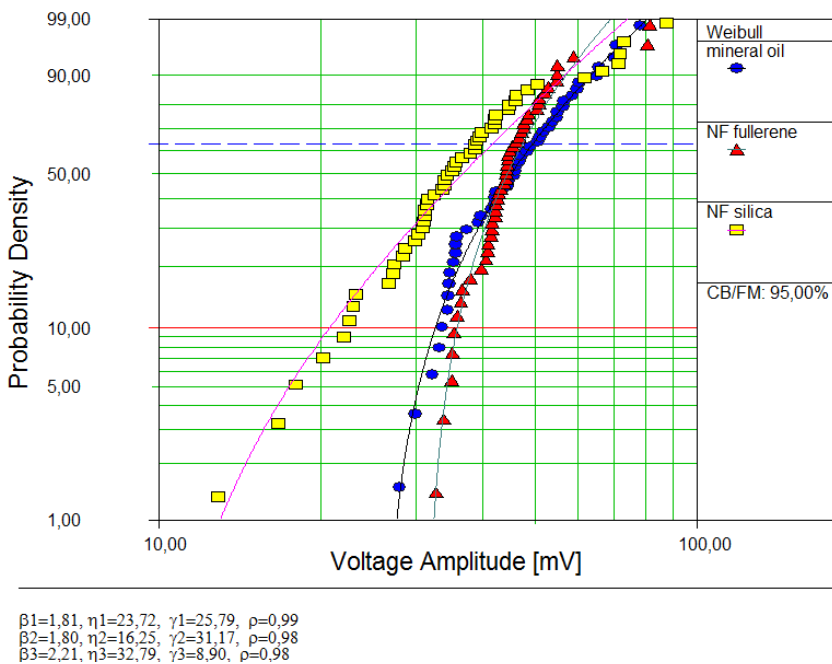


Figure 4.11 3-parameter Weibull distributions of the positive voltage amplitudes of discharge in mineral oil, silica and fullerene nanofluids.

It can be seen from Fig. 4.11 that the difference of voltage amplitudes between mineral oil and fullerene nanofluids is not significant. Silica nanofluid still shows lower voltage amplitudes than mineral oil. Table 4.3 shows the 50% and 63.2% Weibull plot value of voltage amplitudes of discharge in the three fluids.

Table 4.3 Positive voltage amplitude of mineral oil, silica and fullerene nanofluids at 50% and 63.2% probabilities.

Probability density [%]	Mineral oil	0.01% SiO ₂ NF		0.01% fullerene NF	
	Voltage amplitude [mV]	Voltage amplitude [mV]	change	Voltage amplitude [mV]	change
50	45 (±4)	37 (±4)	-19%	44 (±3)	-2%
63.2	50 (±4)	42 (±4)	-16%	47 (±3)	-4%

The mean voltage amplitude of PD in silica nanofluid is around 19% lower than that in mineral oil. For fullerene nanofluid, it is only 2% lower than mineral oil.

4.4.2.5 Summary

In this section, the results of PD measurements under positive DC voltage in mineral oil, 0.01% silica and fullerene nanofluids were compared. The results show that the inception voltage of silica nanofluid is some 20% higher than that of mineral oil, while the enhancement of the inception voltage due to fullerene nanofluid is not significant. From the observation of a PD sequence, it can be seen that the difference among the three fluids is the number of discharge pulses in one PD sequence, which for mineral oil is 3 times higher than that for silica nanofluid and 2 times higher than that for fullerene nanofluid. The total discharge magnitudes of silica nanofluid and fullerene nanofluids are both lower than that of mineral oil. For silica nanofluid, the reduction is 60%, and for fullerene nanofluid the reduction is 33%. The voltage amplitude of mineral oil is reduced by 16% due to the additional silica nanoparticles and 4% due to fullerene nanoparticles.

4.4.3 Results under negative DC voltage

4.4.3.1 Inception voltage

The results of the PD inception voltage of mineral oil, 0.01% silica and fullerene nanofluids under negative DC voltage are shown in Fig. 4.12. It can be seen that the inception voltage of fullerene nanofluid is some 12% higher than that of mineral oil, while the inception voltage of the silica nanofluid and mineral oil show no difference.

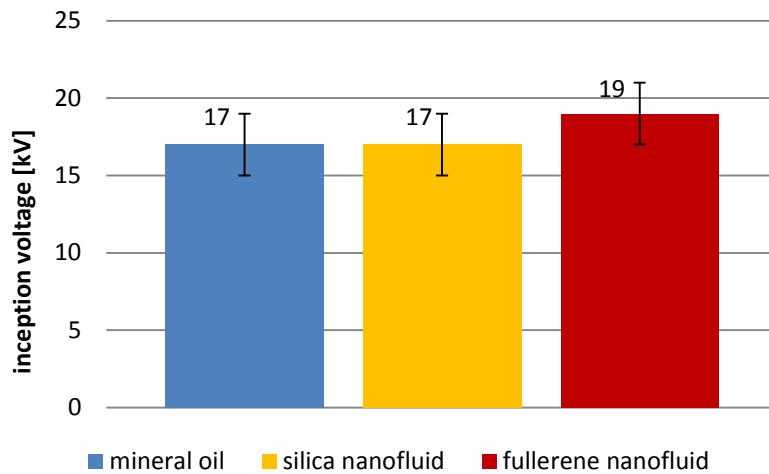


Figure 4.12 Inception voltage of mineral, 0.01% silica and fullerene nanofluids under negative DC voltage.

4.4.3.2 Observation of a PD sequence

In this section, the wave shapes of the three liquids under negative DC voltage are compared. Fig. 4.13 to 4.15 show the wave shapes of the PD in the three fluids. It can be seen that the number of pulses and the voltage amplitude of a single pulse are much different from the wave shapes under positive DC voltage. During one PD sequence, the numbers of pulses under negative DC voltage are less than 5 for all three liquids. The negative voltage amplitudes for the three liquids are around 8 times smaller than that under positive voltage. However, the rise time of a single pulse for all three fluids is around 2 ns, which is the same as that under positive voltage.

Within one discharge sequence, silica nanofluid shows more numbers of pulses than the other two fluids. The voltage amplitude of a single pulse of mineral oil is slightly higher than the other fluids.

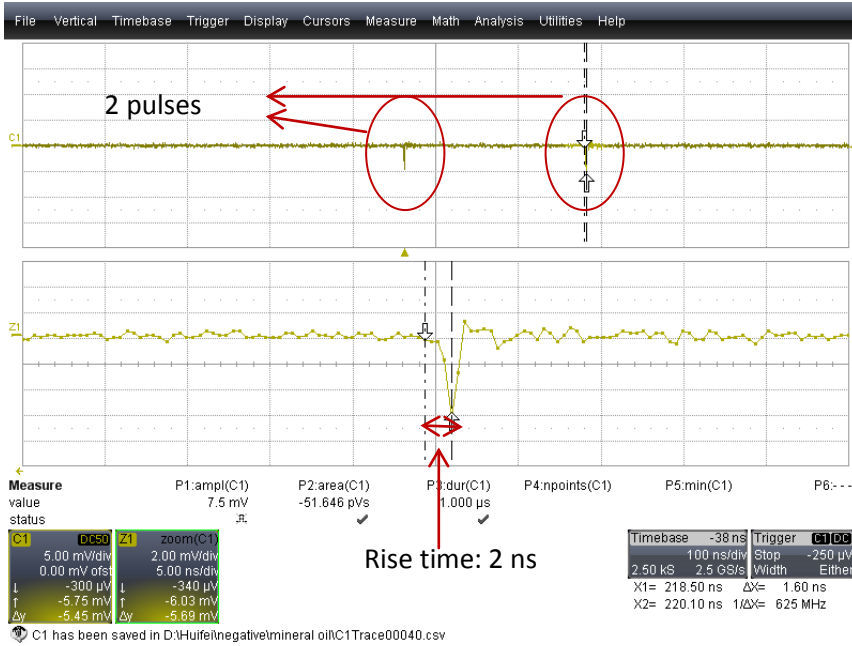


Figure 4.13 One PD sequence for mineral oil under negative DC voltage.

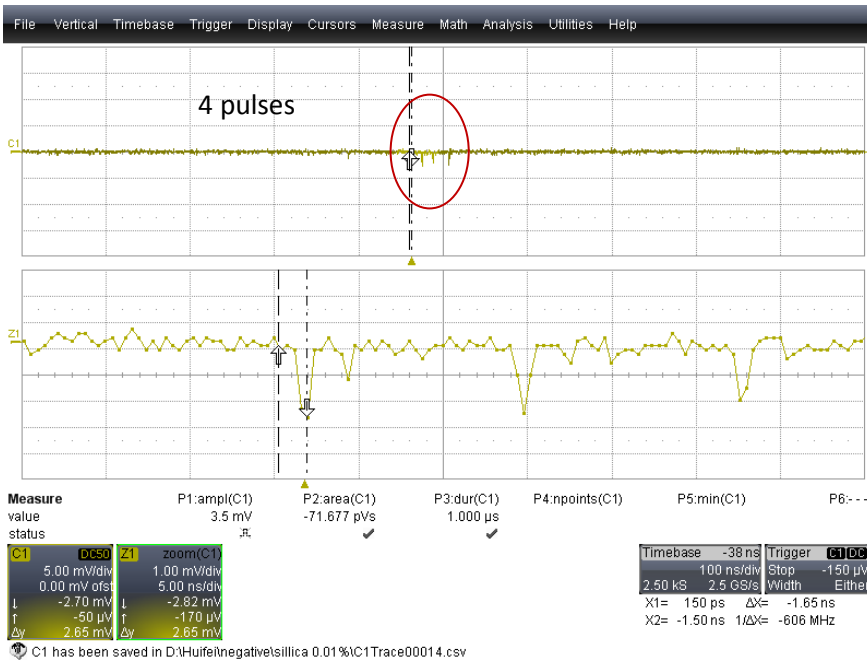


Figure 4.14 One PD sequence for silica nanofluid under negative DC voltage.

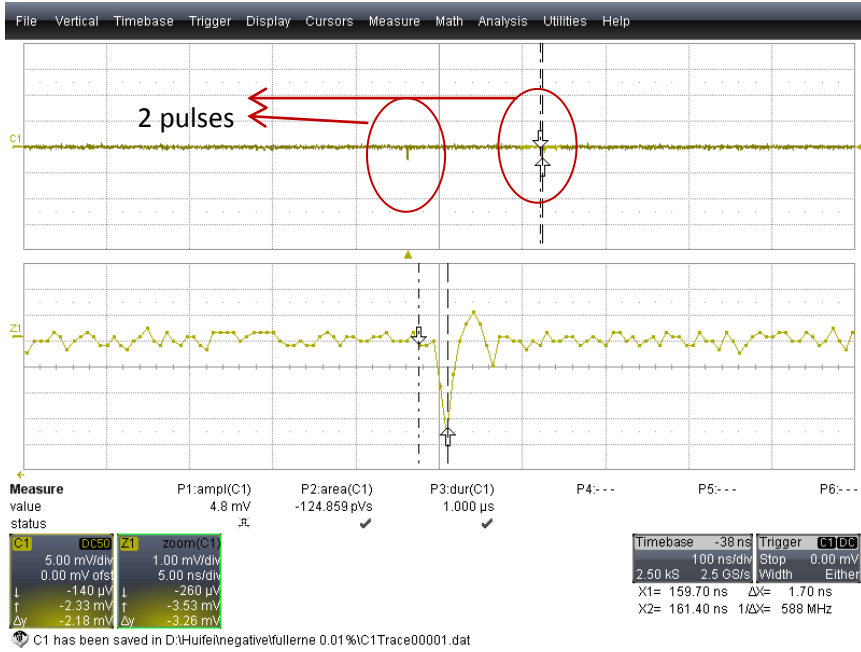
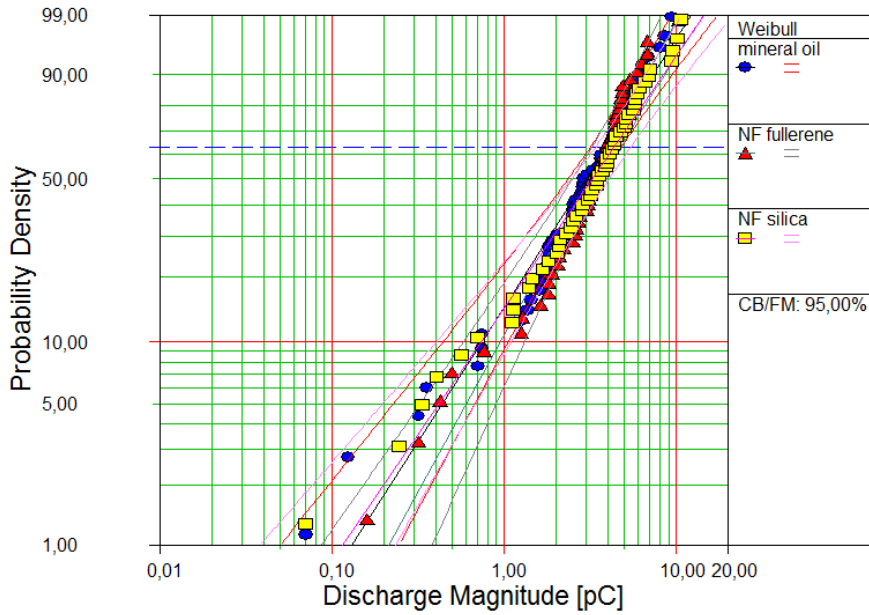


Figure 4.15 One PD sequence for fullerene nanofluid under negative DC voltage.

4.4.3.3 Total discharge magnitudes

Fig. 4.16 shows the 2-parameter Weibull distribution of the negative discharge magnitudes of the three liquids. In Fig. 4.16, the distributions of the three liquids are almost identical. Table 4.3 shows the 50% value of 63.2% value of the discharge magnitudes. It can be seen that silica nanofluid has 10% higher discharge magnitude than that of mineral oil. And fullerene has the same value as that of mineral oil.



$\beta_1=1.35, \eta_1=3.91, \rho=0.98$
 $\beta_2=1.58, \eta_2=3.94, \rho=0.97$
 $\beta_3=1.27, \eta_3=4.33, \rho=0.99$

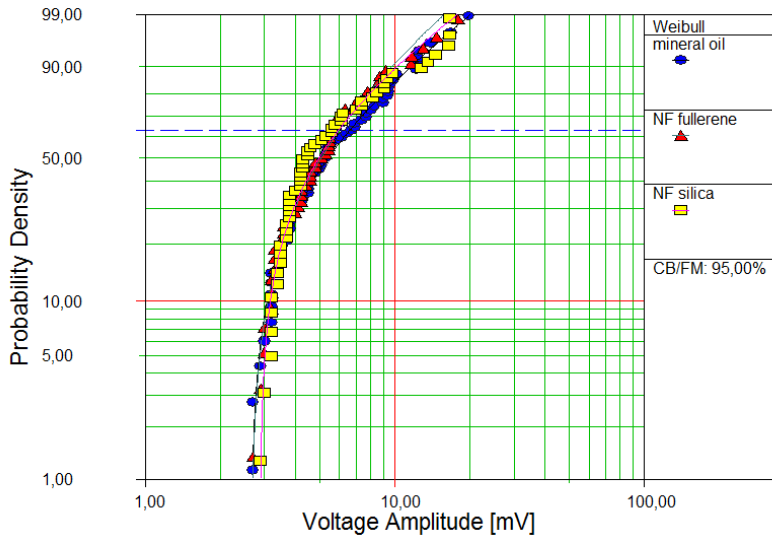
Figure 4.16 2-parameter Weibull distributions of the negative discharge magnitude in mineral oil, silica and fullerene nanofluids.

Table 4.4 Negative discharge magnitude of mineral oil, silica and fullerene nanofluids at 50% and 63.2% probabilities.

BD probabilities [%]	Mineral oil	0.01% SiO ₂ NF		0.01% fullerene NF	
	Discharge magnitude [pC]	Discharge magnitude [pC]	change	Discharge magnitude [pC]	change
50	2.9 (±0.5)	3.2 (±0.9)	+10%	3.1 (±0.6)	+7%
63.2	3.9 (±0.8)	4.3 (±1)	+10%	3.9 (±0.7)	0%

4.4.3.4 Voltage amplitude

Fig. 4.17 shows the 3-parameter Weibull distribution of negative voltage amplitude of single pulse of the three liquids. In Fig. 4.17, the distributions of the three liquids are almost the same. Table 4.5 shows the 50% value and 62.3% value of voltage amplitude. For the value at 63.2% probability, the silica and fullerene nanofluids both are around 10% lower than that of mineral oil.



$\beta_1=1,03, \eta_1=3,97, \gamma_1=2,64, \rho=0,99$
 $\beta_2=1,12, \eta_2=3,37, \gamma_2=2,64, \rho=0,99$
 $\beta_3=0,96, \eta_3=3,08, \gamma_3=2,87, \rho=0,98$

Figure 4.17 3-parameter Weibull distributions of the negative voltage amplitudes of discharge in mineral oil, silica and fullerene nanofluids.

Table 4.5 Negative voltage amplitude of mineral oil, silica and fullerene nanofluids at 50% and 63.2% probabilities

BD probabilities [%]	Mineral oil	0.01% SiO ₂ NF		0.01% fullerene NF	
	Voltage amplitude [mV]	Voltage amplitude [mV]	change	Voltage amplitude [mV]	change
50	5.4 (±1.1)	4.9 (±0.6)	-8%	5.0 (±0.8)	-6%
63.2	6.6 (±1.0)	5.9 (±1.4)	-10%	6.0 (±0.9)	-9%

4.4.3.5 Summary

The PD results under negative DC voltage in the three liquids differ a lot from the results under positive DC voltage. The numbers of pulses during one PD sequence under negative DC is much less than under positive DC voltage. For mineral oil, the negative discharge magnitude is around 20 times smaller than the positive value. The negative voltage amplitude is around 8 times smaller than the positive voltage amplitude. This phenomenon can be explained by the difference between positive and negative streamers introduced in section 4.2. The larger ionization zone in front of the positive charged needle allows positive streamer grow faster than negative streamer. The effect of the nanoparticles on the negative PD behaviour of mineral oil is not significant.

4.5 Discussion

Similar to the results of AC breakdown strength of mineral oil, silica and fullerene nanofluids, silica and fullerene nanofluids show increased inception voltages and decreased total discharge magnitudes than that of mineral oil, especially under positive DC voltage. The reduction due to 0.01% silica nanoparticles is more remarkable than fullerene nanoparticles. This is contrary to the expectation that conductive nanoparticles have more influence on the electrodynamic behaviour of mineral oil. The relaxation time constant of silica nanoparticles is too long to effect the PD dynamics in the oil. Hence the hypothesis is that the hydroxyl group on the surface of silica nanoparticles can adsorb water, acid or particles in the oil, which reduce the effect of these additives on the dielectric strength of mineral oil. This assumption can be verified by examining the constituents in mineral oil and nanofluids. Many materials have unique spectral fingerprints in the THz range, which means that THz radiation can be used to identify them. Fourier transform infrared terahertz spectroscopy (FTIR-THz) is used to study the interaction and vibration of large molecules. The terahertz band is located between light and radio waves and combines the characteristics of both, such as coherence and transparency. The detailed introduction of the FTIR-THz system will be given in appendix E. Recent studies showed that constituents in oils can be examined with terahertz spectroscopy and the results can be used to study the moisture content, oxidation level and acid value in the oil [23, 24].

A Fourier transform (FT) terahertz spectrometer (JASCO type) was used to measure the transmittance spectra of the mineral oil, silica and fullerene nanofluids at 3-18 THz. Fig. 4.18 shows the transmittance spectra of the liquids.

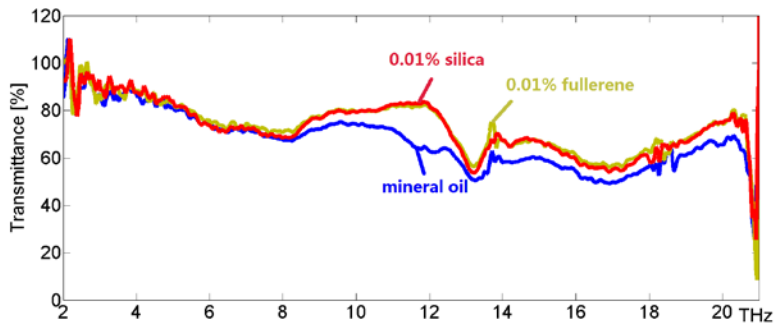


Figure 4.18 Transmittance of mineral oil, silica and fullerene nanofluids in the range of 3 to 18 THz.

The main difference between mineral oil and the nanofluids appears between 9 and 12 THz. A study shows that at 10.4 THz, the transmittance of insulating oil decreases due to an increase of acid value [24]. Mineral oil usually contains some weak organic acid, such as fatty acids. Theoretically, that fatty acid can be used as surfactants for treating nanoparticles. Hence, one possible explanation for the higher inception voltage and reduced partial discharge magnitudes due to nanoparticles is that acid is adsorbed on the surface of nanoparticles in the oil.

4.6 Summary

In order to evaluate the shape of the discharge pulses during the partial discharge process, a time-resolved detection setup with needle-plane electrode was built. The quantities which are used for comparing the PD phenomena for mineral oil, 0.01% silica and fullerene nanofluids are: inception voltage, PD duration, PD rise time, discharge magnitude and PD voltage amplitude.

For all the three fluids, the positive PD events show more pulses and higher voltage amplitudes than for the negative PD events. The positive discharge magnitude is around 20 times larger than the negative value. The positive voltage amplitude is around 8 times larger than the negative voltage amplitude. This phenomenon can be explained by the difference between positive and negative streamer introduced in section 4.2. The

larger ionization zone in front of the positive charged needle allows positive streamer grow faster than negative streamer.

Under positive DC voltage, the PD inception voltage of silica nanofluid is some 20% higher than that of mineral oil. The discharge magnitudes of silica nanofluid and fullerene nanofluids are both lower than that of mineral oil. For silica nanofluid, the reduction is 60%, and for fullerene nanofluid the reduction is 33%. From the observation of one PD sequence, the main difference among the three fluids is the numbers of pulses in one PD sequence, which for mineral oil is 2.8 times higher than that for silica nanofluid and 1.9 times higher than that for fullerene nanofluid. The voltage amplitude of mineral oil is reduced by 16% due to the additional silica nanoparticles and 4% due to fullerene nanoparticles. Under negative DC voltage, the effect of 0.01% silica and fullerene nanoparticles on the PD behaviour of mineral oil is not significant.

The relaxation time constant of silica nanoparticles is too long to capture any electrons in the oil. Hence the mechanism behind the PD reduction due to silica nanoparticles can be hypothesized to be that the hydroxyl group on the surface of silica nanoparticles can adsorb water, acid or particles in the oil, which reduce the effect of these additives on the dielectric strength of mineral oil. This assumption can be verified by examining the constituents in mineral oil and nanofluids. According to the results of the transmittance spectra of the mineral oil, silica and fullerene nanofluids at 3-18 Hz, one possible explanation is that the hydroxyl groups on the nanoparticle could adsorb acid in the mineral oil. This leads to less effect of acid on the partial discharge behaviour in the nanofluids. The larger effect of silica nanoparticles on the dielectric strength of mineral oil compared with fullerene nanoparticles can be a result of the combination of acid and moisture adsorption on the surface of the nanoparticles.

4.7 References

- [1] O. Lesaint and T.V. Top, "Streamer Initiation in Mineral Oil part I", IEEE Transactions on Dielectrics and Electrical Insulation, Vol. 9, pp. 84-91, 2002.
- [2] T.V. Top and O. Lesaint, "Streamer Initiation in Mineral Oil part II", IEEE Transactions on Dielectrics and Electrical Insulation, Vol. 9, pp. 92-96, 2002.
- [3] H. Yamashita, H. Amano and T. Mori, "Optical Observation of Pre-breakdown and Breakdown Phenomena in Transformer oil", Journal of Physics D: Applied Physics, Vol. 10, pp. 1753-1760, 1976.

- [4] D. Linhjell, L. Lundgaard and G. Berg, "Streamer Propagation under Impulse Voltage in Long Point-plane Oil Gaps", IEEE Transactions on Dielectric and Electrical Insulation, Vol.1, pp. 447-458, 1994.
- [5] J.F. Kolb, R.P. Joshi, S. Xiao and K.H. Schoenbach, "Streamer in Water and Other Dielectric Liquids", Journal of Physics D: Applied Physics, Vol. 41, pp. 1-22, 2008.
- [6] R.E. Hebner, *Measurement of Electrical Breakdown in Liquids*, NATO ASI series, Vol. B193, Plenum press, 1988.
- [7] O. Lesaint, "Propagation of Positive Discharges in Long Liquid Gaps", Proceeding of the 12th International Conference on Conduction and Breakdown in Dielectric Liquids, pp. 161-166, 1996.
- [8] O. Lesaint and P. Gournay, "Initiation and Propagation Thresholds of Positive Prebreakdown Phenomena in Hydrocarbon Liquids", IEEE Transactions on Dielectrics and Electrical Insulation, Vol. 1, pp. 702-708, 1994.
- [9] H. Yamashita, K. Yamazawa and Y.S. Wang, "The Effect of Tip Curvature on the Prebreakdown Streamer Structure in Cyclohexane", IEEE Transactions on Dielectrics and Electrical Insulation, Vol. 5. pp. 396-401, 1998.
- [10] A. Denat, J.P. Gosse and B. Gosse, "Electrical Conduction of Purified Cyclohexane in a Divergent Electric Field", IEEE Transactions on Dielectric and Electrical Insulation, Vol. 23, pp. 545-554, 1988.
- [11] M. Haidara and A. Denat, "Electron Multiplication in Liquid Cyclohexane and Propane", IEEE Transaction on Electrical Insulation, Vol. 26, pp. 592-597, 1991.
- [12] R. Katten, A. Denat and O. Lesaint, "Generation, Growth and Collapse of Vapor Bubbles in Hydrocarbon Liquids under a High Divergent Electric Field", Journal of Applied Physics, Vol. 66, pp. 4062-4066, 1989.
- [13] N.V. Dung, F. Mauseth and H.K. Hoidalen, " Streamers in Large Paraffinic Oil Gap", Proceeding of the International Conference on Conduction and Breakdown in Dielectric Liquids, paper 113, 1996.
- [14] L. Dumitrescu, O. Lesaint, N. Bonifaci and A. Denat, "Study of Streamer Inception in Cyclohexane with a Sensitive Charge Measurement Technique Under Impulse Voltage", Journal of Electrostatics, Vol. 53, pp. 135-146, 2001.
- [15] IEC Publication 60270, *High Voltage test techniques – Partial Discharge Measurement*, 2000.
- [16] F.M. O'Sullivan, "A Model for the Initiation and Propagation of Electrical Streamers in Transformer Oil and Transformer Oil Based Nanofluids", PhD thesis, Massachusetts Institute of Technology, 2007.
- [17] D.A. Bolliger, "Influence of the Chemical Composition of Dielectric Fluid on Partial Discharge Characteristics for Diagnostic Purposes", Doctoral Dissertations, University of Connecticut Institute of Materials Science, 2013.
- [18] W. Sima, C. Jiang, P. Lewin, Q. Ynag and T. Yuan, "Modelling of the Partial Discharge Process in a Liquid Dielectric: Effect of Applied voltage, Gap Distance and Electrode Type", Journal Energies, Vol. 6, pp. 934-952.
- [19] H. Raether. *Electron avalanches and Breakdown in Gases*, Butterworth, London, 1964.
- [20] N. Pattanadach, F. Paratomosiwi, B. Wieser, M. Baur and M. Muhr, "The Study of Partial Discharge Inception Voltage of Mineral Oil Using Needle-Plane Electrode Configuration", Proceeding of International Conference on High Voltage Engineering and Application, pp.174-177, 2012.
- [21] P.H.F. Morshuis, "Partial Discharge Mechanisms: Mechanism Leading to Breakdown, Analyzed by Fast Electrical and Optical Measurements", PhD thesis, Technische Universiteit Delft, the Netherlands, 1993.
- [22] Z. Liu, Q. Liu, Z.D. Wang, P. Jarman, C.H. Krause, P.W.R. Smith and A. Gyore, "Partial Discharge Behaviour of Transformer Liquids and the Influence of Moisture Content", IEEE International Conference on Liquids Dielectrics, Bled, Slovenia, 2014.

- [23] R. Ogura, N. Nishimura, S. Matsumoto, M. Mizuno and K. Fukunaga, "Transmittance Characteristics of Various Insulating Oils Evaluated by Terahertz Spectroscopy", XVII International Symposium on High Voltage Engineering, Hannover, Germany, 2011.
- [24] N. Nishimura, Y. Takaku, S. Matsunoto, K. Fukunaga and M. Mizuno, "Transmittance Characteristic of Insulating Oil in Terahertz Wave-band", The 4th South East Technical University Consortium, Vol. E-09, pp. 192-195, 2010.

5 Thermal Conductivity

5.1 Introduction

In an oil-filled transformer, the magnetic circuit and windings are the main sources of losses. The heat generated due to all these losses must be conducted to the environment without allowing the core, winding and structural parts to reach a temperature that will cause deterioration of insulation [1]. So transformer oil needs to have a good thermal conductivity to conduct the heat generated in the core and windings. Heat conduction into the oil will cause a local temperature rise around the core and winding area, which results in a temperature difference within the oil. The temperature difference will cause a density variation in the oil. This variation will bring natural convection into play, the convection will pass the heat to the walls of the tank, and from there it dissipates into the atmosphere. Therefore, the transformer oil's most important intrinsic properties for heat transfer are thermal conductivity and convection.

This convection relies upon the "natural circulation" produced by the difference in density between the liquid's hotter part and its cooler part. The natural convection flow is therefore very dependent on the fluids' viscosity [2]. The results of nanofluids shown in Chapter 3 indicate that the addition of up to 0.1% of nanoparticles has a negligible effect on the mineral oil's viscosity. Therefore natural convection of nanofluids will not be researched here.

For the thermal conductivity of nanofluids, a rapid progress has taken place in research activities concerning the extraordinary enhanced thermal conductivity of nanofluids [3-10]. Thus, the focus of this chapter is on the thermal conductivity of mineral oil-based nanofluids.

This chapter contains the theoretical background, and the experimental and modelling results concerning the thermal conductivity of mineral oil and nanofluids. Section 5.2 starts with an introduction of the mechanism of heat-transfer conduction in liquids. Then, Section 5.3 contains a literature review on the thermal conductivity of nanofluids. Additionally, this section contains a description of the effect of nanoparticles on the thermal conductivity of the base fluids and the possible mechanisms of the enhanced thermal conductivity of nanofluids. Section 5.4 introduces the methods of measuring the thermal conductivity of nanofluids. The

experimental and modelling results of mineral oil-based nanofluids are given in Sections 5.5 to 5.7.

5.2 Conduction heat transfer in liquids

In liquid, heat transfer has three modes: conduction, convection and radiation. Conduction is caused by molecular vibration, which takes place even if the medium is at rest. Convection is the heat transfer that happens because of the mass motion of a fluid when the heated fluid is caused to move away from the source of heat. Radiation is due to emission and absorption of energetic particles or waves. Among these three modes, conduction is the most thoroughly understood phenomenon, since it signifies the liquid's inherent ability of heat transfer, and it can be studied even when liquids remain at rest. Thermal conductivity is a measure of a medium's capability to conduct heat. Thermal conductivity depends on the material and on the temperature.

The French scientist Joseph Fourier in 1822 developed the first comprehensive theory for heat conduction. According to Fourier's law, the heat flux in the direction of heat flow is proportional to the temperature gradient in that direction. The equation can be described as:

$$q_x = \frac{Q_x}{A} = -k \frac{dT}{dx} \quad (5.1)$$

Where q_x is the heat flux in the x direction, Q_x is the heat flowing in the x direction, A is the area perpendicular to x through which heat flows, and k is the constant of proportionality, known as the thermal conductivity [3].

Fig. 5.1 shows the range of the thermal conductivity of different materials. This figure shows that non-metallic liquids, which are commonly used as coolants, have one to three orders of magnitude lower thermal conductivity than solids. Conduction occurs by longitudinal molecular vibration with the velocity of sound, and the kinetic energy is transferred during molecular impact. In liquids, the molecules are much further apart from each other than in solids; therefore, the amount of heat transfer by conduction is also less in liquids than it is in solids.

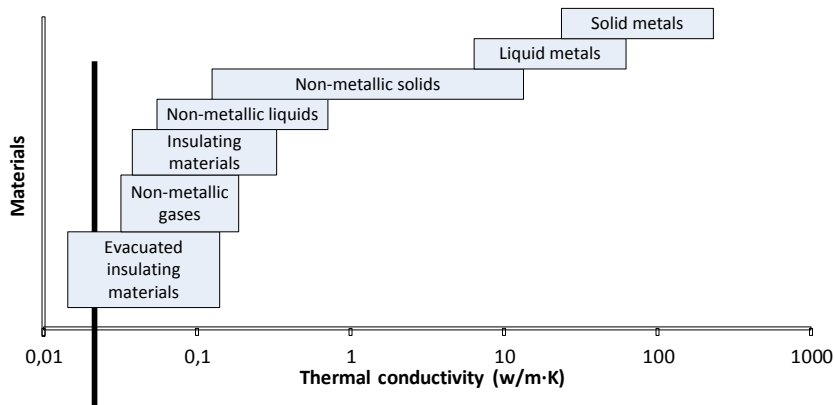


Figure 5.1 Ranges of values of thermal conductivity of various materials [3].

5.3 Thermal Conductivity of Nanofluids

The low thermal conductivity of conventional heat transfer in liquids limits the improvement of performance and compactness of engineering equipment. Because solids possess higher thermal conductivity than liquids, liquids containing a suspension of solid particles are expected to exhibit significant improvement in thermal conductivity. The early studies on the thermal conductivity of suspensions containing millimetre and micrometre-sized particles encountered the problems of rapid settling of particles, particles clogging the flowing channel, and low thermal conductivities at low particle concentrations [4].

Modern nanotechnology made the dispersing of nanometre-sized particles possible in traditional heat-transfer liquids, known as nanofluids. The studies showed that the thermal conductivity of nanofluids strongly depends on the particles' thermal conductivity, on the nanoparticles' size and shape, on the particle concentration, on the aggregations, and on the base-fluid material's properties, temperature and acidity [3-10]. Although the studies of thermal properties of nanofluids are numerous, many conflicting results arise due to the poor characterization of nanofluids and to the inaccuracies in measuring techniques. The stability of nanofluids is still a big issue because nanofluids are prone to forming agglomeration and settling, which possibilities researchers should carefully check.

Four possible reasons exist for the contribution of nanoparticles to the increase of the thermal conductivity [11]:

- Brownian motion of the particles
- the molecular level layering of the liquid at the liquid /solid interface
- the nature of the heat transport in the nanoparticles
- the effect of nanoparticle clusters.

In nanofluids, the nanoparticles are in constant and random movement in the base fluid due to Brownian motion. Such a motion enables direct particle-to-particle heat transport and induces the convective flow of the surrounding fluid, which flow is also called micro-convection [12]. However, another study concluded that the Brownian motion of nanoparticles was too slow in transporting heat through a liquid. This Brownian motion plays an important indirect role in forming nanoparticle clusters, which formations can significantly influence the thermal conductivity [11].

Some studies have proposed that liquid molecules form a layered structure at the liquid/solid interface [11]. The liquid layer's atomic structure is more ordered than the base fluid's [11]. The liquid layer at the interface acts as a thermal bridge between the nanoparticles and the base fluid, which bridge is the key to enhancing the thermal conductivity of the nanofluid [14].

The nature of the heat transport in the nanoparticles is mainly due to the phonon transport in nanoparticles. In non-metal solids, heat is carried by phonons, the thermal vibration of the atoms. These phonons travel at the speed of sound in random directions. The mean free path of a phonon is the distance a phonon travels in a material. When the particle size and the separation between the particles are both small enough to allow the phonons to be initiated from a particle and transmitted to another particle, then the heat transport is significantly increased [11]. However, another study detected thermal resistance at the liquid/solid interface, which resistance is caused by phonon scattering. The phonon scattering is caused by the different rates of phonon transport in the two materials [15]. Unfortunately, the phonon-interface-scattering phenomenon is not well understood.

Recently, a study has shown that clusters of nanoparticles create a local percolation with a lower thermal resistance for heat flow, which resistance leads to the enhanced thermal conductivity in nanofluids [11].

5.4 Thermal conductivity measurement techniques for nanofluids

The generally used methods of measuring the thermal conductivity of nanofluids are the transient hot-wire method, the 3ω method, the thermal constants analyser method, the cylindrical cell method, the temperature oscillation method, and the thermal comparator method [16].

The transient hot-wire method is the oldest and most widely used method. In this method, a thin metallic wire is surrounded by liquid, whose thermal conductivity is to be measured. The wire is used as both a heat source and as a temperature sensor [3]. The wire is heated by applying a constant current into it. The heat dissipated in the wire increases the liquid's temperature. The thermal conductivity determines the liquid's temperature increase [17]. The advantages of hot-wire method are the elimination of natural convection effect, a faster experimental response, and easier setup [16].

The 3ω method is quite similar to the transient hot-wire method as it also uses a radial flow of heat from a single element, which acts both as the heater and as the thermometer. The main difference is that the transient hot-wire method uses a time-dependence response while the 3ω method uses an electric current frequency-dependent response [16].

The thermal constants analyser has the same fundament as the transient hot-wire method. It utilizes the transient plane source (TPS) theory to calculate the thermal conductivity of nanofluid. The TPS element behaves both as temperature sensor and as the heat source. The experimental setup consists of a thermal constants analysis, a vessel, a constant temperature bath, and a thermometer. The probe of the thermal constants analyser is immersed vertically into the nanofluid. The thermal conductivity of the nanofluid is determined by measuring the resistance of the probe [17]. In order to avoid natural convection, the parameters of the analyser should be controlled properly.

The cylindrical cell method is one of the most common steady-state methods used for measuring thermal conductivity of liquids. The equipment consists of a coaxial inner cylinder and an outer cylinder. The nanofluids whose thermal conductivities need to be measured fill the annular space between the two cylinders. Inside the inner cylinder, an

electrical heater is placed. During the experiment, heat flows in the radial direction outwards through the test liquid. Two calibrated Fe–Constantan thermocouples are used to measure the outer surface temperature of the heater and of the inner cylinder. Then the thermal conductivity of the nanofluid can be calculated from the two temperatures, the adjusted voltage, and current of the heater [18].

The temperature oscillation method is based on the propagation of a temperature oscillation inside a cylindrical liquid volume. The measured temperature response of the nanofluid is the result of averaged or localized thermal conductivity in the direction of the nanofluid's chamber height [17].

The thermal comparator method is an indirect technique, based on the principle that when two materials at different temperatures are brought into contact over a small area, heat transfer takes place from the hotter to the colder body. In this method, a heated probe is used, and the temperature between the body of the probe and the tip that makes contact with the sample is measured. The measurement is almost instantaneous. However, precaution and distorting factors should be considered when using this method [17].

5.5 Experimental results of the thermal conductivity of silica and fullerene nanofluids

The thermal conductivity of fullerene and silica nanofluids was measured with the hot-wire method. Silica and fullerene nanoparticles both have positive effects on breakdown strength of mineral oil. Since the nanofluids are to be used as coolants in the transformer, testing the effect of these two nanoparticles on the thermal conductivity of mineral oil. The effects of temperature, time, different materials and particle concentrations on the thermal conductivity of mineral oil were examined. Table 5.1 shows the single particle size, cluster size, and thermal conductivity of the silica and fullerene nanoparticles. Both types of nanoparticles have a spherical shape.

Table 5.1 The particle size and thermal conductivity of silica, titania and fullerene nanoparticles.

Particle type	Nanoparticle size [nm]	Cluster size in the nanofluids [nm]	Thermal conductivity [W/m·K]
Silica	10-20	120	1.38
Fullerene	1	40	0.4

5.5.1 Test Setup

The thermal conductivity of nanofluids is measured with the “Lambda” system, which was purchased from PSL Systemtechnik GmbH. The choice was made due to the advantages of the method, which are the elimination of the natural convection effect, its fast experimental response, and its easy setup.

The operation principle is based on the transient hot-wire method, according to standard ASTM D2717. The hot-wire method is based on the transfer of heat from a controlled source to a material, and the measurement of the temperature changes caused by heat dissipation to determine the thermal properties as a function of time. This optimized electronic device guarantees relatively short measuring times and no additional problems with convection caused by the ignition of the electric energy input to the heat-wire instrument. The measuring principle of the hot-wire method is as follows: A platinum wire with 0.1 mm diameter and a temperature sensor are inserted into the fluid sample (around 50 ml), a constant voltage is applied to the wire to heat it up, which results in a constant heat stream to the surrounding liquid, the resistance of the platinum wire increases, and a decrease of voltage can be monitored. Due to those changes in voltage, the thermal conductivity can be determined. The governing equation of this phenomenon is derived from the non-stationary heat diffusion, Fourier equation with proper boundary condition. Neglecting heat losses from convection and radiation, the diffusion leads to:

$$k = \frac{q}{4\pi(T_1 - T_2)} \cdot \ln \frac{t_2}{t_1} \quad (5.2)$$

Where k is the thermal conductivity of liquid, T_1 and T_2 represent the temperature of the heat source at times t_1 and t_2 , respectively, and q is the heat flow per unit length of the source.

Fig. 5.2 shows the components of the machine. The system consists of the base unit Lambda (on the left side), which calculates the thermal conductivity of the liquid and the thermostat unit “LabTemp 30190” (on the right side), which controls the temperature of the liquid. The sensor head is connected to the Lambda unit and inserted into the thermostat unit, which setup is shown in detail in Fig. 5.3. The sensor head consists of a heat wire, a temperature sensor, a sample cup with an inside thread to screw to the sensor head, and a sensor plug to connect the lambda unit. The accuracy of this system is 1%.



Figure 5.2 Lambda measuring system.



Figure 5.3 Lambda sensor head.

5.5.2 Thermal conductivity as a function of temperature

This section includes a discussion of the measurements of the thermal conductivities of mineral oil, silica and fullerene nanofluids as a function of

temperature. The thermal conductivity of mineral oil decreased with an increase of temperature. The reason for this decrease is that the density of mineral oil is lower at higher temperatures. Temperature also had an influence on the Brownian motion of the nanoparticles. The Brownian motion of the nanoparticles is more intense at higher temperatures [19]. Some studies have shown that nanofluids exhibit more of an enhancement of thermal conductivity than base fluids at higher temperatures [19, 20]. For the effect of mass fraction of nanofluids, studies have shown that the thermal conductivity of nanofluids increases as the mass fraction increases [19, 21-23]. The explanation of this behaviour can be that at higher mass fractions, the distance between nanoparticles decreases, so the particle to particle heat transfer in nanofluids increases.

Both silica and fullerene nanofluids were prepared with 0.01% and 0.1% mass fraction. The reason for choosing these fillgrades stems from the limits of the achieved stability of the nanofluids. To measure the thermal conductivity as a function of temperature from 10°C to 80°C, measurements take two to three hours. Hence the nanofluids need to be stable for at least three hours. For silica nanofluid, 0.1% was the highest concentration for which a stable suspension could be achieved. Figures 5.4 and 5.5 show the measurement results of the thermal conductivity of silica and fullerene nanofluids.

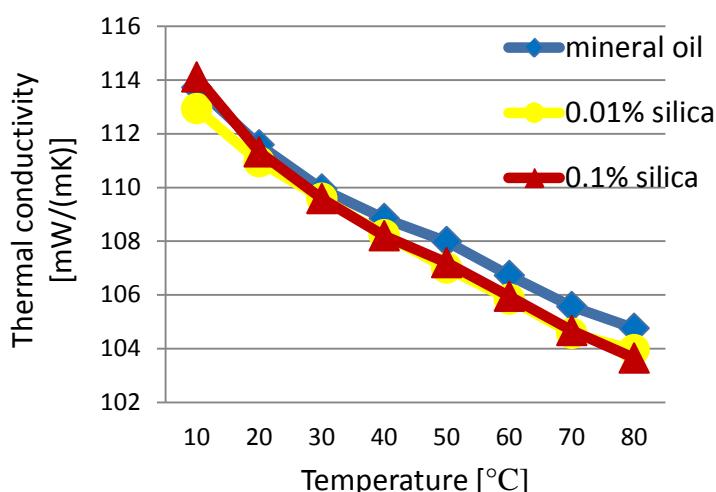


Figure 5.4 Thermal conductivity of silica nanofluids as a function of temperature.

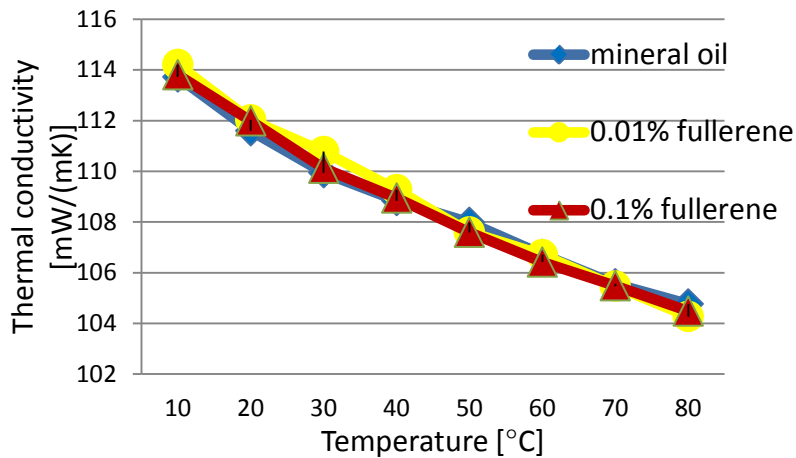


Figure 5.5 Thermal conductivity of fullerene nanofluid as a function of temperature.

Fig. 5.4 and 5.5 show that up to 0.1%, both silica and fullerene nanofluids have a negligible effect on the thermal conductivity of mineral oil. A possible explanation is that the concentrations of the nanofluids are too small to have any effect on the mineral oil. In the reviewed relevant literature, the lowest mass fraction of nanofluids that had a positive effect on the thermal conductivity of nanofluids was 0.5% [19, 21, 23].

5.5.3 Thermal conductivity as a function of time

For this section, the mass fraction of the nanofluids is increased to 0.5%. The thermal conductivity of the nanofluids was analysed as a function of time. In 0.5% silica nanofluid, aggregations were formed and settled within two hours. The duration of the tests was two hours. The study showed that the aggregation and settling of nanoparticles can hinder the thermal conductivity of nanofluids [24]. As other studies have shown, the clusters of nanoparticles create a local percolation, which creates a path with a lower thermal resistance for heat flow, which then leads to the enhanced thermal conductivity in nanofluids [11]. Hence, the two-hour duration tests can also be used to analyse the effect of aggregations on the thermal conductivity of mineral oil.

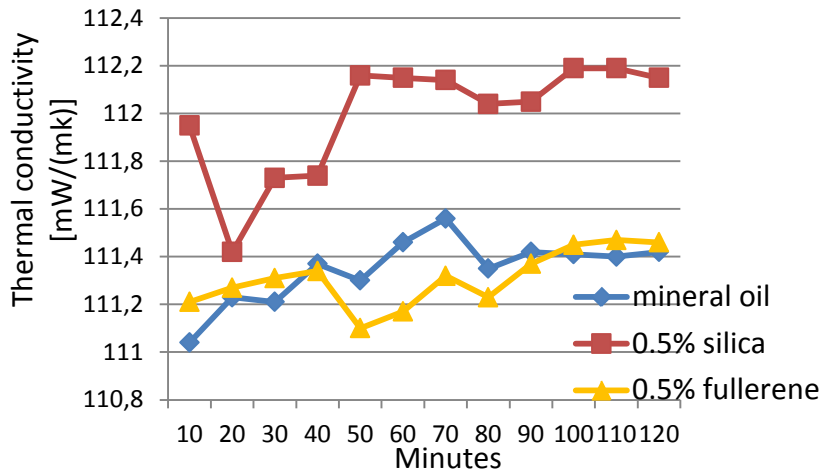


Figure 5.6 Thermal conductivity of mineral oil, 0.5% silica and fullerene nanofluids in function of time.

Fig. 5.6 shows that 0.5% silica has a higher thermal conductivity than the other two fluids, especially after 40 minutes. The enhancement is only by 1%, which is within the accuracy of the instrument. So the enhancement is still negligible. To achieve an increased thermal conductivity by adding nanoparticles, the mass fraction has to increase. The thermal conductivity of silica nanofluid shows changes during the first 40 minutes, which might be due to the forming of agglomerations. However the changes are still less than 1%, which amount is too small to make a conclusion about the effect of agglomeration of silica nanoparticles. During the two-hour test, no agglomerations were formed in fullerene nanofluids, which finding was discussed in Chapter 2. So the test results of the thermal conductivity of fullerene nanofluid didn't show any change.

5.5.4 Summary

The thermal conductivity of silica and fullerene nanofluids has been measured by means of the hot-wire method, and the effects of temperature, mass fraction and time on the thermal conductivity of nanofluids were analysed. The experimental results with the hot-wire method lead to the conclusion that up to a 0.5% concentration of both nanoparticles has a negligible effect on the thermal conductivity of mineral oil.

5.6 Modelling results of the thermal conductivity of silica and fullerene nanofluids

To examine the effect of higher particle concentration on the thermal conductivity of silica and fullerene nanofluids, the thermal conductivity of nanofluids was simulated with the conduction heat transfer module of the COMSOL Multiphysics software. The COMSOL Multiphysics is a finite element analysis, solver and simulation software/FEA software package for various physics and engineering applications. The heat transfer module provides users with interfaces and tools for heat transfer by conduction, convection and radiation. The conduction heat transfer can be modelled in solids and in fluids, or in combination. A more detailed description of the conduction transfer module of COMSOL is in Appendix D.

Sections 5.2 and 5.3 mention that the heat in non-metal solids and in mineral oil is carried by phonons. If the particle size and separation distance between the nanoparticles are small enough, the phonons can be initiated from a particle and transmitted to another particle, and then the heat transport is significantly increased [11]. However, phonon scattering can also cause thermal resistance due to the different rates of phonon transport in the two materials [15]. The results in Sections 5.5.1 and 5.5.2 can lead to the conclusion that small mass fractions of silica and fullerene nanoparticles don't help to improve the thermal conductivity of mineral oil. The possibility exists that losses are generated on the solid/liquid interface and on the interface of the nanoparticles inside a cluster caused by phonon scattering.

In this section, the focus is on the effect of thermal losses and particle concentration on the thermal conductivity of nanofluids. The cluster size of all the nanoparticles in the nanofluids is much larger than the single particle size. Thus, inside the clusters are interfaces among the single nanoparticles. The concentrations of the nanofluids are 0.1%, 1% and 10% mass fraction.

1) Silica nanofluids

For silica nanofluids, the cluster size is 120 nm, on average, and the single particle size is 15 nm, on average. The amount of nanoparticles inside these clusters can be estimated from the volume of the cluster and the volume of a single nanoparticle, based on the following:

$$n_{silica} \approx 0.637 * \frac{v_{cluster}}{v_{nanoparticle}} \approx 0.637 * \frac{\frac{4}{3}\pi * (\frac{120}{2})^3}{\frac{4}{3}\pi * (\frac{15}{2})^3} \approx 512 \quad (5.4)$$

Where n_{silica} is the amount of silica nanoparticles inside a cluster, the value 0.637 is the maximum packing function in the cluster, $v_{cluster}$ is the volume of a silica cluster, and $v_{nanoparticle}$ is the volume of a silica nanoparticle. After estimation, around 512 nanoparticles are inside the cluster.

The total surface (A_t) of the silica nanoparticles inside a 120 nm cluster can be estimated as:

$$A_t \approx n_{silica} * 4\pi * (\frac{15}{2})^2 \approx 3.62 \times 10^5 \text{ nm}^2 \quad (5.5)$$

The effective surface area is defined as the surface area where the silica cluster has contact with the nanofluids (A_e). This area can be estimated as:

$$A_e \approx 4\pi * (\frac{120}{2})^2 \approx 4.52 \times 10^4 \text{ nm}^2 \quad (5.6)$$

The ratio (k) between the total surface area and effective surface is as follows:

$$k = \frac{A_t}{A_e} \approx 8 \quad (5.7)$$

According to the estimation, eight times higher thermal losses are caused by the interface among the single silica particles inside the cluster. To build the model with thermal losses taken into account, instead of introducing 512 thermal barriers, the particle size was reduced in the model. In the model the cluster size was decreased eight times from the cluster size of 120 nm. Fig. 5.7 shows the geometry and total heat flux in the silica nanofluid. The silica nanoparticles have higher heat flux than the host fluids. The input value for the model is the thermal conductivity of the oil and nanoparticles. The temperatures of the right and left sides are set as 180°C and 20°C.

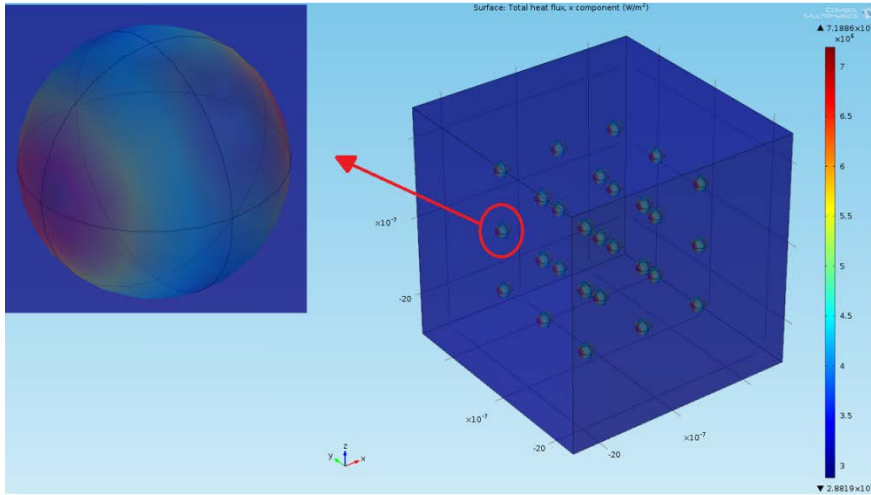


Figure 5.7 Heat flux density in 10% silica nanofluid.

Fig. 5.8 shows the comparison between the thermal conductivity 0.1% silica nanofluid modelled with COMSOL and the experimental data. The values of the modelling result and experimental results are almost the same.

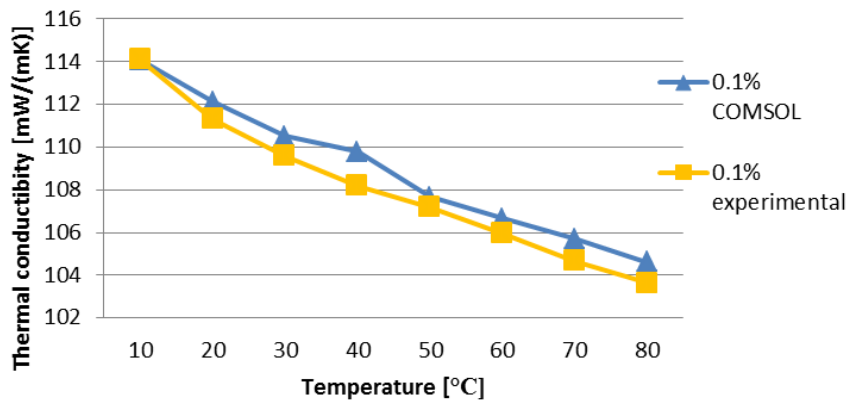


Figure 5.8 Comparison between the experimental and modelling results of thermal conductivity of silica nanofluid.

Fig. 5.9 shows the enhancement of the thermal conductivity of mineral oil due to silica nanofluid. The particle concentrations are 0.1%, 1% and 10% mass fraction. If the thermal losses are taken into account, the enhancement is only 0.8% when the concentration is 10%. If the thermal losses are not considered, then the enhancement of the thermal

conductivity is much higher. With 10% silica nanoparticles, the enhancement is 12%.

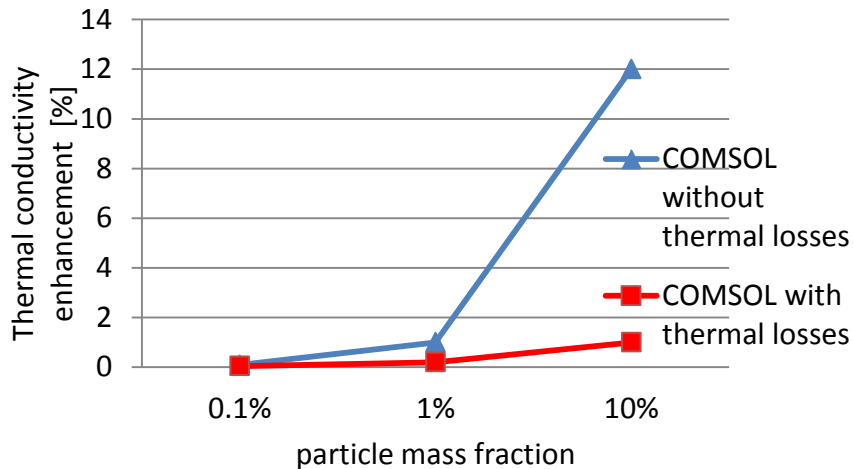


Figure 5.9 Thermal conductivity of silica nanofluids modelled with COMSOL.

2) Fullerene nanofluids

The method to estimate the thermal losses in a fullerene cluster is the same as for silica nanofluids. After estimation, 25 times higher thermal losses arise due to the interface in the fullerene cluster. So the cluster size was decreased 25 times in the model. Compared with silica nanofluid, the particle size is much smaller. The thermal conductivity of fullerene is also smaller than silica. Hence it is expected that the fullerene nanofluid has less effect on the thermal conductivity of the mineral oil. Fig. 5.10 shows the modelling and experimental results of the thermal conductivity of 0.1% fullerene nanofluid and that the values are almost the same. Fig. 5.11 shows the comparison between the thermal conductivity of fullerene nanofluids with thermal losses and without thermal losses. When the thermal losses are taken into account, no effect takes place on the thermal conductivity. If the thermal losses are not taken into account, 10% fullerene nanoparticles improve the thermal conductivity of mineral oil by 1.3%.

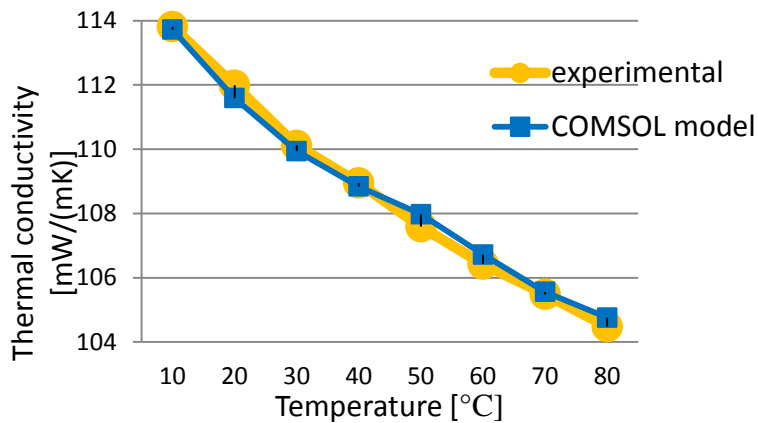


Figure 5.10 Comparison between the experimental and modelling results of thermal conductivity of 0.1% fullerene nanofluid.

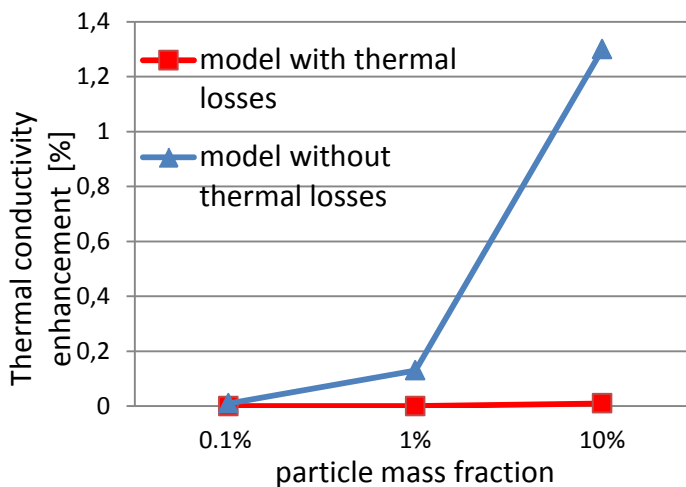


Figure 5.11 Thermal conductivity of fullerene nanofluids modelled with COMSOL.

5.7 Experimental results of thermal conductivity of other types of nanofluids

The negligible effect of silica and fullerene can also be due to the low thermal conductivity of the two materials. In this chapter, the thermal conductivities of copper and titania nanofluids are compared with those of silica and fullerene nanofluids. Titania has a thermal conductivity of 11.7 W/mK, which is around eight times higher than silica and 29 times higher than fullerene. Copper's thermal conductivity is 401 W/mk, which is 290

times higher than silica's and 1000 times higher than fullerene's. The thermal conductivity of the nanofluids was measured in function of time. All the nanofluids were prepared with 0.5% mass fraction.

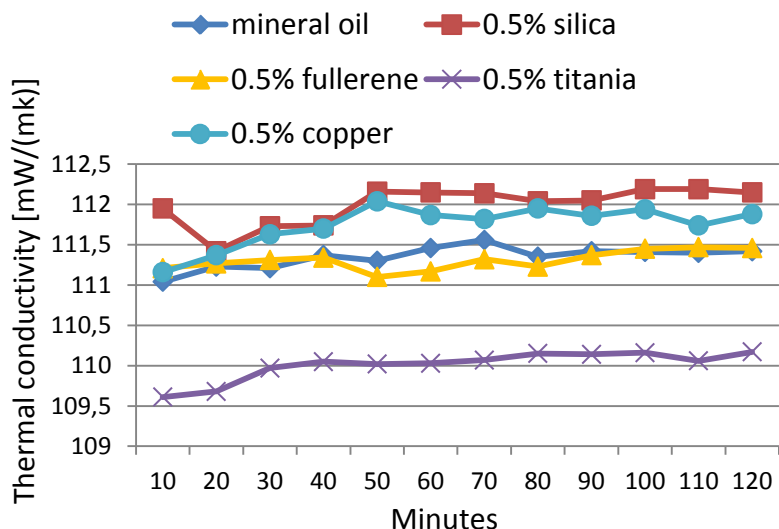


Figure 5.12 Thermal conductivity of mineral oil, 0.5% silica, fullerene, titania, and copper nanofluids as a function of time.

Fig. 5.12 shows that copper and silica nanofluids have similar thermal conductivity values. Titania nanofluid shows a decreased thermal conductivity, and the decrease is up to 1.4%. Copper and titania both have much higher thermal conductivities than silica, but the thermal conductivity of these nanofluids is not higher than that of silica nanofluid.

5.8 Discussion and summary

In this chapter, the measurements of the thermal conductivities of silica and fullerene nanofluids were described. Unfortunately due to the low mass fraction of these nanofluids, the effect on the thermal conductivity of mineral oil due to the two types of nanoparticles was negligible. Based on the COMSOL software's help taking the thermal losses into account, up to 10% fullerene nanofluid had no effect on the thermal conductivity of mineral oil, and 10% silica nanofluids showed a 0.8% enhancement. In an ideal situation, with no thermal losses, the thermal conductivity had a higher improvement rate, according to the simulation. Silica nanofluid with 1% mass fraction increased the thermal conductivity of mineral oil by 1%.

Silica nanofluid with 10% mass fraction showed an 18% enhancement. Fullerene nanofluid with 10% mass fraction can achieve a 1.3% enhancement.

The thermal conductivities of both silica and fullerene is quite low. So the thermal conductivity of titania and copper nanofluids were measured. Titania and copper both had much higher thermal conductivities than silica and fullerene. However, the results showed that 0.5% copper nanofluid has a similar value to 0.5% silica nanofluid, and titania nanofluid showed a lower thermal conductivity than silica nanofluid.

The thermal conductivity of nanofluid depends not only on the thermal conductivity of the particles, but also on the nanoparticle's size and shape, on the particle concentration, on aggregations, and on the base-fluid material's properties, temperature and acidity. Furthermore, the stability of nanofluids is still a big issue because nanofluids are prone to forming agglomerations and settling, especially at higher particle concentrations. The aggregation and settling of nanoparticles can hinder the thermal conductivity of nanofluids [24], so clustering of nanoparticles in the base fluid must be solved before other technical experiments.

5.9 References

- [1] S.V. Kulkarni and S.A. Khaparde, *Transformer Engineering: Design and Practice*, CRC Press, 2004.
- [2] M. Heathcote, *J & P Transformer Book*, Technology & Engineering, 2011.
- [3] S.K. Das, S.U.S. Choi, W. Yu and T. Pradeep, *Nanofluids: Science and Technology*, Wiley-Interscience, 2008.
- [4] J. Philip and P.D. Shima, "Thermal Properties of Nanofluids", *Advances in Colloid and Interface Science*, Vol. 183-184, pp. 30-45, 2012.
- [5] J.A. Eastman, S.U.S. Choi, L.J. Thompson and S. Lee, "Enhanced Thermal Conductivity Through the Development of Nanofluids," *Materials Research Society Symposium Proceedings*, pp. 3-11, 1996.
- [6] M. Liu, M. Lin, I. Huang and C. Wang, "Enhancement of Thermal Conductivity with CuO for Nanofluids", *Chemical Engineering & Technology*, Vol. 29, pp. 72-77, 2006.
- [7] Y. Hwang, H.S.K. Par, J.K. Lee and W.H. Jung, "Thermal Conductivity and Lubrication Characteristics of Nanofluids", *Current Applied Physics*, Vol. 6, pp. 67-71, 2006.
- [8] W. Yu, H. Xie, L. Chen and Y. Li, "Investigation of Thermal Conductivity and Viscosity of Ethylene Glycol based ZnO Nanofluid", *Thermochimica Acta*, Vol. 491, pp.92-96, 2009.
- [9] L.S. Sundar, M.K. Singh, E.V. Ramana, B. Singh, J. Grácio and A.C.M. Sousa, "Enhanced Thermal Conductivity and Viscosity Ofnanodiamond-Nickel Nanocomposite Nanofluids", *Scientific Reports*, Vol. 4, pp. 1-14, 2014
- [10] B.T. Branson, P.S. Beauchamp, J.C. Beam, C.M. Lukehart and J.L. Davidson, "Nanodiamond Nanofluids for Enhanced Thermal Conductivity", *ACS Nano*, Vol. 4, pp. 3183-3189, 2013.
- [11] P. Keblinski, S.R. Rphillpot, S.U.S. Choi and J.A. Eastman, "Mechanisms of Heat Flow in Suspensions of Nano-sized Particles (Nanofluids)", *International Journal of Heat and Mass Transfer*, Vol. 45, pp.855-863, 2002.

- [12] L. Wnag and J. Fan, "Toward Nanofluids of Ultra-High Thermal Conductivity", *Nanoscale Research Letters*, Vol. 6, pp.1-6, 2011.
- [13] J.R. Henderson and F.V. Swol, "On the Interface between a Fluid and a Planar Wall: Theory and Simulations of a Hard Sphere Fluid at a Hard Wall", *Molecular Physics*, Vol. 51, pp. 991-1010, 1983.
- [14] W. Yu and S.U.S. Choi, "The Role of Interfacial Layers in the Enhanced Thermal Conductivity of Nanofluids: A Renovated Maxwell Model", *Journal of Nanoparticle Research*, Vol. 5, pp. 167-171, 2003.
- [15] M.P. Beck, Y. Yuan, P. Warriar and A.S. Teja, "The Effect of Particle Size on the Thermal Conductivity of Alumina Nanofluids", *Journal of Nanoparticle Research*, Vol. 11, pp. 1129-1136, 2009.
- [16] P.C. Mishra, S.K. Nayak and S. Mukherjee, "Thermal Conductivity of Nanofluids – a Extensive Literature Review", *International Journal of Engineering Research & Technology*, Vol. 2, pp. 734-745, 2013.
- [17] G. Paul, M. Chopkar, I. Manna and P.K. Das, "Techniques for Measuring the Thermal Conductivity of Nanofluids: a Review", *Renewable and Sustainable Energy Reviews*, Vol. 14, pp. 1913-1924, 2010.
- [18] H. Kurt and M. Kayfeci, "Prediction of Thermal Conductivity of Ethylene Glycol-Water Solutions by Artificial Neural Network", *Applied Energy*, Vol. 86, pp. 2244-2248, 2008.
- [19] Y. Zeng, X. Zhong, Z. Liu, S. Chen and N. Li, "Preparation and Enhancement of Thermal Conductivity of Heat Transfer Oil-based MoS₂ Nanofluids", *Journal of Nanomaterials*, Vol. 2013, pp. 1-6, 2013
- [20] L.S. Sundar and K.V. Sharma, "Experimental Determination of Thermal Conductivity of Fluid Containing Oxide Nanoparticles." *International Journal of Computational Fluid Dynamics*, Vol. 4, pp.57-68, 2008.
- [21] D. Li, W. Xie, and W. Fang, "Preparation and Properties of Copper-Oil-based Nanofluids," *Nanoscale Research Letters*, Vol. 6, pp. 1-7, 2011.
- [22] B. Wang, B. Wang, P. Wei, X. Wang and W. Lou, "Controlled Synthesis and Size-Dependent Thermal Conductivity of Fe₃O₄ Magnetic Nanofluids," *Dalton Transactions*, Vol. 41, pp. 896–899, 2012.
- [23] G. Colangelo, E. Favale, A. de Risi and D. Laforgia, "Results of Experimental Investigations on the Heat Conductivity of Nanofluids based on Diathermic Oil for High Temperature Applications," *Applied Energy*, Vol. 97, pp. 828–833, 2012.
- [24] N.R. Karthikeyan, J. Philip and B. Raj, "Effect of Clustering on the Thermal Conductivity of Nanofluids", *Materials Chemistry and Physics*, Vol. 109, pp. 50-55, 2008.

6 Stability, health and environmental aspects

The introduction of nanofluids into industry applications requires long term stability of nanofluids and an understanding of the impact of nano-materials on human health and environment. In a transformer, the oil is in motion due to natural or forced convection. In this chapter, the stability of silica nanofluids is investigated when forced convection is applied. The possible harmful effects of nanoparticles on human health and an overview of the impact of nanofluids on the environment are also given in this chapter.

6.1 Stability tests of nanofluids

A nanofluid is theoretically stable as long as particles stay smaller than 100 nm [1]. However, it can be a challenge to maintain this size due to the attractive force between nanoparticles, which can lead to the formation of large particles agglomeration and eventually settle out of suspension. So problems of nanoparticle agglomeration and settling all need to be examined in detail in the applications. Further research still has to be done on the synthesis and applications of nanofluids so that they may be applied as predicted [1].

Due to the gravity and the fact that the density of the nanoparticles is larger than that of mineral oil, most of the nanofluids will have sedimentations after some time. For 0.01% nanofluids, visible sedimentations appear around 1 month after synthesis. This phenomenon can also be observed with a dynamic light scattering (DLS) test. Fig. 6.1 shows the particle size distribution of 0.01% silica nanofluid after synthesis at different moments in time after synthesis. It can be seen that after a week, the peak in the particle size distribution shifts to slightly larger values. This indicates the forming of aggregations. Eventually, these aggregations will settle and visible sedimentation will be formed.

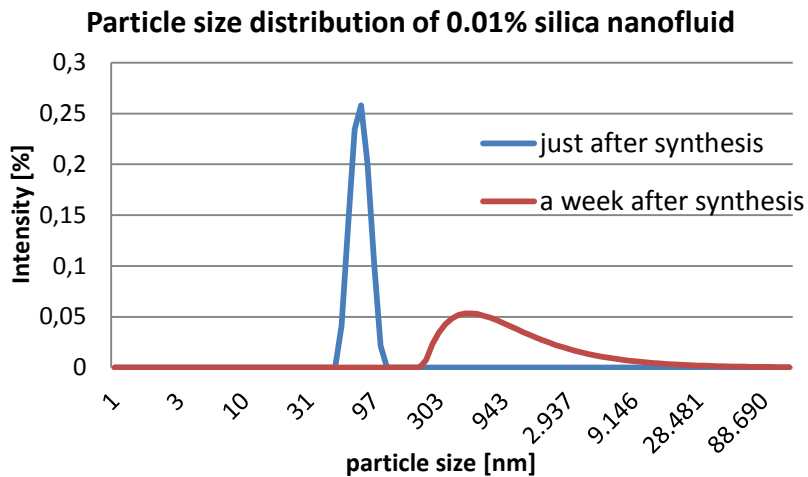


Figure 6.1 Particle size distributions in 0.01% silica nanofluid.

6.1.1 Nanofluids stability test set-up

In a transformer, the oil is in motion due to natural or forced convection. Hence, it is important to find out whether there is still sedimentation when forced convection is applied to the nanofluids. If the convection affects the sedimentation the question arises what is the minimum speed which can prevent sedimentation in nanofluids. Fig. 6.2 shows the experimental setup for observing the stability of nanofluids in the presence of forced convection.

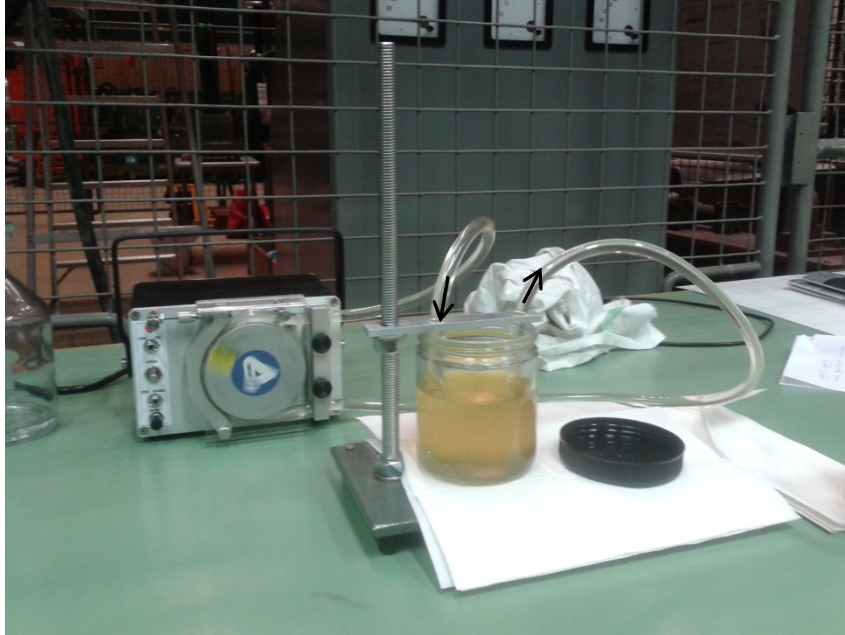


Figure 6.2 Experimental setup for observing the stability of nanofluids with forced convection.

The pump in this setup is a peristaltic pump (tubing pump), Fig. 6.3 shows the squeezing action of the pump. A peristaltic pump contains a flexible tube fitted inside a circular pump casing. A rotor with a number of "rollers" attached to the external circumference of the rotor compresses the flexible tube. As the rotor turns, the part of the tube under compression is closed thus forcing the fluid to be pumped to move through the tube. The maximum pump speed in this study is 300 ml/min.

The sedimentation will be observed optically in the plastic tube and the beaker's corner in a qualitative way. The results are compared with the nanofluids in the still status during this period.

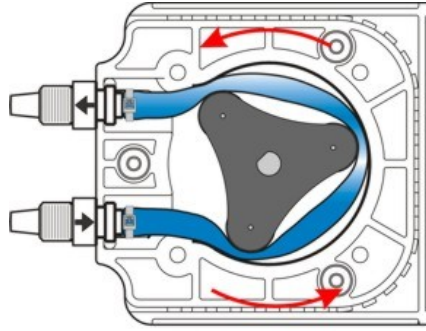


Figure 6.3 Peristaltic pump.

6.1.2 Nanofluids stability test results

Fig. 6.4 shows the test result at 300 ml/min. The test specimen consists of 300 ml silica nanofluid with 0.5% mass fraction. It can be seen that where the tube enters the beaker with the test specimen, there is almost no sedimentation and there are sedimentations where the tube exits the beaker.

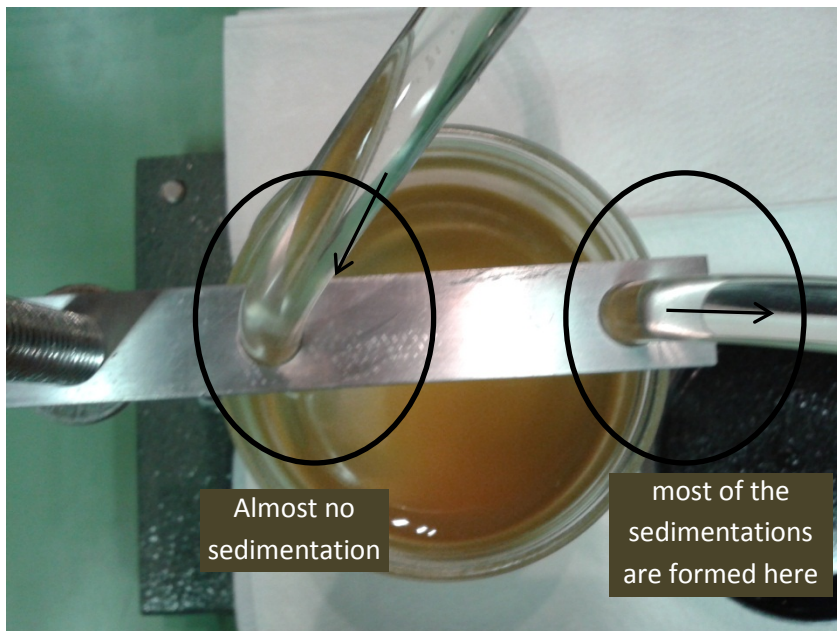


Figure 6.4 Silica nanofluid stability at 300 ml/min.

Due to the fact that sedimentations are prevented only where the tube enters the beaker, the test set-up is modified. Fig.6.5 shows the modified test set-up. The tubes now enter and exit the beaker in the centre.



Figure 6.5 Modified test set-up with the tube entering the beaker in the centre.

Three samples of 50 ml 0.5% mass fraction silica nanofluids were prepared. One sample was kept in still status for 24 hours as a reference. Fig. 6.6 shows the results of 0.5% silica nanofluids stability test. The first test is to pump the silica nanofluid with the maximum speed of 300 ml/min. The result shows that sedimentations are prevented to a large extent in silica nanofluid. Then the second test is to pump the silica nanofluid with a lower speed of 200 ml/min. The result shows that 200 ml/min is not sufficient to prevent sedimentation in silica nanofluid.

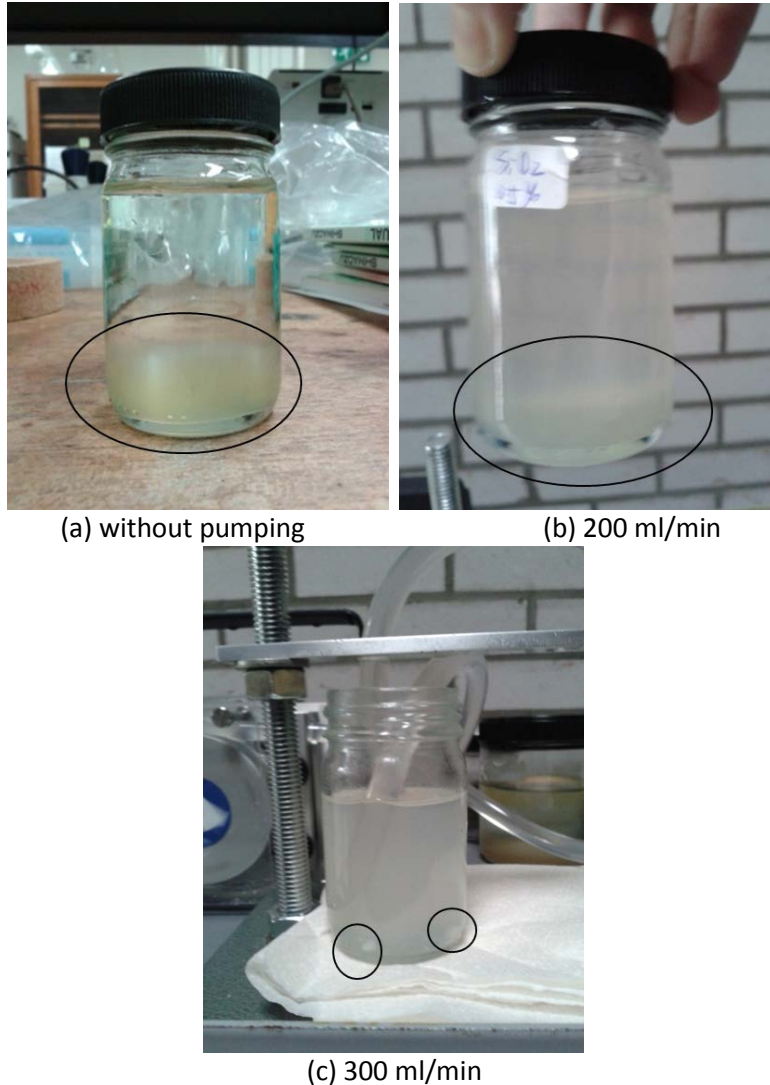


Figure 6.6 Stability tests of 0.5% silica nanofluid at different speed.

6.1.3 Summary and discussion

- 24 hours after synthesis, in a 0.5% silica nanofluid without forced convection, a clear sedimentation layer on the bottom of the liquid was formed.
- Speed of 200 ml/min is not sufficient for preventing sedimentations.
- With 300 ml/min pumping speed, sedimentations are prevented to a large extent.

In a transformer, the average speed of oil movement is 1cm/s according to industrial experience. This speed times the cross section of the tube is around 19 ml/min. So the oil speed in a transformer is 10 times smaller than the 200 ml/min speed used in the experiment. That means for silica nanofluid, the oil speed in a transformer probably is not sufficient to prevent sedimentations.

6.2 Health and environmental aspects

Nanoparticles have been identified as one of the main occupational health and safety (OHS) risks and priorities in review of various national, EU and international regulation and guidelines [2]. Much of the toxicology of nanomaterials is uncertain or unknown. Nano-sized particles are in general more dangerous than their respective micron sized or bulk material due to increased reactivity of their surface area [3]. The most discussed and investigated exposure route of nanoparticles to human body is airborne exposure with inhalable uptake. Airborne particles can be divided by size into three groups: small particles with an average size smaller than 80 nm, intermediate particles with an average size between 80 and 2000 nm and large particles with an average size larger than 2000 nm. The biggest danger is regarded coming from intermediate particles. The reason is that intermediate particles can remain suspended in air for up to several weeks, while small particles are short-lived and tend to largely agglomerate and form large particles and large particles subject to gravitational settling [4]. The penetration of nanoparticles into human body during inhalation is either through nasal cavity or the alveolar capillary barrier in the lung [5, 6]. The exposure to even small concentrations of those particles may cause inflict acute pulmonary effects of the workers. For example, exposure to iron oxide has been found to cause detrimental changes in the human lungs due to deposition inhaled particles [7]. Exposure to copper, vanadium, chromium and zinc has been reported to produce adverse health effects in lung dysfunction and even cancer. Depending on the base material, size and coating of the nanoparticles, the risk is that some types of nanoparticles may translocate from the respiratory tract and distribute to other organs, including the central nervous systems [4]. The available studies suggest that at high concentration zinc oxide nanoparticle is highly toxic, alumina nanoparticle is moderately toxic and magnetite nanoparticle is slightly toxic [8]. Nanoscale titania is possibly carcinogenic to humans and can travel to the brain by way of olfactory neurons when

inhaled [9]. Carbon nanotubes exhibit the potential for lung toxicity. The high aspect ratio of carbon nanotube makes them more dangerous than carbon black or quartz, since they possess sharp ends due to the needle-like shape [10, 11]. Until toxicologists determine what the safe level is, best laboratory practice would be to prevent all inhalation exposure [3]. Besides inhalation, nanoparticles may also have the ability to penetrate through the skin contact or by digestion. Due to the fact that the thickness of skin is much larger than alveolar membrane, the risk of skin penetration is rather low. After entering the body via digestion system, nanoparticles can penetrate into the blood stream and accumulate in the liver and spleen [12]. Carbon and graphite nanoparticles may cause skin diseases and respiratory infections [13].

The environmental impact of nanotechnology can be split into two aspects: the pollution that nanomaterials might cause if released to the environment and the potential to improve the environment. During production, transportation and deposition, nanoparticles and their by-products can be gotten released to the air and water. Those nanoparticles would accumulate in the soil, water or plants. The impacts of nanomaterials on humans and environment may vary at different stages of their life cycle. For future development, these impacts need to be analysed by using Life Cycle Assessment [3]. On the other hand the potential to improve the environment related to power industry by using nanotechnology mainly reflects in storage, conversion, manufacturing improvements by reducing materials and process rates, energy saving and enhancing renewable energy sources.

6.3 Future research

Although transformer oil based nanofluids exhibit higher dielectric and heat transfer properties, to be used in high voltage transformers in the future, the long-term stability of nanofluids is still a challenge. Great efforts have been made to improve the dispersion stability of nanofluids, for instance by using appropriate surfactants and more efficient dispersion method [14, 15]. However, the potential of nanofluids is still not fully clear regarding cost-effective industrial-scale production of nanofluids. Therefore, more material and chemical research still needs to be done to identify the promising methods to synthesize nanofluids with long-term suspension stability and homogeneity [1].

Researchers have demonstrated in the laboratory that nanofluids exhibit enhanced heat transfer and dielectric properties. Recently, some researchers took one step further into practical applications and demonstrated the ability of nanofluids to improve the performance of real-world devices and systems [16]. In the future, nanofluid properties, dielectric and heat transfer performance should be investigated under potential service conditions. All the experimental results should be collated for designers of industrial cooling systems. The development of nanofluid technology is expected to grow rapidly provided strong collaboration exists between nanofluid researchers in academia and industry [1].

6.4 References

- [1] S.K. Das, S.U.S. Choi, W. Yu and T. Pradeep, *Nanofluids: Science and Technology*, Wiley-Interscience, 2008.
- [2] E. Rial-González, S. Copley, P. Paoli and E. Schneider, "Priorities for Occupational Safety and Health Research in the EU-25", European Agency for Safety and Health at Work, Luxembourg, 2005.
- [3] P. Krajnik, F. Pusavec and A. Rashid, "Nanofluids: Properties, Applications and Sustainability Aspects in Materials Processing Technologies", Proceedings of the 8th Global Conference on Sustainable Manufacturing, Advances in Sustainable Manufacturing, pp. 107-113, 2011.
- [4] R. Kochetov, P.H.F. Morshuis, J. J. Smit, T. Andritsch and A. Krivda, "Precautionary Remarks Regarding Synthesis of Nanocomposites", Electrical Insulation Conference, pp. 51-54, 2014.
- [5] A. Nemmar, P.H.M. Hoet, B. Vanquickenborne, D. Dinsdale, M. Thomeer, M.F. Hoylaerts, H. Vanbilloen, L. Mortelmans and B. Nemery, "Passage on Inhaled Particles into the Blood Circulation in Humans", *Circulation*, Vol. 105, pp. 411-414, 2002.
- [6] M. Geiser, B. Rothen-Rutishauser, N. Kapp, S. Schürch, W. Kreyling, H. Schulz, M. Semmler, V. Im Hof, J. Heyder and P. Gehr, "Ultrafine Particles Cross Cellular Membranes by Nonphagocytic Mechanisms in Lungs and in Cultured Cells", *Environmental Health Perspectives*, Vol. 113, pp. 1555-1560, 2005.
- [7] J.W. Sutherland, V.N. Kukur, N.C. King and B.F. von Turkovich, "An Experimental Investigation of Air Quality in Wet and Dry Turning", *CIRP Annals - Manufacturing Technology*, Vol. 49, pp. 61-64, 2002.
- [8] H.A. Jeng and J. Swanson, "Toxicity of Metal Oxide Nanoparticles in Mammalian Cells", *Journal of Environmental Science and Health*, Vol. 41, pp. 2699-2711, 2006.
- [9] J. Wang, Y. Liu, F. Jiaom F. Lao, W. Li, Y. Gu, C. Ge, G. Zhou, B. Li, Y. Zhao, Z. Chai and C. Chen, "Time-dependent Translocation and Potential Impairment on Central Nervous System by Intranasally Instilled TiO₂ Nanoparticles", *Toxicology*, Vol. 254, pp. 82-90, 2008
- [10] C. Lam, J.T. James, R. McCluskey, S. Arepally and R.L. Hunter, "A Review of Carbon Nanotube Toxicity and Assessment of Potential Occupational and Environmental Health Risks", *Critical Reviews in Toxicology*, Vol. 36, pp. 189-217, 2006.
- [11] J. Muller, F. Huaux and D. Lison, "Respiratory Toxicity of Carbon Nanotubes: How Worried Should We Be?", *Carbon*, Vol. 44, pp. 1048-1056, 2006.
- [12] B. Baroli, M.G. Ennas, F. Loffredo, M. Isola, R. Pinna and M.A. Lopez-Quintela, "Penetration of Metallic Nanoparticles in Human Full-Thickness Skin", *Journal of Investigative Dermatology*, Vol. 127, pp. 1701-1712, 2007.
- [13] R.H. Hurt, M. Monthiux and A. Kane, "Toxicology of Carbon Nanomaterials: Status, Trends, and Perspectives on the Special Issue", *Carbon*, Vol. 44, pp. 1028-1033, 2006.
- [14] Y.Z. Lv, S.N. Zhang, Y.F. Du, T.M. Chen and C.R. Li, "Effect of Oleic Acid Surface Modification on Dispersibility of TiO₂ Nanoparticles in Transformer Oils," *International Journal of Inorganic Materials*, Vol. 28, pp. 1-5, 2013.
- [15] P.P.C. Sartoratto, A.V.S. Neto, E.C.D. Lima, A.L.C. Rodrigues de Sá, and P.C. Morais, "Investigation of the Molecular Surface Coating on the Stability of Insulating Magnetic Oils," *The Journal of Physical Chemistry C*, Vol. 114, pp. 179-188, 2010

- [16] K.V. Wong and O. de Leon, "Applications of Nanofluids: Current and Future", *Advances in Mechanical Engineering*, Vol. 2010, pp. 1-11, 2010.

7 Conclusions and recommendations

7.1 Conclusions

Oil based nanofluids are considered to be candidates to replace conventional transformer oil because nanofluids exhibit improvement in both electrical and thermal properties. This thesis focused on the synthesis, AC breakdown strength, partial discharge behaviour, thermal conductivity and viscosity and stability of mineral oil based silica and fullerene filled nanofluids. The main contributions of this study are:

- The achievement of enhanced breakdown strength of mineral oil due to the addition of nanoparticles;
- A possible explanation for this enhancement: the adsorption of moisture and acid on the surface of nanoparticles.

Nanofluids synthesis

The stability of nanofluids is one of the biggest challenges in this project. At steady status, aggregations in nanofluids are caused by attractive forces between nanoparticles which finally result in settling down of the nanoparticles. We found there are two ways to prevent aggregation between particles: modifying the surface of the nanoparticles to increase the repulsive energy and increasing the distance between particles to decrease the attractive energy. In our study, titania, silica and fullerene nanofluids were synthesized. Aggregations of nanoparticles were broken with the help of magnetic stirring and ultrasonic bath. The size distribution of the nanoparticles in the oil was examined with a dynamic light scattering (DLS) test. Without surface treatment, the DLS results showed that:

- In fullerene nanofluids up to 0.5% mass fraction, a long-term stable dispersion is obtained.
- Silica nanofluids with 0.01% mass fraction have visible sedimentations within 1 month; silica nanofluids with 0.02% mass fraction have visible sedimentations within 1 week.
- In 0.01% titania nanofluids, sedimentations are formed within 24 hours

The reason for the stable dispersion of fullerene nanofluids is the hydrophobic surface. In order to achieve a stable dispersion at a higher particle concentration, a hydrophobic surface of nanoparticles is necessary. Silane coupling agent Z6011 and surfactant span80 were used to modify the hydrophilic nanoparticles and to obtain a hydrophobic surface. In this way, nanofluids with smaller size distributions were obtained by keeping the nanoparticles apart, but sedimentations were not prevented.

AC breakdown strength of nanofluids

For nanofluids to be considered as insulating liquids, it is important to evaluate the ability of nanofluids to withstand the electrical stress. Recent studies suggested that conductive nanoparticles can act as electron traps, which help to increase the breakdown strength of transformer oil [1]. In our study, the AC breakdown strength of silica and fullerene nanofluids was investigated. Silica is insulating material with a dielectric relaxation time constant of 25 to 37 s. The time scale for streamer propagation in mineral oil is nano to micro seconds. Therefore the relaxation time constant of silica is not small enough to effect the streamer dynamics. Fullerene is a semi conducting material with a relaxation time constant of 75 to 80 ns, short enough to influence to streamer dynamics.

Due to the limited stability of nanofluids, the achievable mass fractions of silica nanofluids are 0.01% and 0.02% and that of fullerene nanofluids are 0.05% and 0.1%. The effect of different kinds of nanoparticles, particle concentration and humidity on the breakdown strength of mineral oil was investigated. The AC breakdown voltage results of the nanofluids showed:

- For both nanofluids, the breakdown voltage increases with an increase of mass fraction.
- The effect is more significant at 25 ppm moisture content than at 15 ppm moisture content.
- The enhancement of the average AC breakdown voltage due to silica nanoparticles is larger than for fullerene nanoparticles.

Due to the fact that silica is an insulating material, the breakdown behaviour of silica nanofluids can't be explained by the theory of conductive nanoparticles acting as electron traps. Since moisture plays an important role in the breakdown behaviour of nanofluids, one possible

mechanism behind the enhanced AC breakdown voltage of silica nanofluids is that moisture is absorbed on the hydrophilic surface of silica nanoparticles. This hypothesis was confirmed by comparing the AC breakdown voltage of untreated silica and surface modified silica nanofluids. The surface of modified silica nanoparticles is hydrophobic, so it won't adsorb any moisture. The results showed that the treated silica nanofluids have a negative effect on the AC breakdown strength of mineral oil. To a certain extent, these results indicate that the hydrophilic surface of silica nanoparticles, which can adsorb moisture on the surface, can be the reason for the breakdown enhancement. However, fullerene is hydrophobic, therefore moisture adsorption can't be the reason for the enhanced breakdown strength of fullerene nanofluid.

Partial discharge behaviour of nanofluids

Further investigation on the dielectric strength of silica and fullerene nanofluids was performed with the measurement of partial discharge. Partial discharge measurements gave a more detailed view on the pre-breakdown phenomenon of dielectric nanofluid by recording the discharge pulse shape, inception voltage, total discharge magnitude and single discharge pulse amplitude. The PD results of mineral oil, 0.01% silica and 0.01% fullerene nanofluids were compared. The results showed:

- Silica nanoparticles increase the inception voltage and decrease the total discharge magnitude, and pulse amplitude of mineral oil significantly.
- The effect due to fullerene nanoparticles is similar but less than the effect of silica nanoparticles.

The hypothesis is that the adsorption of moisture, acid or other additives in the oil by the nanoparticles is the mechanism behind the improved breakdown strength. This hypothesis can be verified by examining the constituents in mineral oil and nanofluids. Recent studies showed that constituents in oils can be examined with terahertz spectroscopy and the results can be used to study the moisture content, oxidation level and acid value in the oil [3, 4]. The results of terahertz spectroscopy measurements for mineral oil and nanofluids showed that it is possible that the acid value in the nanofluids is lower than in the mineral oil. One possible mechanism is that acid is adsorbed on the surface of the nanoparticles. The increased

inception voltage and decreased PD discharge of silica and fullerene nanofluids can be due to the decreased amount of acid in the oil. The larger effect of silica nanoparticles on the dielectric strength of mineral oil compared with fullerene nanoparticles can be a result of the combination of acid and moisture adsorption on the surface of the nanoparticles.

Thermal conductivity of nanofluids

Compared with the effect on dielectric strength, the effect of silica and fullerene nanoparticles up to 0.1% mass fraction on the thermal conductivity of mineral oil is negligible. This is mainly due to the low concentration and limitation of stability of nanofluids.

Viscosity and stability of nanofluids

The viscosity and stability of silica and fullerene nanofluids were also studied. We concluded that up to 0.1% mass fraction, silica and fullerene have negligible effect on the viscosity of mineral oil. The stability of the nanofluids was investigated in a condition of forced convection with different speed. To prevent the sedimentations of 1% silica nanofluids, the required speed should be around 15 times higher than the average speed of oil in a transformer.

7.2 Recommendations

In this study, the mechanism behind the dielectric strength enhancement due to silica and fullerene nanofluids could not be determined by direct observation. A breakthrough could be realized if the adsorption of either moisture or acid could be directly detected. Therefore it is recommended that the surface properties of the nanoparticles in the oil are further investigated. Since silica and fullerene nanofluids showed lower acid value than mineral oil, it is suggested to investigate the effect of those nanoparticles on the aging effect of mineral oil. Besides, other factors, such as the structure of the nanoparticles and the effects of surfactant or coupling agent should be considered.

The possible mechanism behind the enhanced breakdown strength of silica and fullerene nanofluid is the absorption of moisture and acid. Then, for further work, the pre-breakdown and breakdown behaviour of nanofluids should be investigated in a condition of precisely controlled acid and

humidity level. The research objectives are shown in the following four statements:

1. It is very important to measure the acidity and moisture content in mineral oil and nanofluids carefully.
2. The acid tolerance and moisture tolerance of mineral oil and nanofluids should be studied.
3. The effect of acid and moisture content on the breakdown strength and PD discharge behaviour of mineral oil and nanofluids should be investigated.
4. The breakdown strength and PD discharge of mineral oil should be measured with decreased amount of acid and moisture content according to the adsorption amount due to nanoparticles. And the results can be compared with that of nanofluids.

In order to utilize nanoparticles to increase the thermal conductivity of mineral oil the barrier of the stability of oil based nanofluids should first be crossed. In this study, fullerene nanofluid can be evenly dispersed and stable for at least 3 years. However, the highest mass fraction that can be obtained is still lower than 1%. Most kinds of nanoparticles are not hydrophobic, so surface treatment would be necessary. Further investigation should be focussed on how to obtain stable dispersed nanofluids.

Convection is one of the dominant heat transfer modes for transformer oil. Further study should also look into the nature of forced convective heat transfer of nanofluids. The Brownian motion of the nanoparticles can induce the flow of the surrounding fluids, which is also called micro-convection [2]. This may contribute to the increase of convective heat transfer in the base fluids.

7.3 References

- [1] F.M. O'Sullivan, "A Model for the Initiation and Propagation of Electrical Streamers in Transformer oil and Transformer oil based nanofluids", PhD thesis, Massachusetts Institute of Technology, 2007.
- [2] L. Wang and J. Fan, "Toward Nanofluids of Ultra-High Thermal Conductivity", *Nanoscale Research Letters* 2011, Vol. 6, pp. 1-9, 2001.

- [3] W. Jin, K. Zhao, C. Yang, C. Xue, H. Ni and S. Chen, "Experimental Measurements of Water Content in Crude oil Emulsions by Terahertz Time-domain Spectroscopy", *Applied Geophysics*, Vol. 10, pp. 506-509, 2013.
- [4] N. Nishimura, R. Ogura, S. Matsumoto, M. Mizuno and K. Fukunaga, "Transmittance Spectra of Oxidized Insulation Oil Using Terahertz Spectroscopy", *IEEE international Conference on Dielectric Liquids*, pp. 1-4, 2011.

Appendix A. Dynamic light scattering

A.1 Introduction

Dynamic light scattering (DLS), also called Photon Correlation Spectroscopy, is a technique in physics that is used to determine the size distribution profile of small particles in suspension or polymers in solution [1]. DLS measures Brownian motion and relates this to the size of the particles. Brownian motion is a random movement of particles suspended in a fluid resulting from their collision with quick atoms or molecules in the liquid. The motion depends on particles size, liquid viscosity and temperature [2]. For DLS analysis, the Stokes-Einstein equation is used to relate the velocity of the particle to its hydrodynamic radius [3]. The diameter that is obtained by this technique is the diameter of a sphere that has the same translational diffusion coefficient as the particles. The translational diffusion coefficient is a proportionality constant between the molar flux due to the molecular diffusion and the gradient in the concentration of the species (or the driving force for diffusion).

$$D = \frac{kT}{6\pi\eta a} \quad (\text{A.1})$$

Where D is the translational diffusion coefficient of the particle, k is the Boltzmann constant, T is the temperature, η is the viscosity of the solution/suspension and a is the hydrodynamic radius of the particles. The diffusion velocity of the particles is inversely proportional to the hydrodynamic radius. This shows that for a system undergoing Brownian motion, small particles should diffuse faster than large particles, which is a key concept in DLS analysis [4].

A.2 Collecting data

In a typical DLS experiment, a suspension/solution is irradiated with monochromatic light source, usually a laser light is shot through a polarizer into a sample [5]. Brownian motion in the sample leads to fluctuations in the scattered light intensity. The scattered light signal is collected with a photomultiplier. The intensity of the scattered light is detected as a function of scattering angle θ and time t [6]. In general, when a sample of particles with diameter much smaller than the wavelength of light is irradiated with light, each particle will diffract the incident light in all

directions [4]. A schematic representation of the light-scattering experiment is shown in Fig. A.1

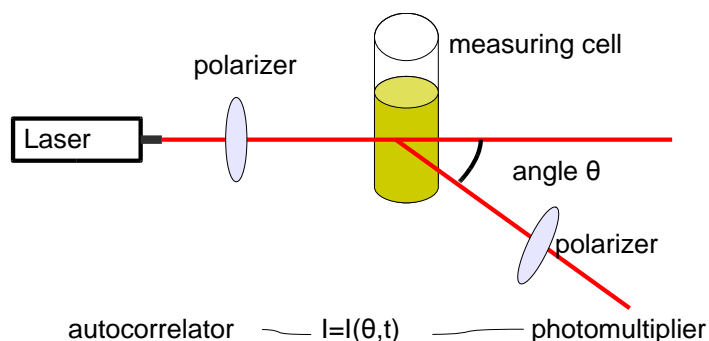


Figure A.1. A schematic representation of the light-scattering experiment, I is the scattered light intensity, θ is the scattering angle, t is the time [6].

A.3 Data analysis

It is inefficient to directly measure the spectrum of frequencies contained in the intensity fluctuations arising from the Brownian motion of particles. The best way is to use a device called a digital autocorrelator. A correlator is basically a signal comparator. It is designed to measure the degree of similarity between two signals, or one signal with itself at varying time intervals. If the intensity of signal at time (t) is compared to the intensity at nanoseconds or microseconds later ($t+\Delta t$), there will be a strong relationship or correlation between the intensities of the two signals. If the signals at $t+2\Delta t$, $t+3\Delta$ etc. are compared with the signal at t , the correlation of signal arriving from the random source will decrease with time [7].

Once the autocorrelation data has been generated, different mathematical approaches can be employed to analyse the particle size distribution in the sample. The simplest approach is to treat the first order autocorrelation function as a single exponential decay.

$$G(t) = e^{-\Gamma t} \quad (A.2)$$

Where $G(t)$ is the correlation function for a system experiencing Brownian motion, Γ is the decay rate and τ is the decay time.

Γ is related to the diffusivity of the particle by

$$\Gamma = -Dq^2 \quad (\text{A.3})$$

Where D is diffusion coefficient of the particle and q is the wave vector

$$q = \frac{4\pi n_0}{\lambda} \sin\left(\frac{\theta}{2}\right) \quad (\text{A.4})$$

Where λ is the incident laser wavelength, n_0 is the refractive index of the sample and θ is the angle at which the detector is located with respect to the sample cell [4].

There are two most common approaches to obtain the particles size from the correlation function: cumulant method and CONTIN algorithm. For the cumulant method, a single exponential is fit to the correlation function to obtain the mean size and an estimate of the width of distribution. The calculation is defined in ISO 13321 and ISO 22412. CONTIN algorithm is an inverse Laplace transform developed by Steven Provencher for analysing the autocorrelation [8]. The CONTIN analysis is ideal for heterodisperse, polydisperse and multimodal systems that can't be resolved with the cumulant method.

References

- [1] B.J. Berne and R. Pecora, *Dynamic Light Scattering: With Applications to Chemistry, Biology, and Physics*, Courier Dover Publications, 2000.
- [2] University of Florida - Department of Physics, PHY4803L – Advanced Physics Laboratory, "Dynamic Light scattering: Experiment DLS", 2012.
- [3] R. Pecora, *Dynamic Light Scattering*, Plenum Press New York, 1985.
- [4] ChemWiki: http://chemwiki.ucdavis.edu/Analytical_Chemistry/Instrumental_Analysis/Microscopy/Dynamic_Light_Scattering
- [5] J. Goodman, "Some Fundamental Properties of Speckle", *Journal of the Optical Society of America*, Vol. 66, pp. 1145-1150.
- [6] Biophysics of Macromolecules: <http://www.dkfz.de/Macromol/research/dls.html>
- [7] MARVERN Instruments Ltd "Technical note-Dynamic light scattering: An introduction in 30 minutes" MRK656-01.
- [8] S. Provencher, "CONSTIN: A General Purpose Constrained Regularization Program for Inverting Noisy Linear algebraic and Integral equations", *Computer Physics Communications*, Vol. 27, pp. 229-242, 1982.

Appendix B. Moisture content measurement

In this study, the moisture content of mineral oil and nanofluids was measured with Vaisala Hand-held Moisture Meter MM70 for spot-checking in oil device. The device consists of two main units: MI70 indicator and MMP78 probe. The device is shown in Fig. B.1.



Figure B.1 MM70 Hand-held moisture and temperature meter [1].

HUMICAP technology enables the device reliable and high performance moisture in oil measurement. HUMICAP is a capacitive thin-film polymer sensor consisting of a substrate on which a thin film of polymer is deposited between two conductive electrodes. The sensing surface is coated with a porous metal electrode to protect it from contamination and exposure to condensation. The substrate is typically glass or ceramic. The thin film polymer either absorbs or realises water vapour as the relative humidity of the ambient air rises or falls. The dielectric properties of the polymer film depend on the amount of absorbed water. As the relative humidity around the sensor changes, the dielectric properties of the polymer film change, so does the capacitance of the sensor. The instrument's electronics measure the capacitance of the sensor and convert it into a humidity reading [2].

The water absorption on the thin film polymer is proportional to the water activity of the fluid. Water activity is the amount of water in a substance relative to the total amount of water it can hold. It is defined as:

$$a_w = \frac{p}{p_0} \quad (\text{B.1})$$

Where a_w is the water activity, p is the partial pressure of water in a substance above the material and p_0 is the saturated vapour pressure of pure water at the same temperature [3].

The water activity in a fluid changes as a function of the saturation point, as well as the actual water content in the oil. The traditional unit of measure for quantifying water content in oil is ppm (parts per million). However, a ppm measurement has one major limitation that it doesn't account for any variation in oil's saturation point. In other words, in a dynamic oil system with a fluctuating saturation point, a ppm measurement would provide no indication of how close the moisture level is to the oil's saturation point. Hence by measuring water activity instead of ppm, the above problem can be avoided. The water activity will always provide a true indication of the margin to saturation point. The absolute humidity of the liquid can be calculated from the water activity, which is:

$$ppm = a_w \times 10^{((\frac{A}{T} + 273.15) + B)} \quad (\text{B.2})$$

Where ppm is the absolute humidity of the liquid, a_w is the water activity, A and B are the coefficients specific to the analysed fluid, and T is the fluid temperature [4].

In this study, the value of the absolute humidity is used, which is a more direct indicator of the moisture content in the oil. The levels of absolute humidity in mineral oil and nanofluids discussed in chapter 3 are around 25 ppm and 15 ppm. At 20°C temperature, the water activity for 25 ppm humidity is around 0.45 and for 15 ppm humidity is around 0.27.

References

- [1] <http://www.vaisala.com/Vaisala%20Documents/Brochures%20and%20Datasheets/MM70-Datasheet-B210960EN-D.pdf>.
- [2] <http://www.vaisala.com/Vaisala%20Documents/Technology%20Descriptions/HUMICAP-Technology-description-B210781EN-C.pdf>.
- [3] http://www.vaisala.com/Vaisala%20Documents/Application%20notes/OilMoistureExpressedWaterActivity_B210806EN-A.pdf.
- [4] <http://avenisense.com/en/chimie/knowledge-center/-13.html>.

Appendix C. Bandwidth of partial discharge detection system

Bandwidth determines an oscilloscope's fundamental ability to measure a signal. Bandwidth is a sine wave specification that simply defines the frequency at which the peak to peak amplitude of the sine wave on the screen is attenuated to 70.7% of the actual sine wave amplitude, known as down by 3 dB, a term based on a logarithmic scale. To obtain an accurate signal, the bandwidth of the oscilloscope should be 3 to 5 times higher than the highest frequency component of the signal [1]. The bandwidth of the signal can be calculated from the rise time, the following formula can be used [2]:

$$\frac{0.35}{BW} = T_r \quad (E.1)$$

Where BW is the specified bandwidth, T_r is the rise time. This 0.35 relationship between bandwidth and rise time is based on a one-pole model for 10 to 90% rise time. The measurement result of the rise time of a PD pulse shown in chapter 4 is around 2 ns. The oscilloscope used in this study is Lecroy waverunner 44xi, the bandwidth is 400 MHz, so the rise time of the equipment is 875 ps. The actual rise time of the signal can be calculated as [3]:

$$T_m = \sqrt{T_s + T_d} \quad (E.2)$$

Where T_m is the measured rise time of the signal, T_s is the actual signal rise time (the actual signal means the PD signal after adding the effect of all the capacitors, inductors and resistors in the PD circuit) and T_d is the digitizer's rise time. After calculation, the actual signal rise time is around 1.8 ns, which is around 2 times more than the rise time of the oscilloscope. So there will be small distortion on the amplitude of the signal and some edges of the signal will vanish. To determine whether the oscilloscope is sufficient to record the PD signal, the frequency spectroscopy of the measured signal was analysed with MATLAB, which is shown in Fig. E.1. The bandwidth of the signal is within 400 MHz, but there are still signals which are happened above 400 MHz.

The recorded results in chapter 4 are total discharge magnitude, PD voltage amplitude, pulse shapes and inception voltage. The purpose is to

compare the PD behaviour of mineral oil, silica and fullerene nanofluids. According to standard IEC60270, the required maximum bandwidth of a PD detector for measuring total discharge under DC voltage is 500 kHz. The main difference of pulse shapes of mineral oil and nanofluids is repetition rate. Since the bandwidth of the oscilloscope is 2 times higher than the signal, then it is sufficient to record the rise time and repetition rate of the signal. The limit of the oscilloscope will only have effect on the PD voltage amplitude. There will be small distortion on the value of the PD voltage amplitude.

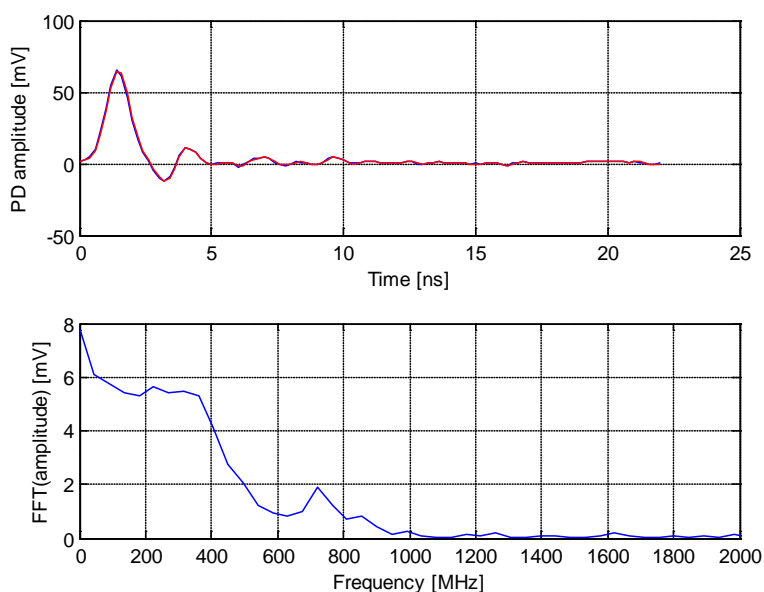


Figure C.1 PD pulse and frequency spectrum.

References

- [1] "Fundamentals of Signal Integrity", Tektronix, www.tektronix.com/signal_integrity.
- [2] Technical Brief, "Understanding Oscilloscope Bandwidth, Rise time and Signal Fidelity" Tektronix, 55W-18024-0.
- [3] <http://www.ni.com/white-paper/3016/en/>

Appendix D. Thermal conductivity calculation of nanofluids in COMSOL Multiphysics heat transfer module

The thermal conductivity calculation of nanofluids in COMSOL contains the heat transfer in solids model and heat transfer in liquid model. The heat transfer in solids model uses the governing equation:

$$\rho C_p \frac{\partial T}{\partial t} - \nabla \cdot (k \nabla T) = Q \quad (D.1)$$

Where ρ is the density of the material, C_p is the heat capacity, k is the thermal conductivity, Q is the heat source, T is the temperature and t is the time.

The heat transfer in fluids model uses the governing equation:

$$\rho C_p \frac{\partial T}{\partial t} + \rho C_p u \cdot \nabla T - \nabla \cdot (k \nabla T) = Q \quad (D.2)$$

Where ρ is the density of the material, C_p is the heat capacity, k is the thermal conductivity, Q is the heat source, T is the temperature, t is the time and u is the fluid velocity field. To calculate the thermal conductivity of the liquid, the velocity would be zero, then the governing equations of solid and liquid models are the same.

In the thermal conductivity calculation model of nanofluids, the input values are the density, thermal conductivity of the nanoparticles and mineral oil, the diameter of the nanoparticles/nano-clusters, the temperature on the left and right size of the nanofluids cubes shown in Fig. 5.7 in chapter 5. First, the conductive heat flux in the nanofluids is given by

$$q_i = - \sum_j k_{ij} \frac{\partial T}{\partial x_j} \quad (D.3)$$

Where q_i is the conductive heat flux, k is the anisotropic thermal conductivity in the nanofluid cube, T is the temperature, the heat is conducted in the positive x direction.

The effective thermal conductivity of the nanofluid can be calculated as:

$$k_{eff} = - \frac{q_i}{\nabla T} \quad (D.4)$$

Where $-k_{\text{eff}}$ is the effective thermal conductivity of the nanofluids, q_i is the conductive heat flux and T is the temperature.

Appendix E. Fourier transform infrared terahertz spectrometer

Fourier transform infrared spectroscopy (FTIR) is a technique which is used to obtain an infrared spectrum of absorption, emission, photoconductivity or Raman scattering of a solid, liquid or gas [1]. In this technique, a Fourier transform is required to convert the raw data into actual spectrum. An FTIR spectrometer simultaneously collects spectral data in a wide spectral range. The goal of the FTIR technique is to measure how well a sample absorbs light at each wavelength. This technique shines a beam containing many frequencies of light at the sample, and measures how much of that beam is absorbed by the sample. Infrared spectroscopy exploits the fact that molecules absorb specific frequencies that are characteristic of their structures. The frequency of the absorbed radiation matches the transition energy of the bond or group that vibrates. The energies are determined by the shape of the molecular potential energy surfaces, the mass of the atoms and the associated vibronic coupling [2]. The whole wavelength range is measured using a Fourier transform instrument and then a transmittance or absorbance spectrum is generated. Analysis of the position, shape and intensity of peaks in this spectrum reveals details about the molecular structure of the sample.

The Terahertz (THz) spectroscopic technique allows a material probed with short pulses which last only a few picoseconds. Many materials have unique spectral fingerprints in the THz range, which means that THz radiation can be used to identify them.

Fig. E.1 shows the FTIR-THz system (JASCO), the samples are mineral oil, silica and fullerene nanofluids, the experiments were performed in National Institute of Information and Communications Technology in Japan.

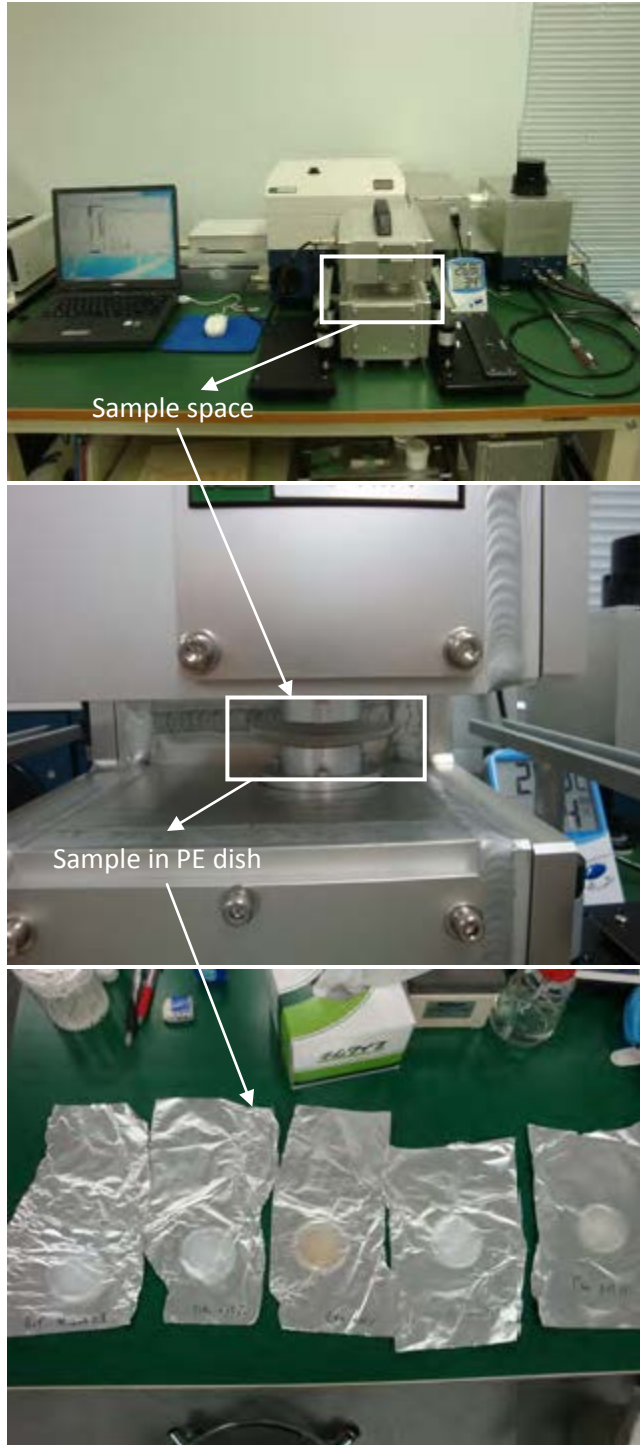


Figure E.1 the FTIR-THz system (JASCO) and test samples.

References

- [1] P. Griffiths, J.A. de Hasseth, *Fourier Transform Infrared Spectrometry (2nd edition)*, Wiley-Blackwell, 2007.
- [2] B. Jaganathan, "Benefits of Vibrational Spectroscopic", *International Research Journal of Management Sciences & Technology*, Vol.4, issue 1, 2013.

List of Symbols and Abbreviations

Symbols	Description	Unit
V_R	Repulsive electrostatic potential	-
V_A	Van der Waals force	-
V_D	Attractive aggregation potential	-
V_M	Energy barrier	-
HLB	Hydrophilic-lipophilic balance	-
M_h	the molecular weight of the hydrophilic group	$\text{g}\cdot\text{mol}^{-1}$
M	the molecular weight of the surfactant	$\text{g}\cdot\text{mol}^{-1}$
m_{span80}	the mass of span80	g
M_{span80}	the molecular weight of span80	$\text{g}\cdot\text{mol}^{-1}$
v_{OH}	the amount in moles of OH groups on the surface of nanoparticles	mol
v_{span80}	the amount in moles of span80	mol
$F(x)$	the cumulative probability of breakdown	%
x	the AC breakdown voltage	kV
β	the Weibull slope	-
η	the scale parameter of Weibull distribution	-
ρ	correlation coefficient of Weibull distribution	-
γ	the location parameter of Weibull distribution	-
τ	the charge relaxation time constant	s
ϵ	electrical permittivity	-
σ	electrical conductivity	S/m
q	partial discharge magnitude	C
I	current	A
t	time	s
q_x	the heat flux in the x direction	W/m^2

Q_x	the heat flowing in the x direction	W
A	the area perpendicular to x	m^2
k	thermal conductivity	W/mK
n_{silica}	the amount of silica nanoparticles inside a cluster	-
V_{cluster}	is the volume of a silica cluster	m^3
A_t	the total surface of the silica nanoparticles	m^2
A_e	the effective surface area of silica cluster	m^2

Abbreviations Description

span 80	sorbitan monooleate
Z6011	silane coupling agent Dow Corning Z6011
TEM	transmission electron microscopy
TGA	thermal gravimetric analysis
DLS	dynamic light scattering
NF	nanofluid
AC	alternating current
BD	breakdown
PD	partial discharge
FTIR-THz	Fourier transform infrared terahertz spectrometer

Acknowledgments

Many people have made contributions to this thesis. Without their kind support and help, this thesis wouldn't have been possible.

First of all, I would like to thank my promoter Prof. Dr. Johan Smit for giving me the opportunity to work in this group. I am grateful to him for trusting in my ability to complete this work and for his helpful ideas and suggestions during this work.

Of great importance for this thesis was my daily supervisor Dr. Ir. Peter Morshuis. The time we spent on discussions over this research and other topics are valuable for me. I appreciate the insightful advice given by him, not only about the technical issues but also about my future.

Without any doubt my daily supervisor Thomas Andritsch is the person who contributed most to this thesis. I am deeply grateful for his guidance all these years, even after he moved to England. His encouragement and support are most valuable and unforgettable. Thank you for helping me planning this work, discussing all the details, proofreading my reports publications and this thesis and helping me improving my English.

It was a great pleasure to work within the framework of the Triumvirate group, which funded this research, chaired by Dipl.-Ing. Arne Lunding. I want to express my gratitude to the Triumvirate members, who showed patience with me in the beginning and shared their ideas since then.

I specially would like to thank Paul van Nes, Wim Termorshuizen and Aad van der Graaf from HV laboratory for indispensable technical support and efficient solutions, especially in design and construction of all the setups I needed for my research. I would also like to thank Marcel Bus, Klaas Besseling, Ben Norder and Pieter Droppert from Delft Chemtech. Their advice and support were fundamental for my research.

I would like to thank my colleagues Andreas, Barry, Dennis, Gautam, Jur, Mo, QiKai, Tom, Ravish, Roy and Xiaolin. Thank you for being great colleagues and providing a friendly atmosphere in the group. I owe special thank to my roommate Roman. Thank you for regularly checking whether I needed any help and providing all the help I needed. It was really enjoyable to work with you. I would also like to thank my roommate Alex.

Thank you for helping me with my first journal paper, interesting discussion and advice. Your curiosity provoked some ideas in this thesis. I especially would like to thank Lukasz, who was my supervisor for my master project. I appreciate all your help ever since I started my master project in this group. Armando, thank you for patiently help me building my partial discharge setup. Your experience and advice were very helpful. Dhiradj, thank you for helping me with all the slow and complicated Dutch employment procedures.

I especially would like thank Kaori Fukunaga from National Institute of Information and Communications Technology in Japan. Thank you for your cooperative research on the Terahertz spectroscopy measurement of the nanofluids samples.

I would like to express my gratitude to my master supervisor Dr. Ir. Edward Gulski. Thank you for recommending me to Prof. Smit and trusting me that I can manage a PhD work.

One important part of my life is Aikido. Special thank to my Aikido teacher, Martin. I learned a lot during the past six years from you, not only Aikido techniques but also the spirit. Thanks all the Aikidokas, you helped me releasing most of the pressure from my work.

Special thanks to my Dutch teacher Carolien. Thank you for helping me with the samenvatting, stellingen and improving my Dutch.

Many thanks to my friend and high school classmate Xuexue from Civil Engineering and my friend Diyun. Thank you for listening to all my complains.

Special thanks to my friend Baobao. I appreciate your talented contribution for the cover of this thesis.

I address my gratitude to my parents for their love, support and confidence in me during all the time I am living far away from them. I would like thank Hans and Trees. Thank you for letting me be part of the family, een warm nest is de basis voor alles. Finally, I am extremely grateful to Pieter for being with me during all these years.

Publications

- H. Jin, P.H.F. Morshuis, T. Andritsch, A.R. Mor, "An Investigation into the Dynamics of Partial Discharge Propagation in Mineral Oil based Nanofluids" International Conference on Dielectric Liquids (ICDL), Bled, Slovenia, July 2014.
- H. Jin, T. Andritsch, P.H.F. Morshuis, J.J. Smit, "The Effect of Surface Treatment of Silica Nanoparticles on the Breakdown Strength of Mineral Oil " International Conference on Dielectric Liquids (ICDL), Bled, Slovenia, July 2014.
- H. Jin, T. Andritsch, I.A. Tsekmes, R. Kochetov, P.H.F. Morshuis, J.J. Smit, "Properties of Mineral Oil based Silica Nanofluids", IEEE Transactions on Dielectrics and Electrical Insulation, Vol. 21, Issue 3, pp. 1100-1108, June 2014.
- H. Jin, T. Andritsch, P.H.F. Morshuis, J.J. Smit, "AC Breakdown Voltage and Viscosity of Mineral Oil based Fullerene Nanofluids", Conference on Electrical Insulation and Dielectric Phenomena (CEIDP), Shenzhen, China, October, 2013.
- H. Jin, T. Andritsch, I.A. Tsekmes, R. Kochetov, P.H.F. Morshuis, J.J. Smit, "Thermal Conductivity of Fullerene and TiO₂ Nanofluids", Conference on Electrical Insulation and Dielectric Phenomena (CEIDP), Shenzhen, China, October, 2013.
- H. Jin, T. Andritsch, P.H.F. Morshuis, J.J. Smit, "AC Breakdown Voltage and Viscosity of Mineral Oil based SiO₂ Nanofluids", Conference on Electrical Insulation and Dielectric Phenomena (CEIDP), Montreal, Canada, October, 2012.
- L. Chmura, H. Jin, P. Cichecki, J.J. Smit, E. Gulski, F.D. Vries, "Use of Dissipation Factor for Life Consumption Assessment and Future Life Modeling of Oil-filled High-Voltage Power Cables", Electrical Insulation Magazine, January/February, 2012.
- H. Jin, P.H.F. Morshuis, T. Andritsch, A.R. Mor, J.J. Smit, "Partial Discharge Behaviour of Mineral Oil based Nanofluids" IEEE Transactions on Dielectrics and Electrical Insulation, submitted in December 2014.

Curriculum Vitae



Huifei Jin was born in 1985 in China. She received her B.S degree in electrical information engineering in 2008 from North-Eastern University, China. In 2010, she received her master degree in electrical power engineering from Delft University of Technology. In 2010 she started her Ph.D. research in the department of High Voltage Components and Power Systems at TU Delft. Her current Ph.D. research focuses on the nanofluids technology. The aim of the research is to facilitate the design of smaller, high power density components by improving the thermal and electrical properties of the cooling medium.

